

https://dspace.org/

Process mineralogy and extraction of rare earth elements from a beach placer deposit

Moila, Awelani Veronica

2019

https://hdl.handle.net/10539/28846

Moila, Awelani Veronica. (2019). Process mineralogy and extraction of rare earth elements from beach placer deposit. University of the Witwatersrand, https://handle/10539/28846

Downloaded from a DSpace repository. https://dspace.org/

FACULTY OF ENGINEERING AND THE BUILT ENVIRONMENT

School of Chemical and Metallurgical Engineering



PROCESS MINERALOGY AND EXTRACTION OF RARE EARTH ELEMENTS FROM A BEACH PLACER DEPOSIT

AWELANI VERONICA MOILA

A dissertation submitted to the Faculty of Engineering and the Built Environment University of Witwatersrand, Johannesburg, in fulfilment of the requirements for the degree of Master of Science in Engineering

DECLARATION

I declare that the research project, **Process mineralogy and extraction of rare earth elements from a beach placer deposit**, is my own work and that each source of information used has been acknowledged by means of a complete reference. This thesis has not been submitted before for any other research project, degree or examination at any university.

Awelani Veronica Moila

……
(Signature of the student)

……
(Date)

……., South Africa
(Signed at)

ABSTRACT

Rare earth elements (REE) are a group of the lanthanides and are significant in the world's economic growth and modern technology market. This REE technological resource is globally distributed and highly monopolised in China. The global demand in REE led to China – "the leading economic producer of REE", limiting its export quotas of the commodity, thus reducing the supply of REE. The decline in REE supply opened up opportunities for other countries to explore alternative and additional sources of REE.

This research aims to investigate alternative sources of REE and to explore an efficient means of processing REE minerals from an existing beach placer deposit operation, currently being mined for titanium. Mineralogical characterisation and hydrometallurgical testwork were chosen for this study.

The sample represented a tailings fraction from heavy mineral concentration. The sample was screened into four size classes namely; +212µm, –212+150µm, –150+106µm and –106µm. Each size class was mineralogically characterised. Mineralogy is an important factor in plant optimisation and process route predictions. In order to process REE efficiently, an upfront mineralogy is a necessity to reduce the rising hefty ore-processing costs.

An integration of X-ray diffraction, optical microscopy, scanning electron microscopy (SEM), electron microprobe analysis (EMPA), automated SEM and bulk chemical analysis was employed in defining the mineralogical characteristics of the tailing sample.

The mineralogical analysis of the tailing sample showed monazite as the prominent REE-bearing mineral, followed by zircon. Other minerals such as epidote, amphibole, rutile, quartz, leucoxene, titanite and almandine were identified in the sample. The results also revealed that the mineralogy of the sample varies per size fraction. The concentrations of REE in other minerals were confirmed in zircon, leucoxene, titanite and almandine by means of EMPA.

The mineralogy findings showed that zircon and monazite are well liberated, with the majority of these minerals distributed in the–150+106µm and –106µm finer fractions. Approximately 50 mass% of the sample, constituting the finer fraction, has concentrated monazite and zircon. The naturally concentrated monazite and zircon in the finer size

fractions showed that the fraction does not require ore upgrading and it is amenable to direct leaching. Subsequent to the mineralogical findings, the leaching testwork was carried out on the combined –150+106µm and –106µm finer fractions in three stages: caustic cracking, water leaching and HCl leaching. The leached products and residues were investigated for their REE extraction success. The extraction findings showed a 55% extraction efficiency of rare earth elements extracted from monazite only. The mineral zircon was identified as an alternative source of REE, apart from monazite, although processing of zircon proved to be inefficient.

ACKNOWLEDGEMENTS

First and foremost, I want to thank God the almighty for the wisdom and strength bestowed upon me in order to complete my research project. I am grateful to my parents (my mother and my late father) for reminding me and my siblings that education is the key to many doors of success. Special thanks to my son, Leseli Hasandi Moila, for enduring and understanding that mommy had to work every night and every weekend. Special thanks also go to my mother, Grace Moila, for her continuous support and prayers.

My appreciation also extends to my supervisor, Prof Sehliselo Ndlovu, from Wits University (School of chemical and metallurgical engineering) and my Co-supervisor, Dr Deshenthree Chetty, (Mintek, mineralogy Division) who kept me constantly engaged in my research. I thank them for their time and for believing in me. Their support and availability whenever I needed their input did not go unnoticed.

I would also like to give recognition to the following people and institutions: -

- Mintek, for funding my studies and allocating funds and time for my project.
- The Mintek, Hydrometallurgy Division with Sam Mokoena, Vusi Makama and Thabiso Motlhamme, for their consulting services, patience and assistance in conducting hydrometallurgical test work.
- The Mintek, Mineralogy Division sample preparation team, for preparing my samples.
- The entire Mintek mineralogy team, for your encouragement and support.
- Archie Corfield for assisting with electron microprobe analyses.
- The Analytical Service Division at Mintek for conducting chemical analysis on my samples.
- My former Mintek colleagues:
    - Itumeleng Molebale and his team, for their assistance in obtaining the samples for my project.
    - Keshree Pillay, for her advice during the writing of my thesis, your time, support and guidance.
    - Themba Mothupi, for assisting with running the samples on the MLA and presenting the data.

Finally, I would like to express my sincere gratitude to all my friends, and the people who directly and indirectly contributed to my Master of Science research project.

LIST OF PUBLICATIONS AND PRESENTATIONS

Moila, A.V., Ndlovu, S. and Chetty, D. (2017) The application of process mineralogy of the rare earth elements (REE) containing tailings sample from a beach placer deposit. SAIMM, *3rd Young Professionals Conference*, Innovation Hub, 9-10 March 2017, pp. 99, Pretoria

Moila, A.V., Ndlovu, S. and Chetty, D. (2017) The application of process mineralogy of the rare earth elements (REE) containing tailings sample from a beach placer deposit, *The Southern African Institute of Mining and Metallurgy*, Vol. 177, pp. 615-621, 1 July 2017 https://issuu.com/saimm/docs/saimm-201707-jul

DEDICATION

This thesis is dedicated to my son, **Leseli Hasandi Moila**, whose time I had to sacrifice to complete this research project.

TABLE OF CONTENTS

1. CHAPTER 1 – INTRODUCTION 1

1.1. Introduction 1
1.2. Problem identification 4
1.3. Research aims 5
1.4. Research questions 6
1.5. Research structure 6
1.6. Thesis layout 7

2. CHAPTER 2 – LITERATURE REVIEW 9

2.1. Introduction 9
2.2. Mineralogy and geology of REE 10
2.2.1. Mineralogy of REE ores 10
2.2.1.1. *Placer deposits* 15
2.3. The extraction of REE 16
2.3.1. Physical and chemical beneficiation of REE 17
2.3.1.1. Gravity separation 18
2.3.1.2. Magnetic separation 18
2.3.1.3. Froth flotation 19
2.3.2. Leaching of REE 19
2.3.2.1. Sulfuric acid leach/ acid baking 20
2.3.2.2. Mechanochemical treatment prior to sulfuric acid leaching 20
2.3.2.3. Caustic soda (NaOH) cracking - leaching 20
2.3.2.4. HCl leaching 21
2.4. Process mineralogy 22

3. CHAPTER 3 – MATERIALS AND METHODS 26

3.1. Introduction 26
3.2. Sample preparation 26
3.3. Chemical analysis 30
3.4. Mineralogical characterisation of feed sample 31
3.4.1. X-Ray Diffraction analysis 31
3.4.2. AUTOSEM analysis (MLA) 31
3.4.3. Scanning Electron Microscopy analysis 32
3.4.4. Electron microprobe analysis 32
3.5. Metallurgy testwork and product characterisation 33
3.5.1. Caustic (NaOH) cracking 34
3.5.2. Water (H_2O) leaching 35
3.5.3. Selective (HCl) leaching 36
3.5.4. Characterisation of REE leaching products 37
3.5.4.1. Mineralogy of REE leach residues 37

3.5.4.2. Chemical analysis 37

4. CHAPTER 4 – CHARACTERISATION OF FEED TAILING SAMPLE 38

4.1. Introduction 38
4.2. Chemical analysis, mineralogy and mineral chemistry 38
4.2.1. Chemical analysis 39
4.2.2. Particle Size Distribution (PSD) of the tailings feed sample 40
4.2.3. Bulk Mineralogy by size of the tailing feed sample 41

4.2.3.1. Data Reconciliation 44

4.2.4. Mode of occurrence of the tailing feed sample 45

4.2.4.1. Size fraction +212µm 45

4.2.4.2. Size fraction –212+150µm 46

4.2.4.3. Size fraction –150+106µm 46

4.2.4.4. Size fraction –106 µm 47

4.2.5. Mineral Chemistry of the tailing feed sample 48
4.2.6. Characterisation of REE containing minerals 50

4.2.6.1. The REE species 50

4.2.6.2. Mineral associations of REE species 50

4.2.6.3. Liberation of REE species 51

4.2.6.4. Elemental Deportment of REE species 54

4.2.6.5. Grain size distribution of REE species 56

4.3. Summary and discussion 58

5. CHAPTER 5 – CHARACTERISATION OF LEACH FEED AND PRODUCTS 61

5.1. Introduction 61
5.2. Chemical and mineralogy data of the REE leaching results 62
5.2.1. Chemical assay of leach residues and filtrates 62

5.2.1.1. Chemical assay of leach residues 63

5.2.1.2. Chemical assay of the leachates 65

5.2.2. Mineralogical characterisation of REE leach residues 68

5.2.2.1. Mineralogy of caustic (NaOH) cracking residues 68

5.2.2.2. Mineralogy of water (H_2O) leach residues 71

5.2.2.3. Mineralogy of selective (HCl) leaching residues 73

5.2.3. Extraction Efficiency 75
5.3. Summary and discussion 75

6. CHAPTER 6 – CHARACTERISATION OF ZIRCON 77
6.1. Introduction 77
6.1.1. Alkali fusion 78
6.1.2. Lime fusion technique 78
6.1.3. Plasma decomposition technique 79
6.1.4. Thermal dissociation technique 79
6.2. Experimental procedures 79
6.2.1. Alkali fusion 79
6.2.2. Chemical analysis 80
6.2.3. Hydrometallurgy tests 80
6.2.4. Mineralogical characterisation of the zircon rich sample 82
6.2.4.1. Sample preparation 82
6.2.4.2. X-Ray Diffraction 82
6.2.4.3. Scanning Electron Microscopy analysis 82
6.3. Results 82
6.3.1. HCl leaching targets 82
6.3.2. Minerals and phase compositions 83
6.4. Summary and discussion 84
7. CHAPTER 7 – CONCLUSIONS AND RECOMMENDATIONS 86
7.1. Conclusions 86
7.1.1. Introduction 86
7.1.2. The value of mineralogy 86
7.1.3. Role of mineralogy in selection of metallurgical process 87
7.2. Recommendations and further work 90
REFERENCES 91
APPENDIX A: ELEMENTAL MAPS 99
APPENDIX B: EMPA DATA 107
APPENDIX C: MASS BALANCE 122
APPENDIX D: MASS BALANCE CALCULATIONS 128
APPENDIX E: CALCULATED ZR/SI RATIO 131
APPENDIX F: BULK MODAL MINERALOGY 132

LIST OF FIGURES

Figure 1: A demand and supply curves 2

Figure 2: Thesis layout 7

Figure 3: A periodic table indicating the rare earth elements 9

Figure 4: The major REE deposits and world distribution 12

Figure 5: An ideal flowsheet of extracting REE 17

Figure 6: An image showing the 50kg bucket of the research sample 27

Figure 7: Images showing coning and quartering of the sample 28

Figure 8: A flowsheet showing the sample preparation 29

Figure 9: The experimental approach of the three leaching stages. 33

Figure 10: Particle size distribution 40

Figure 11: Bulk mineral composition of the tailing feed sample. 42

Figure 12: Data validation 44

Figure 13: Backscattered electron (BSE) images 45

Figure 14: BSE images showing an overview (image A) 46

Figure 15: BSE images showing an overview (image A) of the –150+106 µm 47

Figure 16: An overview (image A) of the –106µm 48

Figure 17: Ideal liberation classes (adapted from Cropp, 2013). 52

Figure 18: Liberation analysis of REE containing minerals. 53

Figure 19: Deportment of REE containing minerals of the bulk sample 55

Figure 20: Monazite grain size distribution, n = number of grains measured 56

Figure 21: Xenotime grain size distribution, n = number of grains measured 57

Figure 22: Zircon grain size distribution, n = number of grains measured 57

Figure 23: BSE images of residues from caustic cracking and washing tests 69

Figure 24: BSE images of residues 71

Figure 25: BSE images of residues from HCl leaching 73

Figure 26: A photograph showing the sample mixture before alkali fusion. 80

Figure 27: The XRD spectra of the leached fused zircon. 84

Figure 28: Estimated cost analysis 89

LIST OF TABLES

Table 1: Common REE bearing minerals 11

Table 2: Selected primary and secondary REE deposit types 13

Table 3: Particle size distribution 30

Table 4: Experimental conditions for the caustic cracking test 34

Table 5: Experimental conditions for the water leaching test 35

Table 6: Experimental conditions for HCl selective leaching test 36

Table 7: Analysed Rare Earth Element concentrations, in ppm 39

Table 8: Particle size distribution (in 2D, note, underestimation compared with 3D) 41

Table 9: Bulk mineral composition of the tailing feed sample 43

Table 10: Mineral chemistry 49

Table 11: Normalised proportions of major REE containing minerals 50

Table 12: Mineral associations of REE 51

Table 13: Liberation analysis of REE containing minerals by free surface % 54

Table 14: Deportment of REE containing minerals of the bulk sample. 55

Table 15: Previous results of the bulk mineral assemblage of the sample 61

Table 16: The REE Chemical analysis of the composited sample “leach feed” 62

Table 17: Elemental composition of caustic cracking residues 63

Table 18: Elemental composition of water leach residues 64

Table 19: Elemental composition of HCl leach residues 65

Table 20: Elemental composition of caustic (NaOH) cracking filtrate 66

Table 21: Elemental composition of water leach filtrate 66

Table 22: Elemental composition of HCl selective leaching. 67

Table 23: Averaged chemical compositions from the analysed points 70

Table 24: Averaged chemical compositions from the analysed points 72

Table 25: Averaged chemical compositions from the analysed points 74

Table 26: Summary of REE extraction 75

Table 27: Experimental conditions of selective leaching test 81

Table 28: Leaching conditions of REE extraction from zircon rich sample 83

GLOSSARY

µm	Si unit for microns
Agglomeration	a mass or lumps collection of particles or grains in a sample
Alkali fusion	a chemical method used to break down strong chemical bonds using NaOH, at high temperature and at a given time
Allanite	an epidote group rare earth element mineral
Alm	Almandine
Am	Amphibole
AutoSEM	Automated Scanning Electron Microscopy
Beach placer deposits	"alluvial" deposits of a secondary origin that have a natural concentration of dense or heavy minerals deposited in streams, rivers, and beaches as a result of sediment deposition
BSE	Back Scattered Electron
Calcination	a pyrometallurgy method that involves the use of high temperature for thermal decomposition
Caustic cracking	a leaching process whereby NaOH is the solution of choice
Cracking	to chemically break down compounds/bonds
Crystal lattice	a symmetrical arrangement of atoms in a crystal
DI*water	Deionized water
EDS	Energy Dispersive Spectroscopy
EMPA	Electron microprobe analysis
Ep	epidote

Export quotas	a restriction made by government to export a particular product
Extraction	in chemistry, it is a removal of the element of interest using an acid or base solution
Extraction efficiency	the percentage of dissolved solids
Geological setting	the geological area of origin or location
Gg	Giga grams
Grain size	the size or diameter of a single crystal in a grain or particle
Grs	grossular
Gt	goethite
H_2SO_4	Sulfuric acid
HCl	Hydrochloric acid used for selective leaching
Heavy minerals	a class of minerals with a specific gravity greater than $3g/cm^3$, these minerals are normally deposited along the coastal area and river or shore
HREE	Heavy Rare Earth Elements
Hydrolysis	a chemical breakdown as a result of reacting with water
ICP-AES	Inductively Coupled Plasma - Atomic Emission Spectroscopy
ICP-OES	Inductively Coupled Plasma Optical Emission Spectroscopy
Kv	SI unit for Kilovolt
Leach residue	a solid phase product from leaching/ solid-liquid separation
Leachate	known as leach filtrate, it is the solution resulting from leaching

Lithium tetraborate	a flux for fusing different types of material (i.e oxides, ceramics, steel, silicates, carbonates, oxides and aluminosilicates
LREE	Light Rare Earth Elements
m/m	mass per mass percent
Micro Sieverts	SI units for measuring ionized radiation dosage
Mineral grain	specific minerals that make up a particle in a rock
MLA	Mineral Liberation Analyser
Mnz	Monazite
Monazite	a rare earth phosphate mineral
MREE	Medium Rare Earth Elements
nA	nano amperes
NaOH	Sodium Hydroxide base solution used for REE cracking
Oxidation states	represent the number of electrons gained or lost by an atom
Particle	a small quantity or fragment of any composition that has a grain size and chemical composition.
PLS	pregnant leach solution
ppm	parts per million
Process mineralogy	the application of mineralogy studies in order to design or optimise the metallurgical plant
QEMSCAN	Quantitative evaluation of minerals by scanning electron microscopy

Qtz	Quartz
REE	Rare Earth Elements
Rt	Rutile
SEM	Scanning Electron Microscopy
Solid solution series	elemental substitution that occurs in minerals when specific minerals share the same basic chemical formula
Tailings sample	it refers to the by-products left over from mining and extracting the resource and in this study that sample was used a feed sample.
TREE	Total Rare Earth Elements
WDS	Wavelength dispersive spectroscopy
XBSE	Extended backscattered electron
X-Ray Diffraction	a rapid method used to identify mineral abundance
XRD	X-ray diffraction
Zrn	Zircon

1. CHAPTER 1 – INTRODUCTION

1.1. Introduction

Rare earth elements (REE) belong to a group of the lanthanide series elements from the periodic table. They consist of fifteen elements of the lanthanide suite, including scandium and yttrium (Schweitzer and Pesterfield, 2010). This group of elements is very important in the world's economic growth and modern technology market. The REE are a major constituent of many advanced materials, especially in the high technology and green energy sectors.

The REE are widely and globally distributed, with China in control of approximately 95% of the world's REE market (Chen, 2011; Levkowitz and Beauchamp-Mustafaga, 2010). China has played a principal role in REE mining and production for the past two decades (Massari and Ruberti, 2013); resulting in a fluctuating trend of demand and supply of this technological resource.

In the mid-sixties the majority of the world's REE production was from the Mountain Pass deposit in California, United States of America (USA) (Rare earth elements, 2012). In the 90s, Australia's Mount Weld was the second largest producer of REE, while Mountain Pass remained as the largest producer (Kogel *et al*., 2006; British Geological Survey, 2011).

In 2003, the Mountain Pass rare earth mine ceased its mining operation as a result of environmental impacts and lower prices of REE (U.S. Geological Survey, 2004). This change influenced the rest of the United States of America (USA) REE life chain. Later, the REE application in the U.S. significantly declined by 29% from 8 Kilotonne (**Kt**) in 2003 to 5.7 Kt and 5.2 Kt in 2004 and 2005, respectively. From 1995 to 2007, there was a significant change in the REE market (Alam, 2012) due to the decline in U.S.A. REE, leading to a global increase in REE demand (Du and Graedel, 2011).

A decade later China emerged as the leading economical producer of REE worldwide; other countries became completely dependent upon its exports (British Geological survey, 2011). This subsequently led to the closure of Australian and U.S.A REE mines as they could not compete with the lower production costs of REE in China (Charalampides and Vatalis, 2015).

Most REE in the world are mined in China in Bayan Obo mine, which is a carbonatite deposit in Mongolia. The global REE production is therefore highly monopolised by China (Wübbeke, 2013).

China has the largest world's population, and with most of the countries completely dependent on its REE resource, China was placed in a difficult state of meeting both its own local and international export demand (Morrison and Tang, 2012). China then decided to implement new export regulations to limit its REE exports (Binnemans *et al.*, 2013). This involved prohibiting the REE sales and the establishment of export quotas in order to meet its own REE needs (Seaman, 2010). However, the new changes impacted the rest of the world's demand and supply, creating a supply chain gap that later led to a high demand for this technological resource, as shown in **Figure 1**.

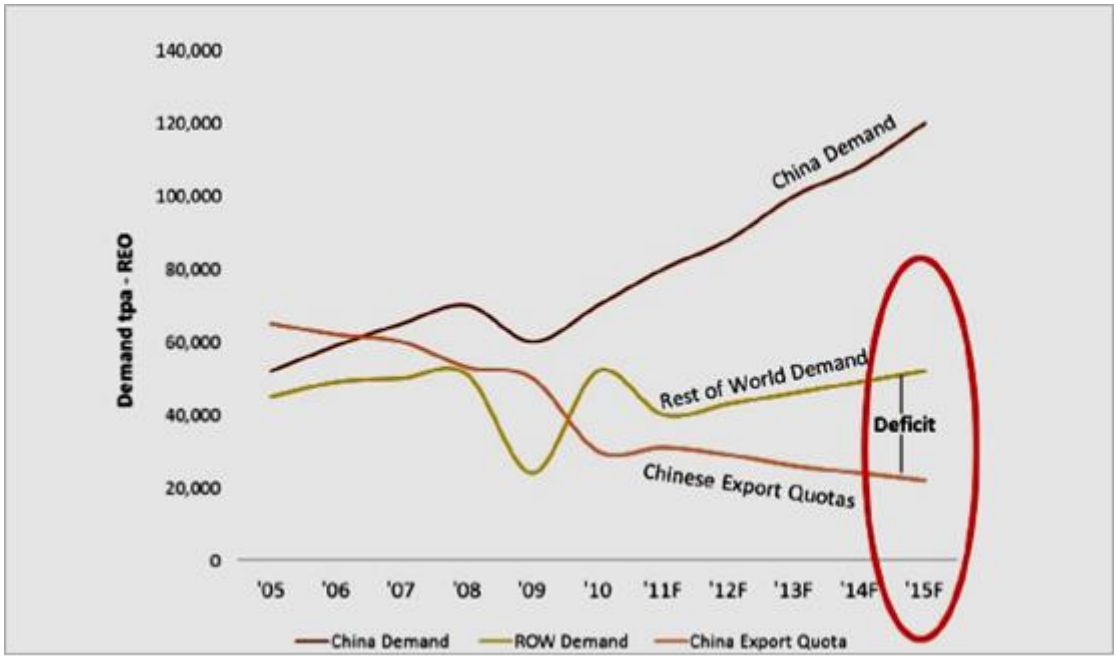


Figure 1: A demand and supply curves, showing 'an' increase in the deficit gap created by the decline in REE export; sourced from (IAMGOLD, 2012).

Due to the changes in the REE mining and production industry as a result of China's attempt to sustain its supply; other countries outside China were compelled to explore other means of closing the REE supply gap created by China. After the closure of Mountain Pass mine in 2003, the United States of America only processed REE concentrates from ores mined before the mine was closed (U.S. Geological Survey, 2004; British Geological survey, 2011). However, the rapid increases in global REE demand led to a rebirth in exploration of other

REE sources, with the US Molycorp renewing the mining permit for Mountain Pass in 2004 (Jacoby and Jiang, 2010) and Mount Weld in Australia renewed by Lynas.

Recently, Mountain Pass and the Australian Mount Weld mine increased the REE production, with other countries such as South Africa and Asian countries such as India, Kazakhstan and Vietnam working towards the REE production stages. These new sources were able to cut China's share of global supply to 86% from over 93% between 2011 and 2012 (Tse, 2011).

In order to fill the demand gap created by China, Japan made plans to extend the search for highly concentrated REE in the deep-sea mud of the Pacific Ocean (Gordon, 2011). Japan also made plans to recycle old batteries and electronics for their REE content and to develop alternative supplies of REE originating from Mongolia (Tabuchi, 2010). India planned to resuscitate its REE production from Indian Rare Earths Limited (IREL), which had been stopped in 2004. Other plans to enhance the development of REE supply in India and Vietnam were also made by Toyota Motor Corporation, for 2011 and 2013 (Jacoby and Jiang, 2010; Montgomery, 2011). According to Jacoby and Jiang (2010), Molycorp announced that it had acquired one of the greatest world's leading Rare earth processing company-Neo Material Technologies Inc. (Neo).

As a result of the changes in REE exports and subsequent developments, this study aims to assist in identifying an additional REE resource as well as the development or optimisation of an efficient ore processing route for REE in South Africa. The Chinese, Americans and Australians have developed technologies to process REE from various geological provenances, whereas South Africa has developed extraction technologies for REE originating from hydrothermal and carbonatite deposits.

The beach placer deposits in South Africa have been explored and beneficiated for their heavy minerals (i.e. ilmenite, magnetite, rutile, leucoxene, garnets, zircon cassiterite, monazite etc.). However, very little work has been conducted to assess beach placer deposits, in terms of REE extraction from monazite and other heavy minerals such as garnets, zircon and leucoxene. The heavy minerals from placer deposits have a potential of REE concentration in their solid solution series, as a result of ore genesis.

This study involves the use of process mineralogy for the development of an extraction route for REE from an existing beach placer deposit, currently mined for titanium and iron as a by-product, with the aim to explore sources of REE other than monazite.

The scope of the work entails mineralogical and hydrometallurgical investigation of the REE ore from a beach placer sand deposit, whereby minerals such as monazite, leucoxene, zircon and apatite etc. are thoroughly investigated for their REE content. This project also aims to reduce the compounding costs that come with processing of REE, by introducing mineralogical characterisation in the early stages of ore processing.

1.2. Problem identification

China's ceasing of their supply quotas in REE led to a drastic global demand for REE and paved ways of exploring other sources of REE production Research studies have been conducted globally on REE from carbonatite deposits and placer deposits. China and the USA contain the largest percentage of the world's rare earth reserves originating from the carbonatite deposits; whereas placer deposits in Australia, Brazil, China, India, Malaysia, South Africa, Sri Lanka, Thailand and the U.S.A. account for the second largest part in the world REE distribution (Haxel *et al*., 2002).

However, it should be noted that not much research has been conducted on the REE originating from placer deposits in the African continent, particularly Southern Africa. Most heavy mineral deposits or placer deposits are mined for titanium-bearing minerals and zircon, with products such as monazite and leucoxene often considered as tailings material in these operations. Leucoxene is an alteration product of titanium minerals and has the potential of carrying REE in its crystal structure or lattice. There is nothing published or literature review in the open on investigating leucoxene and other heavy minerals for their REE content. Heavy minerals such as zircon, leucoxene, titanite, garnet and epidotes also have a potential of carrying REE concentration.

The proposed study will therefore address leucoxene, garnets and zircon as a potential and additional REE resource in placer deposits.

Titanium mining companies have abandoned monazite and other REE-bearing minerals due to environmental issues associated with their radioactive nature (thorium content).

The environmental hazards associated with monazite and the difficulty in obtaining a nuclear license to treat monazite could be a possible reason why most titanium mining companies do not mine monazite as a by-product. The Eneabba placer deposit in Australia is an example of a placer deposit that mined titanium as a primary product and monazite as a by-product. However, this is not the case with African deposits including Southern Africa.

Often times, during ore processing or minerals extraction, mineralogy is used as a problem-solving tool. The behaviour of the ore affects the processing route; hence mineralogy is a vital component or factor in determining the ease or difficulty of processing and extracting REE beforehand, which can be looked at as a cost cutting measure. Mineralogy should therefore, be used at the beginning of a project as a decision-making tool for the processing and extraction routes to pursue in relation to ore processing. This would eliminate numerous issues that metallurgists or engineers encounter prior to mineral extraction of this high technological resource, since its extraction is very complex and costly.

To address the identified problem, the scope involves a detailed mineralogy investigation to give guidance on the hydrometallurgy to be conducted in extracting the REE. In addition, the process mineralogy and extraction of REE from placer deposit leucoxene, zircon and monazite studies will aid in achieving the main objective of this research study.

1.3. Research aims

The main aim of this research is to evaluate the development of an efficient processing route for the extraction of rare earth elements from alternative sources (i.e. other heavy minerals). This study will focus on the following: -

- The characterisation of REE containing minerals from an existing heavy mineral beach placer deposit currently being mined for titanium and iron, in order to explore an additional and potential REE resource. This additional and potential REE resource refers to other minerals that contain REE and the possibility of extracting REE from those minerals.

  This will involve the study of monazite and other heavy minerals from a beach placer deposit for their REE content. The identified heavy minerals will be investigated further for their mineral chemistry in order to locate the proportions of REE within

their crystal lattice. Monazite will be examined and other minerals such as leucoxene, zircon and garnet will be investigated as an additional REE resource from an existing placer or beach sand operation, currently mining ilmenite and rutile for titanium production. Monazite, garnet, zircon and leucoxene mainly report to the tailings and can be investigated as a by-product from this existing titanium production operation, as a means of maximising the potential of the resource. A tailings sample from a Ti operation will be investigated.

- Evaluating if conducting mineralogical characterisation prior to processing route selection, can serve as an economical decision-making tool.

  The processing route of REE will be drawn from mineralogical findings, and these findings will aid in assessing the possibility of ore upgrading or direct ore leaching.

1.4. Research questions

- What are the different REE-bearing species found in this placer deposit?
- Apart from monazite, are there REE present in other heavy minerals from the beach placer deposit?
- What is the best possible approach of extracting REE from REE containing minerals and heavy minerals (i.e. alkaline route or acidic route)?
- Can the different REE species be treated simultaneously or separately, and what will be the advantages and constraints of treating REE in each of these ways? Will the use of mineralogical techniques prior to processing provide an effective decision-making tool to act as cost-effective means of REE extraction?

1.5. Research structure

The research will include the following:

- Literature review
- Acquiring samples for the study
- Sample preparation for the entire study
- Mineralogical analysis
- Metallurgical testwork
- Reporting findings

1.6. Thesis layout

The thesis layout comprises seven chapters, as shown in **Figure** 2.

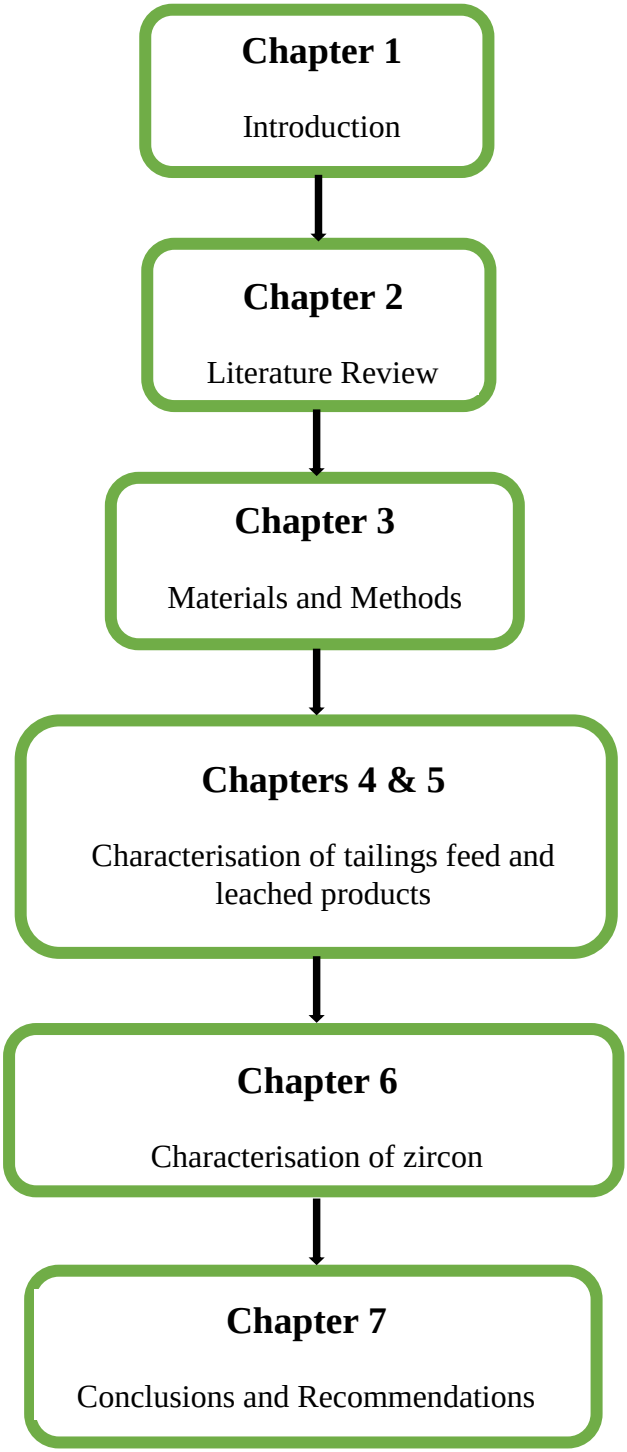


Figure 2: Thesis layout

Chapter 1 introduces the scope of the project, the history of REE global supply and demand, the problem identification and the main objectives.

Chapter 2 contains a comprehensive literature review, which begins with the background of REE and the importance of REE globally, as well as the geology and mineralogy of REE, different deposit types and REE global distribution. This is followed by a review of both physical and chemical methods used to extract REE. The literature review also emphasises the importance of integrated mineralogical techniques as a decision-making tool in the mineral processing approach for this study.

Chapter 3 details the methodological approaches used to answer the research questions and meet the research objectives.

Chapters 4 and **5** present the results and discussion of the tailings "feed" sample, leach feed and leach products of the study i.e. mineralogical characterisation and extraction results.

Chapter 6 provides additional work on the zircon characterisation and the extraction of REE from zircon.

Chapter 7 concludes the main findings of the study and provides recommendations for further work.

2. CHAPTER 2 – LITERATURE REVIEW

2.1. Introduction

Rare earth elements (REE) refer to a group of seventeen periodic table elements, in which fifteen of these elements are a series of lanthanides, as well as yttrium and scandium (Long *et al*., 2010; Kul *et al*., 2007; Kumari *et al*., 2015; Gupta 2003). Lanthanides are elements from atomic numbers 57 to 71 (Schweitzer and Pesterfield, 2010).

The elements, which are lanthanum, cerium, praseodymium, neodymium, promethium, samarium, europium, gadolinium, terbium, dysprosium, holmium, erbium, thulium, ytterbium and lutetium form part of the lanthanides (Massari and Ruberti, 2013; Naumov, 2008). However, scandium and yttrium also exhibit similar physical and chemical properties (i.e. the oxidation states and valence electron orbital configuration) as lanthanides, and are often grouped with them (**Figure 3**).

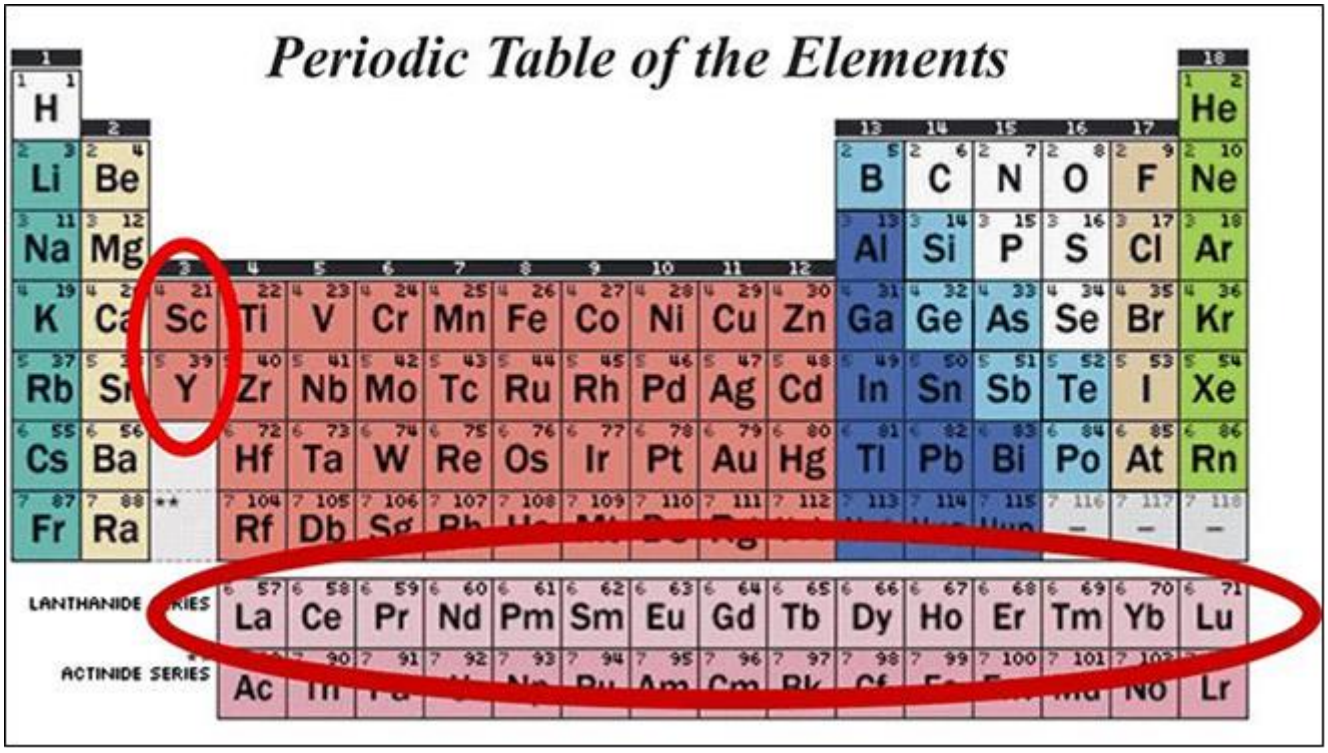


Figure 3: A periodic table indicating the rare earth elements; (including scandium and yttrium) circled. Image from tnahistoryoftechnology.com.

The valence electron configurations are characterised by $6s^25d^14f^{n-1}$ or $6s^24f^n$. The elements cerium to lutetium have the series known as the "inner transition" elements or "f" elements and the 5d and 4f electrons sublevel exhibit similar rare earth atoms energies (Spedding, 1975; Gupta and Krishnamurthy, 2005). The REE are generally grouped into two types – the heavy rare earth elements (HREE) and light rare earth elements (LREE) (British Geological survey, 2011). The LREE are from lanthanum through to europium while the HREE are from gadolinium through to lutetium, including yttrium. Scandium does not belong to either of the two REE types - LREE or HREE (Gupta and Krishnamurthy, 1992). Cerium is the most abundant REE while promethium is the rarest REE. (Koltun and Tharumarajah, 2014; Tyler, 2004). These REE are not rare in nature; they occur in low concentration across the world, with cerium, lanthanum, neodymium and yttrium being the most common REE

The REE are vital to the world's growing market and economy, with their demand and production vastly increasing (IAMGOLD, 2012). The rare earth elements are naturally flexible, soft and react at high temperatures; hence their extensive use in modern technology. Rare earth elements are a major constituent of many advanced materials, especially in modern high technology, for green energy sectors (LED), permanent magnets, rechargeable batteries, catalysts, glass additives, phosphors, hybrid cars, turbines and many more electronic gadgets (Habib and Wenzel, 2014; Long *et al*., 2010; Szumigala and Werdon, 2010; Goonan, 2011). Because of various REE properties such as high electrical conductivity, high metallic lustre and oxidation state ($^{3+}$), these elements have generated a great interest in the mining sector (Helmenstine, 2017).

2.2. Mineralogy and geology of REE

The REE are found in almost all mineral groups (silicates, oxides, carbonates, hydroxides, fluorides and phosphates) and they also occur in different types of deposits.

2.2.1. Mineralogy of REE ores

The REE do not occur as pure elements; they are found in a variety of minerals (**Table** 1). There are over 250 REE-bearing minerals discovered to date, from different types of deposits (Gupta and Krishnamurthy, 2005; Jordens *et al*., 2013).

Table 1: Common REE bearing minerals (adapted from Orris and Grauch, 2002; Castor and Hedrick, 2006)

Mineral name	Ideal chemical formula
Aeschynite- (Ce)	$(Ce,Ca,Fe)(Ti,Nb)_2(O,OH)_6$
Allanite-(Ce)	$(Ce,Y,Ca)_2(Al,Fe^{3+})_2(SiO_4)_3(OH)$
Apatite	$(Ca,Ce)_5(PO_4)_3(OH,F,Cl)$
Bastnaesite	$(Ce,La,Y)CO_3F$
Brannerite	$(U,Ca,Y,Ce)(Ti,Fe)_2O_6$
Britholite-(Ce)	$(Ce,Ca)_5(SiO_4,PO_4)_3(OH,F)$
Eudialyte	$Na_4(Ca,Ce)_2(Fe^{2+},Mn^{2+},Y)ZrSi_8O_{22}(OH,Cl)_2$
Euxenite-(Y)	$(Y,Ce,Ca)(Nb,Ta,Ti)_2(O,OH)_6$
Fergusonite- (Ce)	$(Ce,La,Nd)NbO_4$
Gadolinite- Ce)	$(Ce,La,Nd,Y)2Fe^{2+}Be_2Si_2O_{10}$
Kainosite- (Y)	$(Ca_2(Y,Ce)_2Si_4O_{12}CO_3.H_2O$
Loparite	$(Ce,La,Na,Ca,Sr)(Ti,Nb)O_3$
Monazite-(Ce)	$(Ce,La,Nd,Th)PO_4$
Parisite (Ce)	$Ca(Ce,La)_2(CO_3)_3F_2$
Huanghoite-(Ce)	$BaCe(CO_3)_2F$
Xenotime	YPO_4
Synchysite-(Ce)	$Ca(Ce,Y)(CO_3)_2F$
Florencite-(Ce)	$CeAl_3(PO_4)_2(OH)_6$
Yttrocerite	$(Ca,Ce,Y,La)F_3.nH_2O$
Cebaite-(Ce)	$Ba_3Ce_2(CO_3)_5F_2$
Samarskite-(Y)	$(Y,Ce,U,Fe^{3+})_3(Nb,Ta,Ti)_5O_{16}$

There are generally three mineral species mainly mined for REE. These are bastnaesite; a LREE fluorocarbonate, monazite; a LREE or HREE phosphate and xenotime; a HREE yttrium phosphate (Rabie *et al*., 2013). Most production of REE comes from less than 10 minerals; hence the extraction of REE resources is strongly dependent on the REE mineralogy.

Rare earth elements occur in a variety of geological deposits and environments. The REE minerals normally occur in igneous and metamorphic rocks as well as sedimentary placer deposits (Sappin and Beaudoin, 2015). Gupta and Krishnamurthy (2005) published comprehensive information on REE deposits and their occurrences, with over 200 minerals of REE discovered. The concentration and distribution of these REE mineral deposits are influenced by rock-forming and hydrothermal processes.

The REE mineral deposits are categorised into primary and secondary deposits. The primary carbonatite deposits are associated with igneous and hydrothermal processes, whereas the secondary deposits are linked with sedimentary processes and weathering (Sappin and Beaudoin, 2015). Furthermore, these deposits are further classified according to ore genesis, mineralogy and occurrence. The global distribution of REE resources is presented in

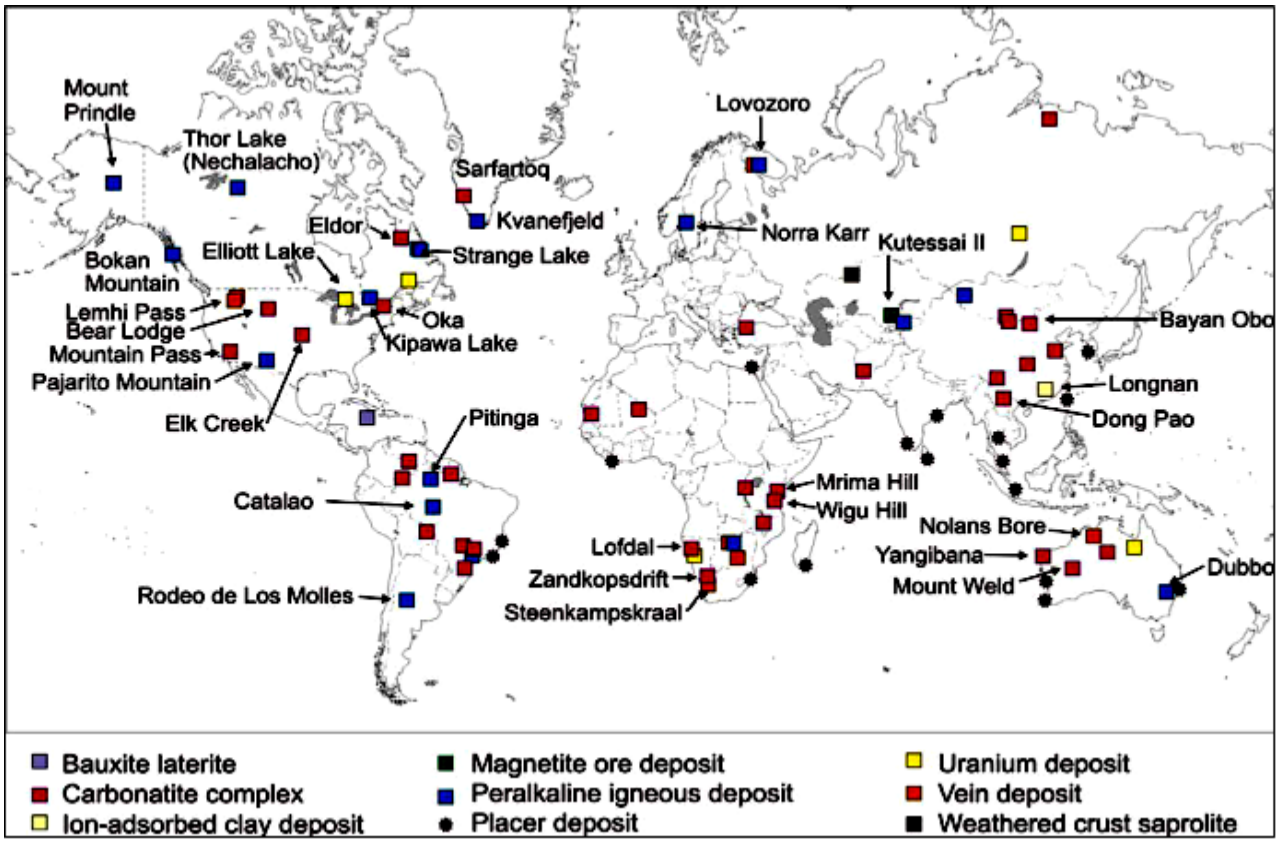


Figure 4.

Figure 4: The major REE deposits and world distribution (modified Szumigala and Werdon, 2010).

The most economic and commercial REE deposits are associated with bastnaesite and monazite minerals, from igneous rocks and carbonatites deposits (Rabie *et al*., 2013). **Table 2** shows the general primary and secondary REE bearing mineral geological settings.

Table 2: Selected primary and secondary REE deposit types and their geological settings (adapted from Orris and Grauch, 2002; Grauch and Mariano, 2008).

Deposit type	Deposit name and Country of origin
REE deposits of primary origin	
REE associated carbonatites	• Bayan Obo in China • Mountain Pass in California, USA • Iron Hill in USA • Ambar Dongar in India • Barra do Itapirapua in Brazil • Iron Hill, USA
REE associated with alkaline igneous rocks	• Ilimaussaq, Greenland • Khibina and Lovozerite, Russia • Thor Lake and Strange Lake, Canada; • Weishan, China; • Brockman, Australia; • Pajarito Mountain, USA
Hydrothermal deposits	• Karonge in Burundi • Naboomspruit, Zandkopsdrift and Steenkampskraal in South Africa • Lemhi Pass, Snowbird and Bear Lodge, USA • Hoidas Lake, Canada
REE deposits of secondary origin	
Beach placer deposit- naturally transported sediments along rivers and coastlines	• Eneabba in Western Australia • Richards bay minerals in South Africa • Chavara, India • Green Cove Springs, USA
Alluvial deposits –heavy minerals	• Perak in Malaysia • Chavara, India • The Carola monazite belt in USA • Guangdong in China
Paleo placer deposits - ancient formed placer deposits	• Elliot Lake in Canada • Bald Mountain in the USA
Chemical weathering formed REE Lateritic deposits	• Mount Weld in Australia • Kangankunde deposit, Malawi
Residual Ion-adsorption clays	• Longnan and Xunwu deposit, China

Carbonatites are the dominant sources of rare earth elements, with major REE-producing deposits mainly of carbonatite origin (Jackson and Christiansen, 1993). The carbonatites are igneous rocks; they are of deeply magmatic origin, rich in carbon dioxide and low in silica that intruded the earth's crust and solidified (Gupta and Krishnamurthy, 2005). The REE mineralization of carbonatites includes mainly LREE minerals such as bastnaesite, synchysite allanite and monazite.

Pegmatite deposits are a hard rock source of REE that begin as granitic magmas formed by re-melting of crustal material (Jackson and Christiansen, 1993). Monazite and allanite are associated with pegmatite deposits, and these deposits tend to have HREE enriched within these minerals.

Primary deposits include hydrothermal deposits, which are unrelated to alkaline igneous rocks, with hydrothermal deposits enriched with HREE minerals such as xenotime (Orris and Grauch, 2002).

Lateritic deposits are a result of chemical weathering (Kanazawa and Kaminati, 2006; Robb, 2005). These are also of economic importance and are formed by the weathering of REE-rich alkaline complexes. Apatite, pyrochlore and monazite are typical residual minerals, and crandallite group minerals are typical secondary minerals formed during weathering (Jackson and Christiansen, 1993).

The ion adsorption clay deposits (e.g. China Longnan REE deposit in China) are weathering alteration products of REE-enriched clay (Grauch and Mariano, 2008).

Placer deposits are concentrations of heavy mineral beach sands and are naturally transported and deposited with sands and gravel by rivers or coastal process (Orris and Grauch, 2002). The most vital REE-bearing minerals in this type of deposit are monazite, sometimes with minimal amounts of xenotime.

2.2.1.1. *Placer deposits*

This project involves mineralogical characterisation and extraction of REE from material and products originating from a beach placer deposit. Placer deposits, also referred to as "alluvial" deposits; are of a secondary origin and have a natural concentration of dense or heavy minerals deposited in streams, rivers and beaches as a result of sediment deposition (Robb, 2005). These heavy minerals also have high specific gravity, and such properties make the minerals chemically resistant to weathering and therefore, durable (van Gosen *et al*., 2010).

The literature on the geology of placer deposits is vast; there has been discussions published by a number of authors: Orris and Grauch, 2002; Castor and Hedrick, 2006; Kanazawa and Kamitani, 2006; Gupta and Krishnamurthy, 1992; Gupta and Krishnamurthy, 2005. Most commercial REE deposits are associated with carbonatite and placer deposits, with placer deposits found in beach sands or along the coast. They are formed by concentration of heavy minerals such as titanium containing minerals with zircon, leucoxene, apatite, xenotime and monazite (Shepherd, 1990; Tyler and Minnitt, 2004) as by-products.

The REE placer deposits are found across the world. In the 1980s, Australia was the third main producer of REE after the Mountain Pass and Bayan Obo deposits. Australia produced about 2500 tonnes of monazite annually from its Eneabba West Coast placer deposit, north of Perth (Castor and Hedrick, 2006). There are several countries that have explored monazite as a by-product and these include Brazil, India, Malaysia, Thailand, China, Taiwan, New Zealand, Sri Lanka, Indonesia, Democratic Republic of Congo, Korea and the United States of America (Sengupta and van Gosen., 2016; U.S. Geological Survey, 2011).

Other examples are:

- Heavy mineral sand - high dune from North Stradbroke Island, an Australian island in the state of Queensland (Hoatson *et al*., 2011).
- Heavy-mineral sand from Murray Basin in Australia.
- Monazite sand from Orissa beach placer in eastern India (Rao and Misra, 2009).
- Heavy mineral sand rich in monazite from a deposit in Southern India.
- The Carolina Piedmont with Monazite alluvial deposit.

2.3. The extraction of REE

Diverse techniques have been applied by different workers to treat REE ores, and these extraction techniques have been used in different operations to process rare earth elements. There are various well-known processes for decomposing the REE-bearing minerals, and in order to select an appropriate beneficiation and leaching method, the mineralogy of the ore has to be carefully considered.

Bastnaesite; a fluorocarbonate mineral and monazite; a phosphate mineral (Peelman *et al*., 2014), are two well-known major commercial REE ore minerals from which predominantly REE can be extracted with relative ease. **Figure 5** below shows an ideal flowsheet of REE extraction from bastnaesite and monazite.

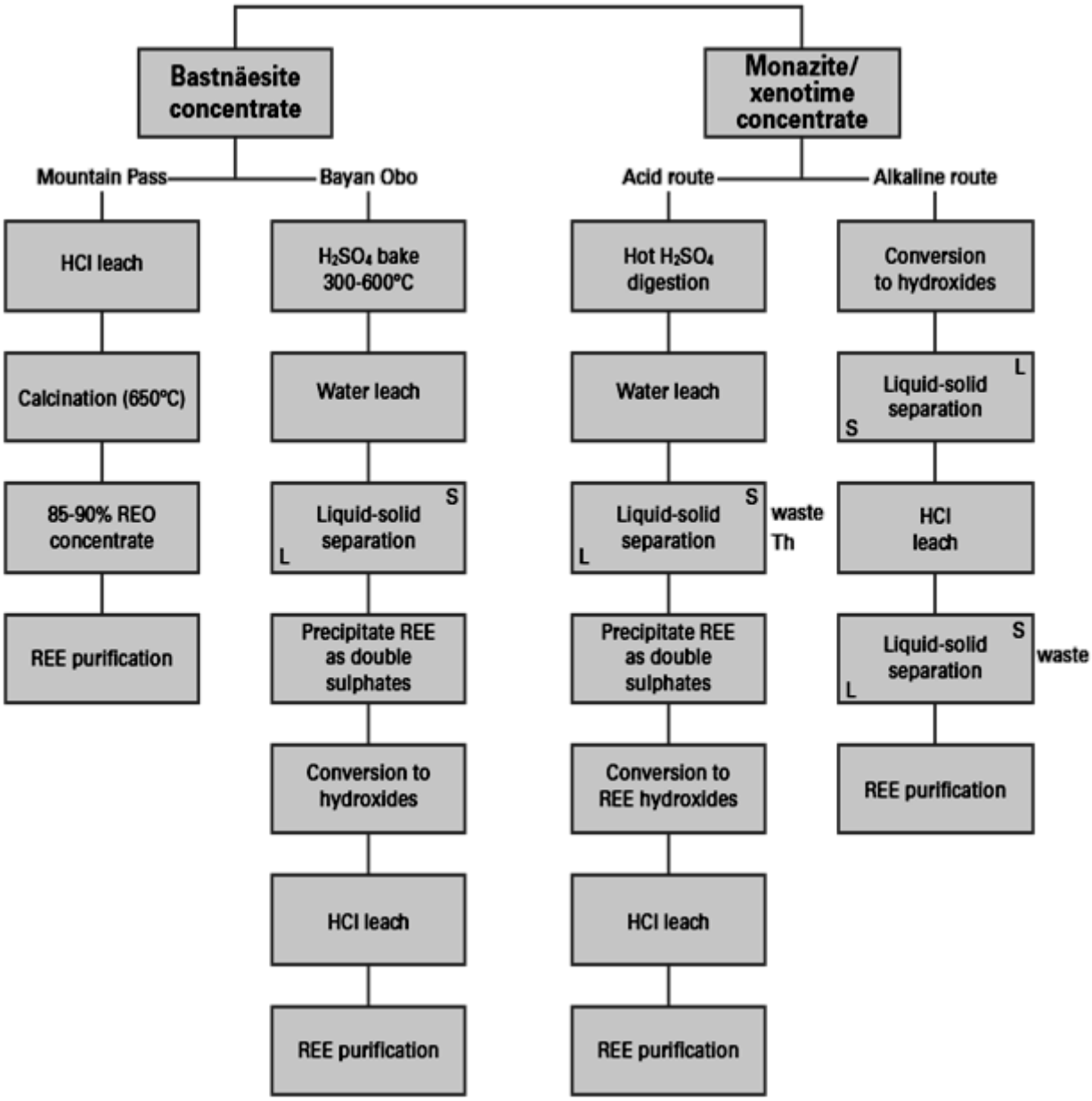


Figure 5: An ideal flowsheet of extracting REE from bastnaesite (carbonatite origin REE) and monazite (placer deposit origin REE), adapted from Chegwidden and Kingsnorth (2002).

2.3.1. Physical and chemical beneficiation of REE

Ore beneficiation involves upgrading the ore by physical or chemical techniques. This is achievable by applying various methods such as crushing, screening, sorting, milling, washing, filtration, gravity and magnetic separation, flotation and agglomeration (Wills, 2006). In terms of ore beneficiation, the selection of the most suitable method for upgrading the ore depends on the ore characteristics. These characteristics are obtained by conducting

mineralogical characterisation of the ore. This shows that mineralogy is an important factor to be considered before embarking on any metallurgical campaign.

The ore can either be beneficiated chemically, physically, or undergo thermochemical beneficiation. Below are some of the well-known beneficiation methods.

2.3.1.1. Gravity separation

Rare earth minerals from beach placer deposits are known to have dense specific gravities ranging from 4 to 7, which makes REE minerals good candidates for gravity separation (Ferron *et al*., 1991). Gravity separation can be unfavourable on ore where gangue minerals have specific gravities similar to the desired rare earth minerals, e.g. barite in Bayan Obo (Guy, 2000).

Gravity separation is less costly to utilise on beach sand, owing to a wide range in specific gravity. It is commonly used in REE beneficiation, mainly for monazite ore. The REE operations in China use both froth flotation and gravity separation (shaking tables, spiral concentrators and conical separators) for ore beneficiation (Chi *et al*., 2001).

2.3.1.2. Magnetic separation

Magnetic separation is a method that separates minerals based on their natural magnetic susceptibility; this stage is also an efficient separation stage in REE beneficiation. This separation stage is used to reject magnetic gangue from non-magnetic REE minerals, or to produce a concentrate of monazite or xenotime since REE have electrons with magnetic components (Gupta and Krishnamurthy, 1992).

Monazites from placer deposits respond well to magnetic separation and gravity separation. These two separation methods are also used to separate paramagnetic monazite from non-magnetic heavy mineral gangue material such as zircon and rutile (Zhang and Edwards, 2012). However, an effective beneficiation of monazite from beach sands involves gravity separation combined with magnetic separation to disregard magnetic susceptible minerals such as magnetite (Jordens *et al*., 2013; Ferron *et al*, 1991). In China, magnetic separators are used to remove Fe-containing gangue prior to REE separation by flotation (Chi *et al*., 2001; Zhang and Edwards, 2012).

2.3.1.3. Froth flotation

Froth flotation is a mineral separation process that is used to produce concentrates of an ore. This process takes place in a water-mineral suspension and separates minerals based on their hydrophobicity properties. Froth flotation can also be used to separate different REE minerals; and this is dependent on the mineral type and geological provenance of REE-containing minerals.

The flotation of monazite from beach sands or placer deposits involves the use of fatty acids or phosphoric acid esters as collectors (Pavez and Peres, 1993; Dixit and Biswas, 2008; Pavez and Peres, 1994). The flotation process of monazite and bastnaesite is different owing to the mineralogical differences of the ore deposits. The gangue minerals in a monazite concentrate from beach placer deposits includes numerous heavy minerals (i.e. ilmenite, zircon, leucoxene, pseudobrookite, rutile, magnetite, quartz, and epidote), which might require high consumption of reagents, in contrast to gangue associated with bastnaesite (from carbonatite deposits), (Pavez and Peres, 1994).

Upgrading of bastnaesite is achieved by using both physical separation and flotation methods; the gravity and magnetic separation stages are conducted prior to flotation (Chi *et al*., 2001). A combination of physical separation and flotation methods can aid in the upgrading of concentrate production. To date, there is very little research available on the investigation of other heavy minerals such as zircon, garnet and leucoxene for their REE concentration extraction potential.

2.3.2. Leaching of REE

The leaching of rare earth elements involves two processing routes namely: - the acid route and the alkaline route (see **Figure 5**). The leaching of REE is carried out on upgraded material in the form of a concentrate. The concentrates or products are then directly treated by either acidic or alkaline reagents depending on their mineralogy. In other instances, the concentrate first undergoes thermal treatment prior to leaching (Fatherly *et al*., 2008).

In terms of REE leaching, there are already established processes available, i.e. the conventional processes, which involve sulfuric acid agitation leaching, known as sulfation roasting or baking; leaching after pyrometallurgical methods such as calcination and

dissolution of ion phosphate from REE phosphate minerals using NaOH cracking and bisulfate fusion procedure.

2.3.2.1. Sulfuric acid leach/ acid baking

Acid baking or sulfuric acid leaching of REE is a cheaper method of REE extraction, compared to caustic cracking (Chin and Wang, 1996). This method is basically an acid digestion method (Verbaan *et al*., 2015), in which the monazite or any REE are converted into REE (SO_4), when SO_4^{2-}ion of H_2SO_4 acts as a ligand that reacts at a high temperature (Fernelius, 1946). This is shown in the chemical reaction below:

$$2REE(PO)_{4(solid)} + 3H_2SO_{4(aq)} \rightarrow REE_2(SO_4)_{3(solid)} + 6H^+_{(aq)} + 2PO^{3-}_{4(aq)} \quad 2.1$$

This leaching process is known as the acid baking method, and is well-known for both beach placer deposits and carbonatite deposit REE extraction. The leaching process takes place at a high temperature environment of 200 to 400 °C over several hours (Fernelius, 1946). The leached product undergoes washing stages for sulfate removal, which is later followed by precipitation (Verbaan *et al*., 2015; Welt *et al*., 1958).

2.3.2.2. Mechanochemical treatment prior to sulfuric acid leaching

Sulfuric acid leaching after mechanochemical treatment is a successful and popular method for treating monazite from placer beach deposits from Malaysia (Kim *et al*., 2009; Zhang and Lincoln, 1994). This process involves mechanochemical treatment of monazite with caustic soda at room temperature (Zhang and Lincoln, 1994). After the formation of REE hydroxides and sodium phosphate, the phosphate components are subsequently removed by washing, and the washed products are later leached by sulfuric acid.

2.3.2.3. Caustic soda (NaOH) cracking - leaching

Caustic decomposition can also be applied to specific ores. The most common process is decomposition through applying sodium hydroxide to phosphate REE minerals (Kim and Osseo-Asare, 2012; Krumholtz, 1957). Meerson (1957) and Habashi, (1997) also reported the use of sodium hydroxide to crack the phosphate ion of monazite using a combination of high temperature and high pressure. During this process, the ore is mixed with 50 to 70 wt.% NaOH and decomposed at temperatures from 140 to 170 °C for 2 to 4 hours (Sulaiman, 1991).

Rare earth elements are transformed into REE hydroxides, while phosphates (from monazite) form trisodium phosphate (Barbosa *et al.*, 2001; Gupta and Krishnamurthy, 2005) or carbonates and fluorides (from bastnaesite). These are transformed into soluble sodium salts that can be washed off with warm to hot temperature water. The chemical reaction below shows the reaction of REE phosphate with NaOH:

$$REE(PO)_{4(solid)} + 3NaOH_{(aq)} \rightarrow REE(OH_3) + 3Na + PO^{3-}_{4(aq)} \qquad 2.2$$

The resulting solids undergo selective leaching with diluted HCl. Often, caustic decomposition results in lots pure products. However, if the ore contains several different minerals, a process capable of decomposing all of them has to be defined (Chin and Wang, 1996). Once REE are solubilised, they have to be separated from co-leached elements. After removal of impurities e.g. by pH dependent precipitation, REE are typically precipitated as oxalates or carbonates, from which REE-oxides can be obtained by calcination.

2.3.2.4. HCl leaching

Decomposition in HCl is commonly applied to carbonate minerals like bastnaesite, parisite, synchysite or similar minerals, but it can also be used to decompose allanite, cerite or gadolinite. The ore is stirred in concentrated HCl at temperatures > 90 °C. If the ore contains fluorine (e.g. bastnaesite), some of the REE forms insoluble REE-fluorides that remain in the solid residue. To recover those REE, the solid residue has to undergo an additional decomposition with sodium hydroxide, to convert the fluorides into hydroxides and soluble sodium fluoride (Kumari *et al.*, 2015). The rare earth hydroxide can then be dissolved in HCL solution as shown by the following chemical reaction:

$$REE(OH)_3 + 3HCl \rightarrow REECl_3 + 3H_2O \qquad 2.3$$

Fluorides are washed away and REE hydroxides are dissolved by excess HCl in the leaching liquor from the HCl decomposition step. In the presence of carbonates, the above reaction (**2.3**) conditions will dissolve unwanted carbonate phases without attacking bastnaesite, resulting in reagent consumption.

2.4. Process mineralogy

Process mineralogy is a practical application of mineralogical methods and understanding to aid in mineral exploration, and to predict and optimise how an ore can best be mined and processed (Cropp, 2013). Process mineralogy contributes greatly in all stages of exploration, metallurgical testwork, pilot plant designing and throughout the production stage (van Rahden, 1979). Over the years, more mining operations have increasingly used mineralogy to characterise complex ore, in treatment of waste dump material, upgrading of tailings, in geometallurgical modelling and plant optimisation as well as process prediction and design. Process mineralogy is also applied to reduce operational costs and other financial or environmental risks.

The application of process mineralogy is considered to predict potential ore grades and recoveries, and the metallurgical difficulties that may arise subsequent to the commencement of a mining process or commissioning of a pilot plant (Lotter *et al*., 2011).

Information on the ore minerals and rock information such as gangue mineralogy of the ore, mineral of interest, elemental deportment, particle size distribution, particle shape, liberation analysis, free surface area and mineral associations can be obtained from process mineralogy studies. Process mineralogy is most likely to address some of the fundamental metallurgical questions listed below: -

- What is the mineralogical makeup of the sample?
- What are the main species in the sample?
- What is the grain size distribution of the target minerals?
- What is the degree of liberation for the target mineral?
- What are the main gangue minerals in the samples?
- Is it possible to upgrade the product?
- Are there any penalties elements in the concentrate?

Process mineralogy is also essential in mineral processing stages such as extraction and beneficiation of ore; both stages require a multi-disciplinary approach. The multi-disciplinary approach involves closely integrated mineralogy in order to provide a meaningful representation of the economic potential of an ore deposit or pilot plant (van Rahden, 1979). Process mineralogy is also beneficial in both pyrometallurgy and hydrometallurgy operations. Hydrometallurgical processes involve leaching of ores, and in order to produce a leach concentrate of the mineral or element of interest, the mineralogy of the ore must be highly considered. It is vital to carry out detailed mineralogical studies since mineral liberation plays a key role in ore leaching. Meloy *et al.*, (1990) have made relevant contributions in the area of process mineralogy.

As Cropp *et al.*, (2013) confirmed, the understanding of gangue types and their textural intergrowth with ore minerals is important in developing metallurgical flowsheets (i.e flotation recovery of copper). Poor liberation is capable of limiting the use of physical separation methods for upgrading REE, which would subsequently interfere with the hydrometallurgical processing. This necessitates deeper understanding of the influence of gangue mineralogy on direct hydrometallurgical extraction routes. Mineralogy also plays a key role in characterising concentrates and their behaviour prior to the pyrometallurgical process of smelting, with the aim to produce metals or slags.

The integrated mineralogical approach involves the use of the traditional mineralogical techniques i.e X-ray diffraction analysis (XRD), electron microprobe analyser (EMPA), scanning electron microscopy (SEM) and petrographic studies together with the modern SEM techniques, Mineral Liberation Analyser (MLA) and Quantitative Evaluation of Minerals by Scanning Electron Microscopy (QEMSCAN). The QEMSCAN is an automated mineral classification technique which operates on a scanning electron microscope and the mineral identification tool uses the mineral's unique energy dispersive X-ray spectra (EDS) (Lotter *et al*.,2011). The mineral liberation analyser (MLA) also uses unique EDS for mineral identification; it gives information such as bulk modal analysis, liberation analysis, grain size distribution and mineral associations of the mineral of interest (Fandrich, 2006).

Both traditional and modern mineralogical techniques are used to describe the ore type, predict and optimise the processing plant, or to minimise arising ore processing difficulties. The traditional mineralogy provides qualitative, semi-quantitative and quantitative mineralogical inputs, whereas the modern and automated methods provide quantitative data. The automated methods have a greater ability to quantify textural features of minerals, provide mineral abundance and detail chemical compositions.

The XRD is used in determining the mineral abundance of the ore and EMPA is used to determine the mineral chemistry or elemental concentration within the minerals. Petrographic studies and SEM can provide information such as the mineral's textural relationships, which can aid in process predictions.

Quantitative mineralogical analysis provides more meaningful quantified and accurate data that can be used in improving, designing and optimisation of metallurgical processes. The QEMSCAN and MLA provide quantifiable data for studies of the various mineral species. This essential mineral ore data includes the bulk modal mineral assemblage, grain size distribution, mineral association, mineral liberation analysis, grade recovery, particle view report, image grid, mineral deportment and mineral associations for both ore gangue minerals and predicted recoveries (Lastra. 2007). This enables QEMSCAN/MLA to provide a full mineral and compositional accounting of a given ore type (Lotter *et al*., 2011).

In other instances, process mineralogy can be used in process optimisation. Process mineralogy showed that the integration of traditional mineralogy techniques such as optical microscopy, quantitative or qualitative XRD and SEM can be used to support mineral processing studies in order to assess and optimise the proposed process.

The knowledge gained from undertaking a well-defined and focused process mineralogy study on material used in an operation can have a significant impact on reducing operational costs, improving recovery and lowering risk (Gu *et al*., 2014). Process mineralogy studies can also be used to guide, interpret and optimise bench scale and pilot projects as well as to audit the plant performance with confidence.

According to Thompson *et al*., (2011), the upfront mineralogical assessment of REE leads to a correct metallurgical planning and provides early predictions in beneficiation testwork.

Thompson *et al*., (2011) also suggested that the use of traditional mineralogical techniques such as XRD, petrographic studies and manual SEM are the best mineralogical techniques for REE ore characterisation; in order to enable the production of a good REE concentrate for hydrometallurgical testwork.

The mineralogical methods applied are used to identify both economical and non-economical minerals, and provide more effective information that can aid in defining and planning a better metallurgical processing route. The mineralogical information sums up the abundance of economical REE minerals present, the REE ores textures and other minerals associated with REE.

Perez-Barnuevo *et al.*, (2013) carried out studies on characterisation of intergrowths in mineral particles. The performed mineralogical investigation demonstrated that liberation analysis of monazite dictated the processing route, and the QEMSCAN elemental deportment information identified the potential processing problem areas.

Studies made by Smythe *et al*., (2013), also indicated the importance of understanding the mineralogy of the ore before embarking on any metallurgical testwork, owing to the variability and complexities of REE-containing ores. Mineralogy does provide a broader understanding of the amount of REE in the ore, together with the REE-containing minerals, grain size distribution, liberation, deportment and other minerals associated with REE-containing minerals. The information was achieved through the use of XRD, EMPA and QEMSCAN, and the combination of these analytical techniques proved that mineralogy is a key factor in reducing cost and achieving meaningful results that can aid in process route prediction (Smythe *et al*., 2013).

3. CHAPTER 3 – MATERIALS AND METHODS

3.1. Introduction

This chapter outlines the materials and methods employed to meet the research objectives of this study. The study was conducted in two phases, with phase one entailing a detailed mineralogical analysis on a beach placer deposit sample. The sample was a tailings sample originally from an existing Ti-production, referred to as a tailings feed sample. Phase two of the study involved the hydrometallurgical testwork on the same sample. Mineralogical characterisation was aimed at facilitating the selection of a suitable physical or chemical processing methods for the extraction of REE from the sample, as well as to identify and characterise other additional REE containing species. Mineralogy was also aimed at exploring a potential REE source. Chemical analysis was conducted to obtain data on the grade of REE, major, minor and trace elements in the material.

3.2. Sample preparation

Sample preparation is important as it helps to ensure that the properties of the sample to be analysed are representative. This is done to eliminate the possibility of obtaining erroneous results. The sample used in this study was 50kg of beach sand material (tailings sample) from an existing titanium production operation. The sample was radioactive and thus, necessary health and safety procedures were considered and undertaken. These safety and environmental measures included measuring the radioactivity of the sample **(Figure 6**), storing the sample in a designated radioactive storage, and ensuring that all the personnel involved in preparation of the sample were well-trained on how to handle radioactive material.



Figure 6: An image showing the 50kg bucket of the research sample, and the recorded radioactive reading of 5.87microsieverts per hour

On receipt, the sample was labelled **AMI/14/495** for traceability purposes. The blending of the sample was achieved by weighing, followed by coning and quartering (**Figure 7**). A homogenous 40kg sample was obtained and set aside for minerals processing and hydrometallurgical testwork. The remaining 10kg of the sample was subjected to rotary splitting with the aim of achieving a feasible 5kg portion for mineralogical characterisation. The remaining 5kg split was stored for repetition or additional mineralogical testwork or bench scale metallurgical work, if required.

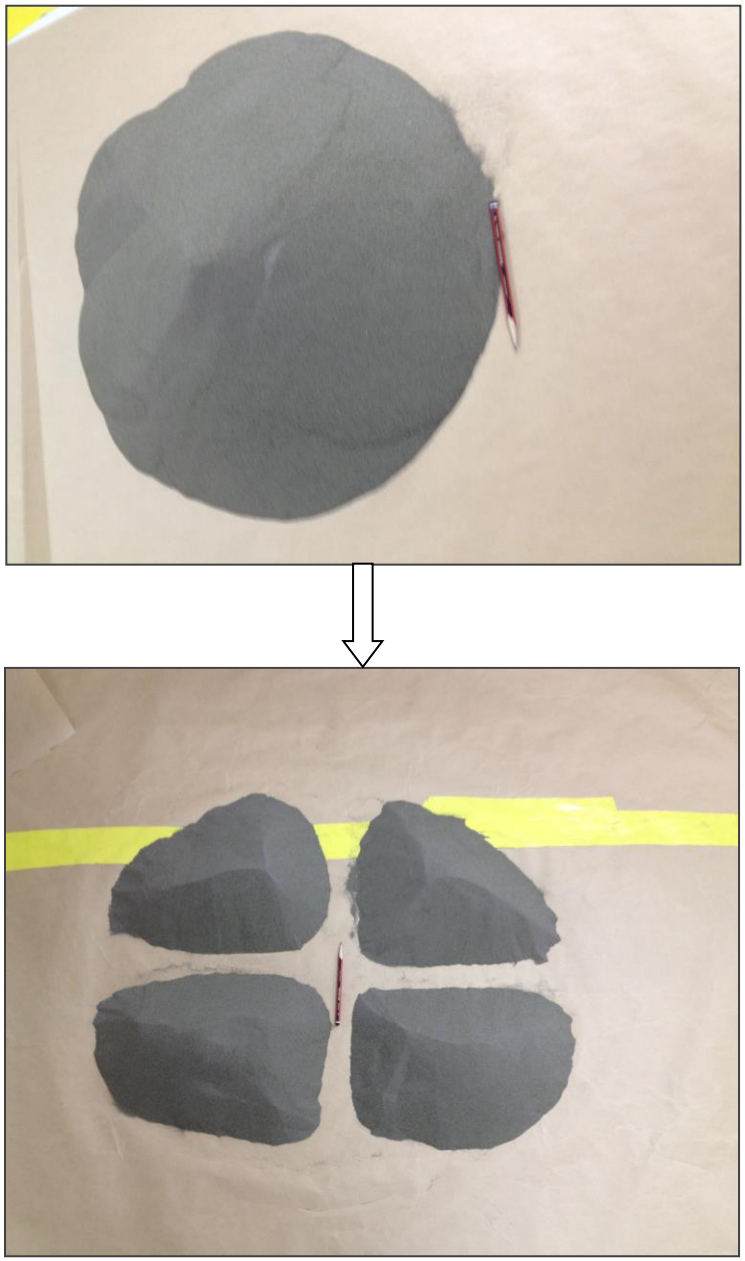


Figure 7: Images showing coning and quartering of the sample

The 5kg mineralogical sample was further reduced to a homogenous ~2kg sample. The ~2kg sample was screened into four size fractions namely: +212µm; –212+150µm; –150+106µm and –106 µm. The ore sample was wet screened using cold tap water. Subsequently, the samples were dried overnight using an oven at 50ºC. The flowsheet in

Figure 8 illustrates the stages followed in attaining homogenous samples for a range of different analysis.

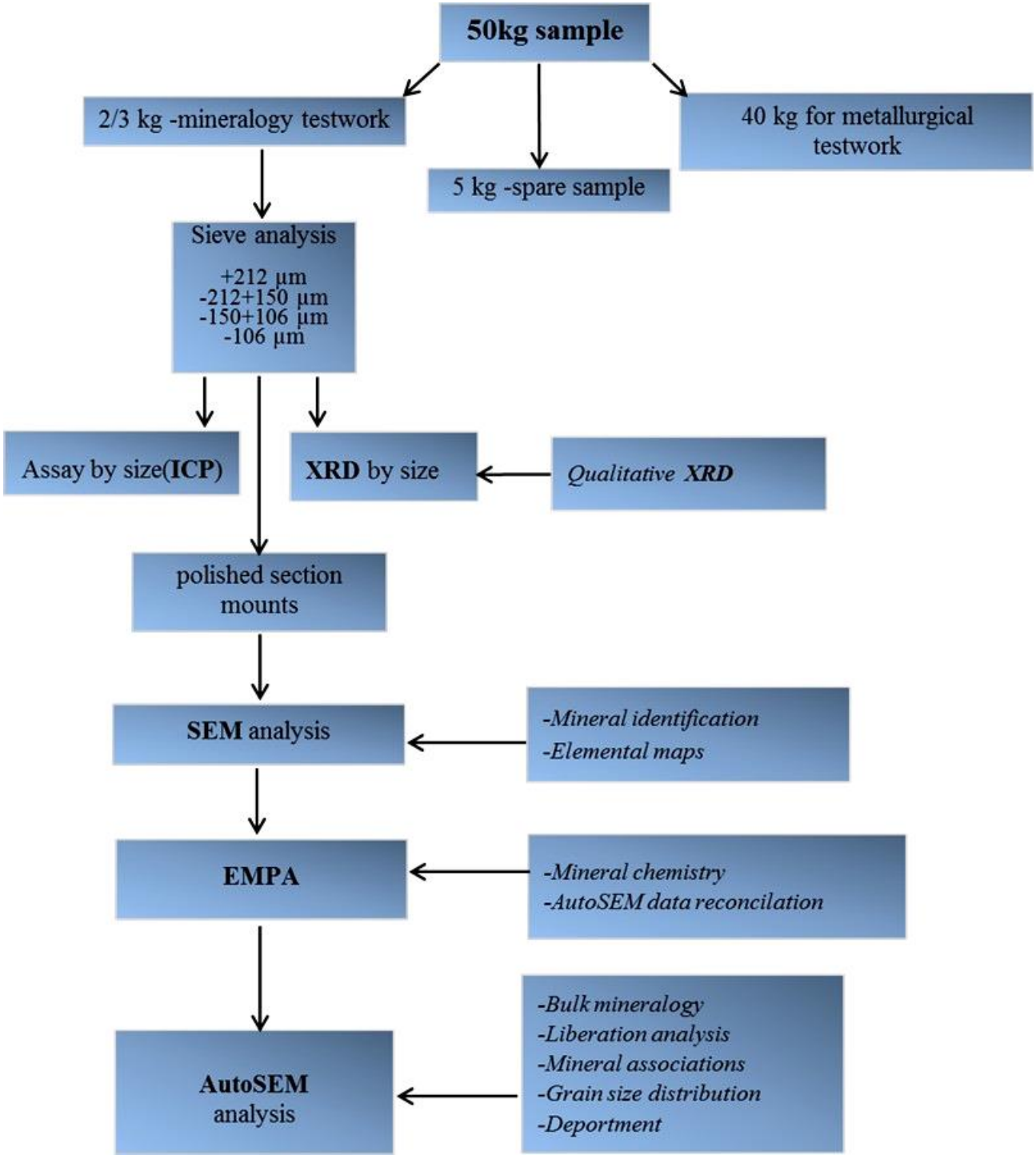


Figure 8: A flowsheet showing the sample preparation procedure and the methods used for mineralogical studies.

Upon drying, each size fraction from the mineralogical sample was weighed and recorded. The particle size distribution is given in **Table 3**.

Table 3: Particle size distribution

Size fractions	Mass (grams)	Mass (%)
+212 µm	198.5	8.5
–212+150 µm	946.9	40.4
–150+106 µm	797.2	34
–106 µm	401.4	17.1
Total	**2343.9**	**100**

A head sample and sub-samples from the individual size fractions were pulverised for XRD and bulk chemical analysis. Sub-samples were also prepared into normal and bottle mounted polished sections for analysis by microscopy methods. Each size fraction was thus mineralogically and chemically studied.

3.3. Chemical analysis

The bulk major, minor and trace element composition, including that of the REE, was determined on each size fraction using Inductively Coupled Plasma Optical Emission Spectroscopy (ICP-OES), particularly to assess REE grades prior to ore processing.

Inductively Coupled Plasma - Optical Emission Spectroscopy is a multi-element technique used to measure the concentration of various elements in a variety of sample matrices. Also known as Inductively Coupled Plasma - Atomic Emission Spectrometry (ICP-AES), the technique is capable of measuring the majority of elements in the Periodic Table and is currently one of the most widely used methods for elemental analysis (Boss and Freeden, 2004).

This type of emission spectroscopy uses high temperature argon plasma to produce excited atoms and ions that emit electromagnetic radiation at wavelengths characteristic of a particular element (Hou and Jones, 2000). The intensity of the emission is indicative of the concentration of the element within the sample or directly proportional to the concentration of the elements in the sample.

3.4. Mineralogical characterisation of feed sample

3.4.1. X-Ray Diffraction analysis

X-Ray Diffraction is a powerful tool used for identifying and quantifying the mineralogy of crystalline compounds in rocks, soils and particulates, to provide information on the bulk mineralogy of the sample. The X-Ray diffractometer works when monochromatic X-rays are projected onto a crystalline material at an angle (θ). Diffraction occurs when the distance travelled by the rays reflected from successive planes differs by an integer (n) of wavelengths (λ).

By varying the angle θ, the Bragg's Law conditions [$n\lambda = 2d \sin\theta$] are satisfied by different d-spacings. Plotting the angular positions and intensities of the resultant diffracted peaks produces a characteristic pattern where different phases are present; the diffraction trace represents the sum of the individual patterns (Bruker axis, 2001)

To obtain the bulk mineralogical composition, the pulverized material was subjected to analysis using a Bruker D8 Advance diffractometer. A Co Kα radiation, a 2θ scan range of 5-80º, a step size of 0.02º 2θ, and a counting time of 3 s per step were employed. Note that only crystalline phases that are present in amounts sufficient to diffract (usually 3-4 mass%), are detectable by this method.

3.4.2. AUTOSEM analysis (MLA)

An MLA was used to quantitatively determine the mineral abundance in the sample. The measurement mode employed in this study was the extended backscattered electron (BSE) liberation analysis (XBSE). The XBSE mode implements area X-ray analysis to efficiently and effectively analyse ore samples containing phases with sufficient BSE contrast to ensure effective segmentation. The backscattered electron (BSE) image is then collected and segmented to delineate mineral grain boundaries in each particle, where each mineral grain is then subjected to an X-ray analysis (Gu, 2003).

The sized bottle mounts polished sections were studied using MLA, in order to obtain the bulk mineral assemblage, grain size distribution, mineral associations, the liberation characteristics and deportment of REE of the head sample and individual size fraction.

3.4.3. Scanning Electron Microscopy analysis

A Zeiss EVO MA15 Scanning Electron Microscopy (SEM), equipped with quantitative energy dispersive spectrometry (EDS), was used to verify the presence of REE-bearing minerals and to determine their elemental compositions of the feed sample.

The prepared normal polished sections and leached products mounted on a stub were examined for mineral characterisation using the SEM. Elemental maps were captured to illustrate and verify the mode of occurrence of REE-bearing minerals and other elements associated with REE-minerals.

Element mapping is a procedure available on the SEM, where specific selected chemical elements can be "searched" within a microscopic field and the relative concentrations of the element are illustrated with different selected colours. If one particular element is present in a particle, the specific particle is highlighted with the element colour. With particles containing more than one mineral phase, the individual element colour concentration is highlighted according to its occurrence in the minerals. If the element is absent, an overall background colour occurs.

3.4.4. Electron microprobe analysis

Electron microprobe analysis provides an understanding of the distribution of chemical components in geological and environmental materials to aid interpretation of their geochemical evolution. This technique provides quantitative major and trace element information for individual minerals grains, with high spatial resolution down to 1 µm. A Cameca SX50 Electron Microprobe equipped with four Wavelength Dispersive Spectrometers (WDS) was used to determine the mineral chemistry on various grains. A maximum of 365 grains was analysed across all size fractions.

Calibration of the rare earth elements was performed on the REE Orthophosphate Reference samples from the Smithsonian Microbeam Standards collection. Other elements analysed were calibrated using appropriate reference standards. The standard excitation conditions used were 20 kV and 30 nA, with a spot size of 5 µm.

3.5. Metallurgy testwork and product characterisation

As stated in the objectives of the study, the metallurgical testwork routes selected will depend on mineralogical findings. Subsequent to the detailed mineralogical analysis undertaken on tailing feed sample size fractions, the findings showed that monazite was the chief REE carrier, and that the 150+106µm and –106µm size fractions were naturally upgraded in monazite, and could be taken further for leaching testwork. The two size fractions: –150+106µm and –106µm were composited to form a –150µm sample (referred to as the leach feed sample).

For hydrometallurgical testwork, previous studies at Mintek have shown that when monazite is the main REE carrier, a cracking procedure (using NaOH) followed by washing and an acid leach constitutes the desired process for extracting REE. For the procedure, 400g of the leach feed was milled to 100% passing 45µm in order to achieve extraction rates of greater than 90% (Peelman *et al*., 2014). The composite sample went through a series of hydrometallurgy tests. The hydrometallurgical testwork conducted involved caustic cracking, water leaching and selective leaching. The experimental approach is illustrated in **Figure 9**.

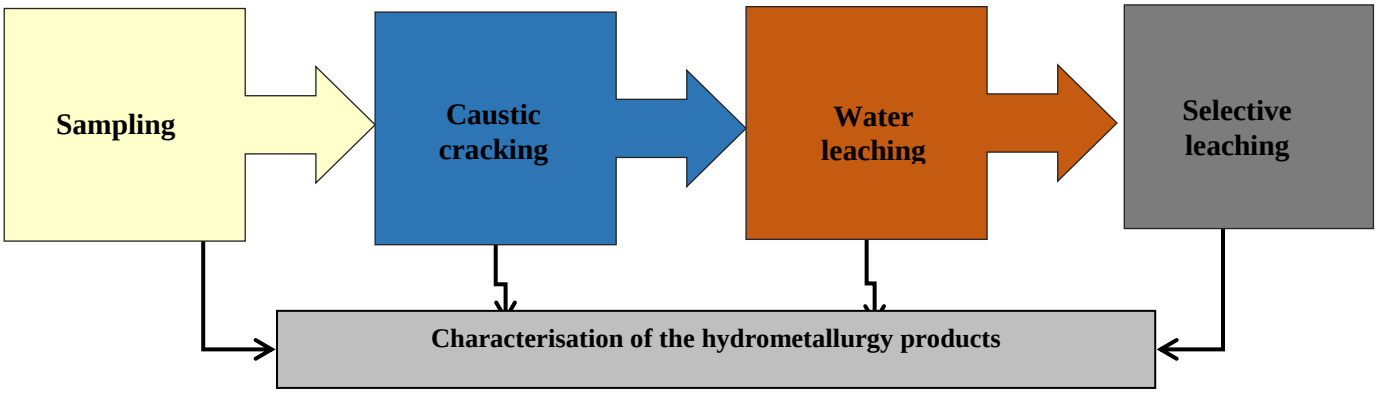


Figure 9: The experimental approach of the three leaching stages.

Caustic cracking is the decomposition of monazite using 50% (m/m) NaOH solution (Gupta and Krishnamurthy, 2005), in order to break down the monazite (Ce,La,Nd,Th)PO_4) into trisodium phosphate and REE. Water leaching is the next stage after caustic cracking. The water leaching method aims to remove NaOH entrainments from the leach residues. Selective leaching involved primarily, the dissolution of REE with HCl.

3.5.1. Caustic (NaOH) cracking

A 400g dry aliquot of the sample was slurried in freshly prepared 50% (m/m) NaOH solution targeting an initial pulp containing 20% (m/m) solids, in a stainless-steel reactor. This corresponded to 2000g of slurried feed. The pulp was agitated with an overhead mechanical stirrer, heated and the temperature controlled and maintained at 140°C for 4 hours (**Table 4**).

Table 4: Experimental conditions for the caustic cracking test

Parameter	**Target**
Temperature	140°C
Residence time	4 hours
Target pH	-
Solids content	20% m/m
Grind size	100% passing 45 µm
Feed Data:	**Target**
Mass of feed solids	400g
Required mass of NaOH solution	1600g
Volume of DI water	800g
Mass of NaOH pellets	800g
Reagent concentration:	**Target**
NaOH concentration	1000g/L
NaOH concentration	50.0% (m/m)

**m/m –percentage by mass*

Thereafter, the pulp was vacuum filtered whilst hot to avoid solution crystallization on the filter. The filter cake was washed two times by re-pulping in de-ionized water and one plug wash at a wash water ratio of five times the mass of wet cake in each step to remove entrained NaOH and other impurities. The wash liquors were combined and the total volume recorded. A sample of the combined wash liquors was taken for chemical analysis.

After each wash, a representative sample of the wet residue was taken for mineralogical analysis. In addition, a sample of the washed leach residue was removed from the cake while in the filter pan for the determination of moisture content and chemical analysis.

3.5.2. Water (H_2O) leaching

The washed residue after cracking was subjected to a further hot water wash step (water leach). The solids from the caustic crack step were slurried in de-ionized water at 60°C in a stainless steel 5L reactor, targeting the required pulp density of 20% (m/m). The reactor contents were agitated with a stainless-steel impeller using a mechanical over-head stirrer. Test parameters such as temperature, pH and redox potential (Eh) were recorded on a half-hourly basis. The temperature was controlled at 60°C (**Table 5**).

Table 5: Experimental conditions for the water leaching test

Parameter	**Target**
Temperature	60 ºC
Residence time	4 hours
Target pH	Variable
Slurry density	20.0 % (m/m)
Feed Data:	**Target**
Required mass of feed wet	488.32 g
Mass of dry feed solids	308.97 g
Mass of *DI water	1056.55 g

**DI water- deionized water*

On completion of the test after 4 hours, the mixture was filtered and the mass of the wet residue recorded. The volume and the mass of the filtrate were also recorded. The filtered residue was weighed, subsequently re-slurried and washed once with de-ionized water, at a wash ratio of 5 times the mass of the wet residue. The wash liquor total volume was recorded.

The washed solids were dried overnight in an oven at 50°C. A representative sample of the washed dried cake was obtained by using the cone and quartering method for mineralogical investigation. The remaining dried filter cake residue was stored and used as feed to subsequent HCl testwork.

3.5.3. Selective (HCl) leaching

The dried filter cake residue from the water leach step was used as feed for selective REE dissolution testwork. The objective of this test was to selectively dissolve the REE from the pre-treatment stage solid residue. The solids were slurried with deionized water to 20% solids (m/m) in a 3L thermoplastic coated reactor. The reactor was equipped with an overhead stirrer with a thermoplastic coated impeller, thermocouple and also pH and Eh meter.

The operating parameters such as temperature, redox potential (Eh) and pH were recorded half-hourly. Concentrated HCl acid (32% m/m) was added timely to control the pH of the mixture at the value of 3 (**Table 6**).

Table 6: Experimental conditions for HCl selective leaching test

Parameter	**Target**
Temperature	Ambient ^{o}C
Residence time	4 hours
Target pH	3.00
Target Eh	variable mV
Feed Data:	**Target**
Required mass of dry feed	284.3 g
Solids content	20 % (m/m)
Mass of *DI water	1137 g
Reagents concentration	**Target**
HCl concentration	32 %

**DI water- deionized water*

On completion of the test, the slurry was filtered by means of vacuum filtration. The filtered wet solids mass, volume and mass of filtrate were recorded. The wet solids were washed three times with two re-pulping washes and one plug wash using deionized water. The washed solids were dried in an oven at 50°C. The dried solids were then homogenized and a representative sample was taken using a cone and quartering technique for mineralogical assessment. The leach liquors were also sampled for chemical analysis.

3.5.4. Characterisation of REE leaching products

3.5.4.1. Mineralogy of REE leach residues

Mineralogy was conducted on residues from each leaching stage, and on residues of all re-pulp and plug washing steps of each leaching stage (as described in sections *3.5.1*, *3.5.2*, and *3.5.3*). This was achieved using SEM.

A total of ten leach and washed residues were representatively prepared for examination using a Zeiss EVO MA15 SEM in order to identify REE-containing phases and mineral compositions present. Due to the smaller amounts of the samples, the samples were prepared on carbon coated stubs for examination. The Zeiss EVO MA15 SEM, equipped with quantitative energy dispersive spectrometry (EDS), was used to verify the presence of REE-bearing phases and to determine their elemental composition. The leach residues were assessed by manual operated Zeiss SEM, since they were no longer minerals but phases making mixed elemental compounds that AutoSEM has a difficulty in identifying.

3.5.4.2. Chemical analysis

The leach residues and leach liquors that were sampled during the leaching and washing stages were chemically analysed for their REE content. These chemical results were used in the mass balance calculations and to calculate the leach efficiencies and accountability.

4. CHAPTER 4 – CHARACTERISATION OF FEED TAILING SAMPLE

4.1. Introduction

This chapter outlines the results and discussion of the testwork carried out in order to fulfil the identified problem statement in **Chapter 1**, using the experimental methods described in **Chapter 3**. The testwork carried out in this study was aimed at achieving the described set of objectives. These objectives were to explore the most suitable processing route for the extraction of rare earth elements from an alternative REE source.

In order to meet the outlined objectives, REE from an existing heavy mineral beach placer deposit currently being mined for titanium and iron were characterised. In addition, the sample's mineralogy was characterised to establish if carrying out mineralogical investigation beforehand can serve as an effective tool to guide the processing route selection.

In an attempt to answer the objectives of the study, a tailings feed sample originating from a current Ti-production operation was mineralogically characterised and further taken for hydrometallurgical test. The results are outlined and discussed in this chapter.

4.2. Chemical analysis, mineralogy and mineral chemistry results of the tailings feed

The chemical analysis by size was performed to measure the TREE % grade of the sample. The mineralogical characterisation involved the bulk mineralogy of the tailings feed sample by size in order to show the distribution of the minerals present across all the size fractions and the head sample. This was aimed at distinguishing the abundance of the known REE species, the abundance of other heavy mineral that have a potential of hosting REE as well as other possible silicates, phosphates and oxide minerals present in the sample.

The MLA was used for bulk mineralogy, coupled with XRD analysis to confirm the gangue mineralogy. The EMPA was used to determine the REE concentrations in the different minerals. The MLA was further used to characterise the identified REE species, for their liberation characteristics, grain size distribution, mineral associations and REE deportment.

4.2.1. Chemical analysis

The chemical analysis data showed that the total rare earth elements (TREE) content is 2.7% (**Table 7**). The chemical assay results also show the abundance of REE in the –106µm size fraction at 1.8%.

Table 7: Analysed Rare Earth Element concentrations, in ppm

Elements	+212µm	–212+150µm	–150+106µm	–106µm
Mass Distribution (in %)	**8.5%**	**40.4%**	**34.0%**	**17.1%**
La	553.8	965.9	7358.5	26642.8
Ce	1000.3	1772.6	14337.5	51597.5
Pr	125.3	207.9	1116.2	6192.6
Nd	405.4	715.2	3814.2	13880.2
Sm	67.0	137.6	672.1	2351.3
Eu	8.3	16.6	40.5	63.8
Gd	75.3	157.3	621.3	1937.8
Tb	13.6	25.7	81.7	210.2
Dy	87.8	160.6	399.3	703.1
Ho	28.3	50.6	114.3	148.4
Er	96.1	169.6	368.9	356.9
Tm	16.4	28.8	62.3	49.7
Yb	115.5	204.0	449.9	342.7
Lu	19.4	33.9	77.4	59.5
Sc	174.5	242.8	357.6	287.0
Y	695.4	640.3	1419.9	1714.2
TREE in ppm	3482.2	5529.4	31291.4	106538.0
Size fraction weighted TREE in %	0.03	0.2	1.1	1.8

4.2.2. Particle Size Distribution (PSD) of the tailings feed sample

The particle size distribution of the sample, as derived from the MLA is in two-dimension (2D). The 2D PSD derived from the MLA showed that the retained wt% of the sample is in accordance with the way the sample was initially sampled and screened into the four size fractions as specified in **Chapter 3**. The PSD trend of the four sizes screened sample and the MLA derived PSD will always be underestimated relative to reality.

Figure 10 presents both cumulative retained wt% curve and a standard retained wt% of the total sample. The detailed particle size distribution is shown in **Table 8**.

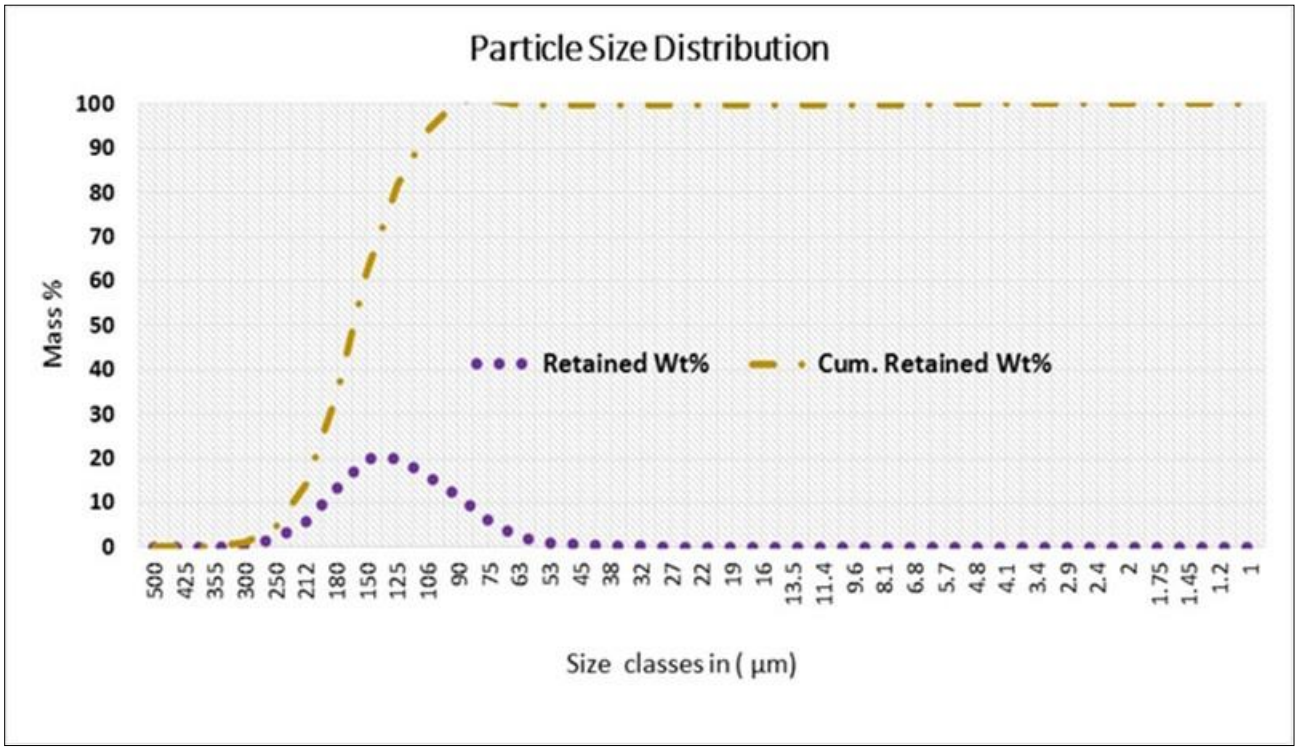


Figure 10: Particle size distribution in retained wt % and cumulative retained wt%.

Table 8: Particle size distribution (in 2D, note, underestimation compared with 3D) in retained wt% and cumulative retained wt%

Size classes in (µm)	Retained wt%	Cum. Retained wt%
500	0.0	0.0
425	0.1	0.1
355	0.1	0.2
300	0.5	0.6
250	1.9	2.5
212	5.9	8.5
180	13.2	21.6
150	20.2	41.8
125	20.0	61.8
106	16.2	78.0
90	11.4	89.4
75	6.0	95.3
63	2.3	97.6
53	1.1	98.7
45	0.5	99.2
38	0.3	99.5
32	0.2	99.7
27	0.1	99.8
22	0.1	99.8
19	0.0	99.9
16	0.0	99.9
13.5	0.0	99.9

4.2.3. Bulk Mineralogy by size of the tailing feed sample

The bulk mineralogy was achieved by means of MLA and XRD. The X-ray diffraction analysis was undertaken on the sample to determine the bulk mineralogical composition, particularly the gangue phases which may affect test work to assist with the AutoSEM bulk modal mineralogy. The MLA was also used for repeatability and reproducibility analysis (**APPENDIX F**) in order to assess the experimental errors.

The mineralogy results show that the mineral distribution is variable across all size fractions. The coarser fractions (+212µm and –212+150µm) are dominated by epidote, followed by minor quantities of diopside, augite and amphibole.

Mineralogical differences are more evident in the two smallest size fractions (–150+106µm and –106µm), where zircon, rutile and monazite are more concentrated.

Quartz is expected to be predominant in beach placer deposit; however, this sample shows quartz in minute amounts. The minor amounts of quartz in the sample are due to the fact that this is a tailings sample originating from an operational titanium plant. In the titania production plants, quartz is normally removed in the early stages, thus, is then unlikely to report into the final tailings. Garnet (almandine and grossular) was only detected in the +212µm, –212+150µm and –150+106µm size fractions. Two types of leucoxene were identified in this sample; one leucoxene containing niobium (Nb) and the other leucoxene lacking Nb. **Figure 11** and

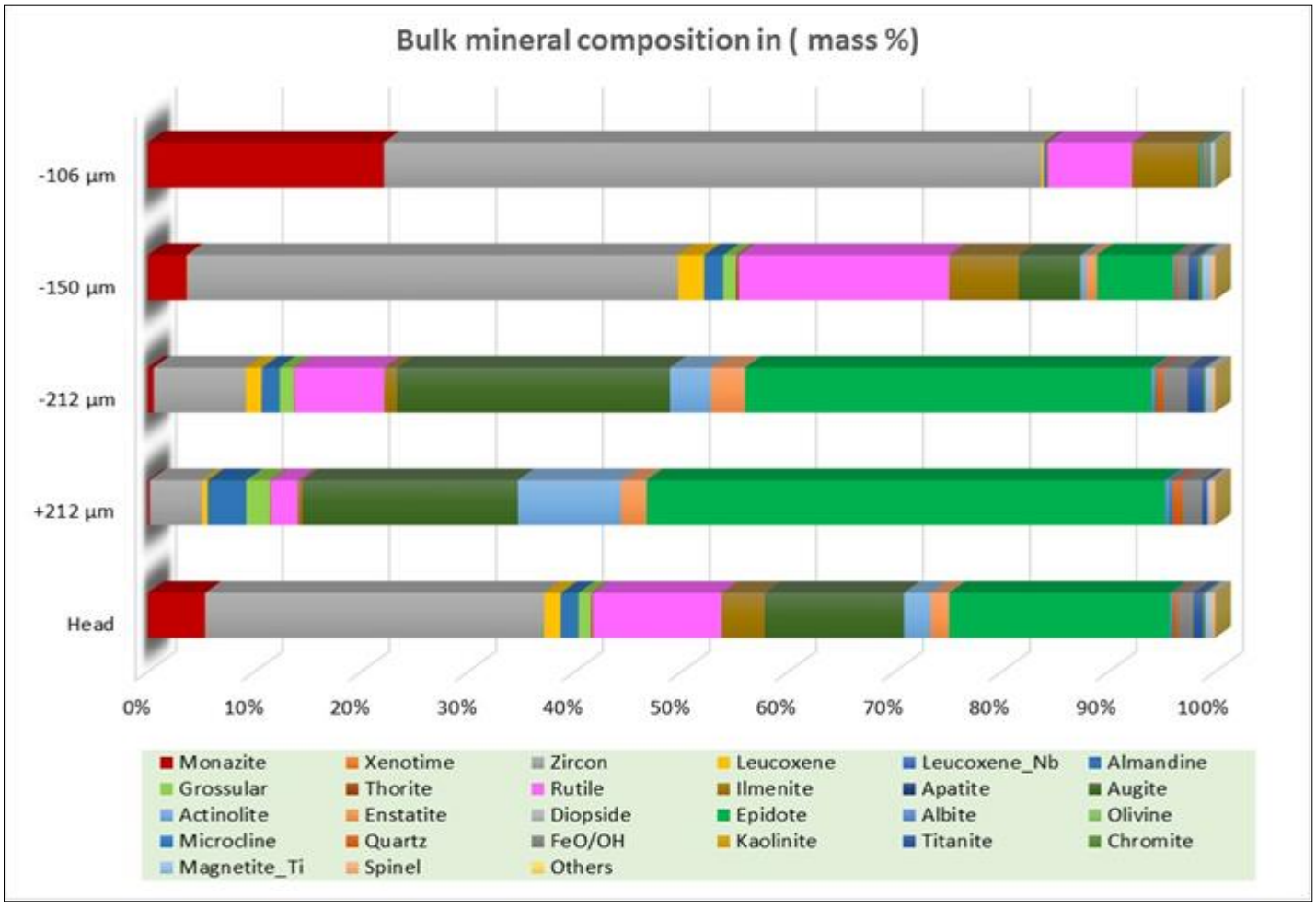


Table *9* contains all the minerals identified using a combination of XRD and MLA.

Figure 11: Bulk mineral composition of the tailing feed sample.

Table 9: Bulk mineral composition of the tailing feed sample

Mineral groups	Mineral	Chemical Formulae	Head	+212µm	–212µm	–150µm	–106 µm
Mass Distribution in %			**100**	**8.5**	**40.4**	**34.0**	**17.1**
REE-containing species	Monazite	$(Ce,La,Nd,Th)PO_4$	5.3	0.2	0.5	3.6	22.1
	Xenotime	YPO_4	<0.1	<0.1	<0.1	0.1	<0.1
	Zircon	$ZrSiO_4$	31.3	4.7	8.4	45.8	61.6
	Almandine	$Fe_3Al_2Si_3O_{12}$	1.6	3.5	1.5	1.7	0.2
	Grossular	$Ca_3Al_2(SiO_4)_3$	1.2	2.2	1.3	1.2	<0.1
	Titanite	$CaTiSiO_5$	0.9	0.5	1.4	0.9	<0.1
	Thorite	$(Th,U)SiO_4$	0.1	0.1	<0.1	0.2	0.1
	Leucoxene		1.5	0.5	1.4	2.4	0.2
	Leucoxene_Nb		<0.1	<0.1	0.1	<0.1	<0.1
Oxides	Rutile	TiO_2	11.9	2.4	8.2	19.6	7.9
	Ilmenite	$FeTiO_3$	4.0	0.5	1.2	6.5	6.3
	FeO/OH	$FeO(OH)$	1.4	1.7	2.1	1.0	0.4
	Chromite	$FeCr_2O_4$	0.3	<0.1	0.2	0.4	0.2
	Magnetite_Ti	Fe_2O_4	0.6	0.2	0.6	0.8	0.4
	Spinel	$MgAl_2O_4$	0.3	0.5	0.3	0.4	<0.1
Phosphates	Apatite	$Ca_5(PO_4)_3(OH,F,Cl)$	<0.1	0.1	<0.1	<01	<0.1
Silicates	Augite	$(Ca,Na)(Mg,Fe,Al,Ti)(Si,Al)_2O_6$	12.8	19.2	24.9	5.7	<0.1
	Actinolite	$Ca_2(Mg,Fe)_5Si_8O_{22}(OH)_2$	2.5	9.2	3.7	0.5	<0.1
	Enstatite	$Mg_2Si_2O_6$	1.7	2.3	3.1	1.0	<0.1
	Diopside	$Ca_3Al_2(SiO_4)_3$	<0.1	<0.1	<0.1	<0.1	<0.1
	Epidote	$Ca_2(Fe,Al)_3(SiO_4)_3(OH)$	20.4	46.5	37.2	7.1	0.1
	Albite	$NaAlSi_3O_8$	0.1	0.3	0.2	0.1	<0.1
	Olivine	$(Mg, Fe)_2SiO_4$	<0.1	<0.1	<0.1	<0.1	<0.1
	Microcline	$KAlSi_3O_8$	0.1	0.3	0.2	0.1	<0.1
	Quartz	SiO_2	0.4	0.9	0.7	0.23	<0.1
	Kaolinite	$Al_2Si_2O_5(OH)_4$	<0.1	0.1	<0.1	<0.1	<0.1
	Andalusite	Al_2SiO_5	1.4	4.3	2.4	0.4	<0.1
	Others		<0.1	<0.1	<0.1	<0.1	<0.1
	Total		**100**	**100**	**100**	**100**	**100**

**<0.1 = Below detection limit of 0.1%*

4.2.3.1. Data Reconciliation

Data reconciliation measures the reliability and confidence of mineralogy data. The chemical assay measured data is used as the control against the MLA calculated assays. The calculated values are derived using the mass proportions of the minerals and their ideal chemical composition. The data validation results show good reconciliation for most of the elements (i.e Fe, Ca, Ce, Ti) particularly Ce (**Figure 12**), providing more confidence in the mineralogy data reported for the REE-containing minerals.

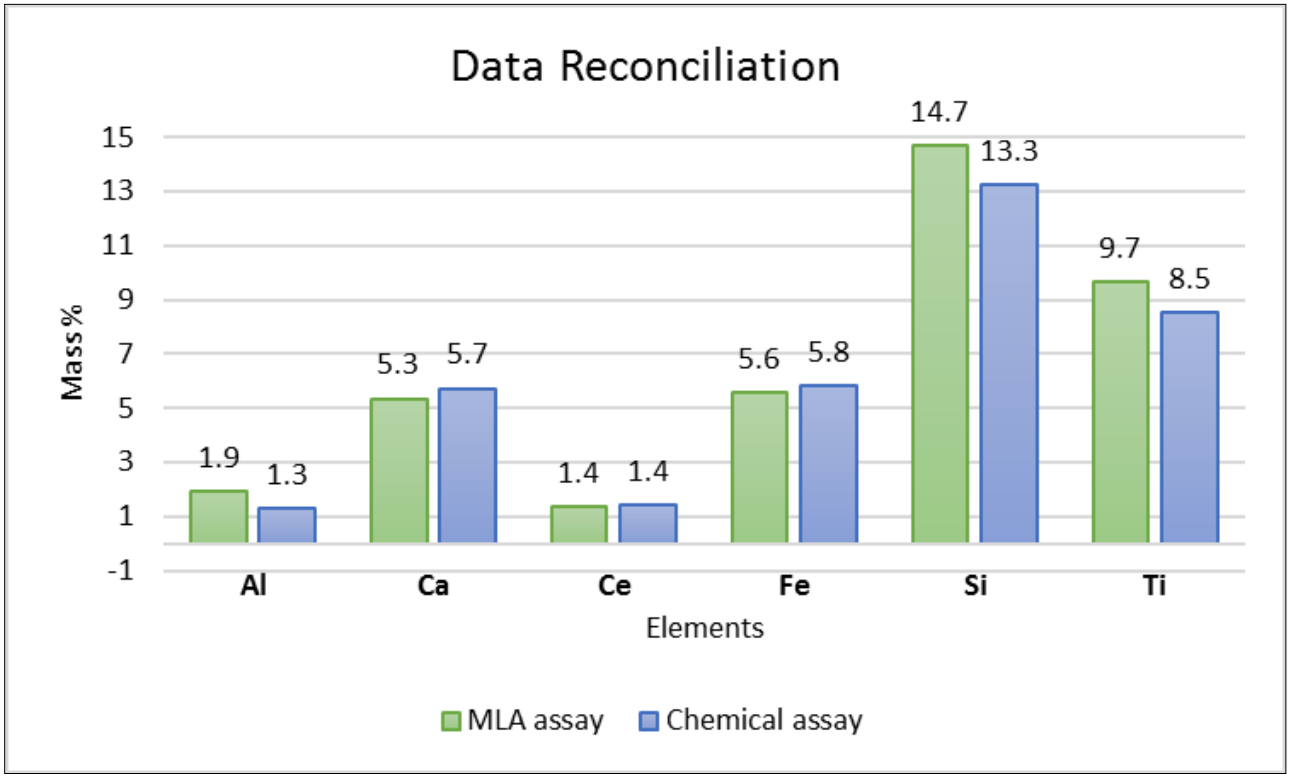


Figure 12: Data validation

4.2.4. Mode of occurrence of the tailing feed sample

This sub section qualitatively describes the minerals present, their mode of occurrence and mineral association in each size fraction, as carried out with the SEM. The detailed SEM analysis images and elemental maps are presented in **APPENDIX A.**

4.2.4.1. Size fraction +212µm

Size fraction +212µm consists mainly of epidote and amphibole (actinolite). Monazite and zircon are present in smaller amounts; garnet (almandine) and quartz also occur in smaller quantities. The majority of monazite and zircon occur as liberated, with a few grains of monazite associated with zircon, quartz and goethite (**Figure 13).**

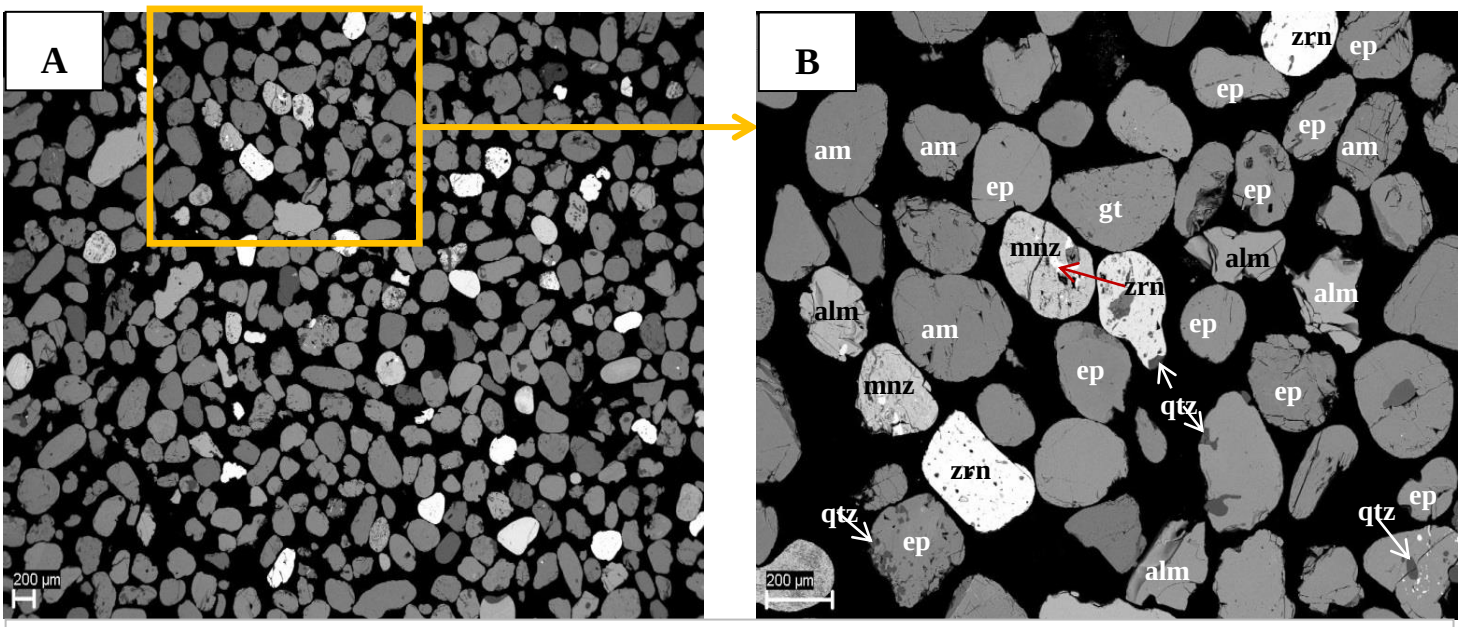
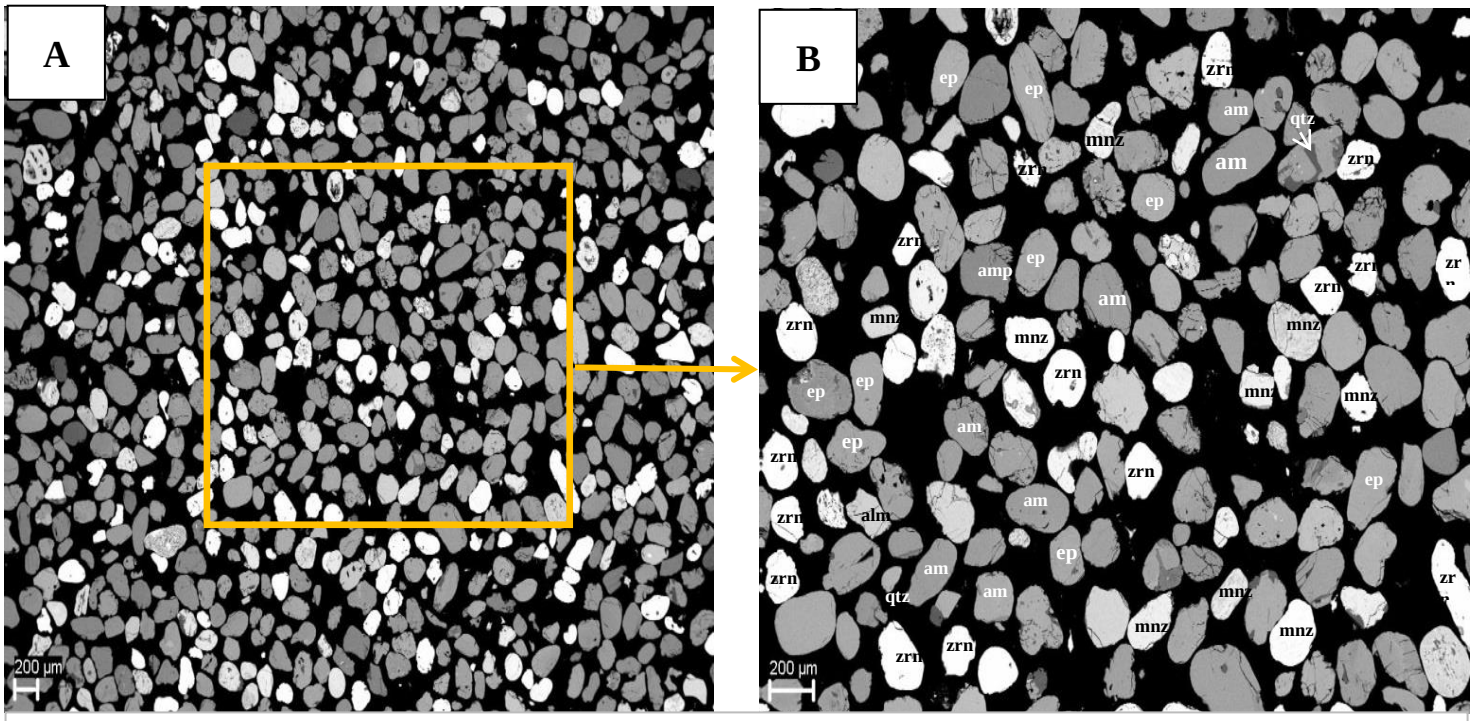


Figure 13: Backscattered electron (BSE) images showing an overview (image A) of the +212µm size fraction illustrating the distribution of several minerals; with selected area in "yellow" presented in image B.

4.2.4.2. Size fraction –212+150µm

The BSE images show discrete and liberated grains of monazite in this fraction. This size fraction clearly shows an increase in monazite and zircon in contrast to the +212µm fraction (**Figure 14**).The grains of epidote and amphibole (actinolite) are widespread in this fraction; indicating the abundance of these two minerals.

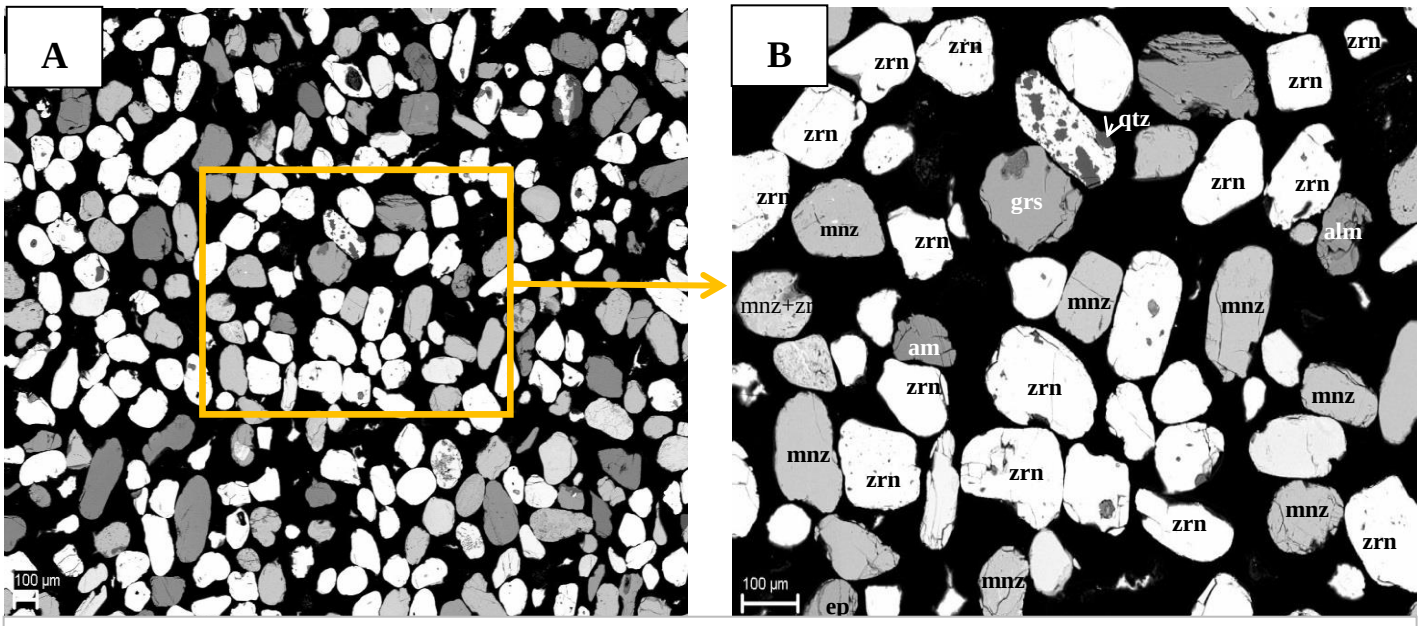


am-amphibole, **ep**- epidote, **zrn**-zircon, **mon**- monazite, **qtz**-quartz,

Figure 14: BSE images showing an overview (image A) of the –212+150 µm size fraction illustrating the distribution of several minerals, with selected area in "yellow" presented in image B.

4.2.4.3. Size fraction –150+106µm

This size fraction shows a decrease in epidote and amphibole (actinolite) content, with a concomitant increase in zircon and monazite (**Figure 13**). This is in contrast to observed abundance of these minerals in size fractions +212µm and –212+150µm. Numerous grains of monazite and zircon are liberated, with very few grains associated with quartz and goethite. Minor amounts of grossular and amphibole (actinolite) were detected in this fraction.



am-amphibole, **alm**-almandine, **zrn**-zircon, **mon**- monazite, **qtz**-quartz, **grs**-grossular

Figure 15: BSE images showing an overview (image A) of the –150+106 µm size fraction illustrating the distribution of several minerals, with selected area in "yellow" presented in image B.

4.2.4.4. Size fraction –106 µm

Monazite and zircon are more evident in this fraction compared to +212µm and –212+150µm, with minor amounts of rutile and ilmenite present. Monazite and zircon mainly occur as liberated and very few grains of these minerals are associated with trace amounts of quartz. Certain grains of zircon display zoning defined by variable amounts of silica and zirconium, compared with theoretical concentrations of the elements for zircon (**Figure 16**)

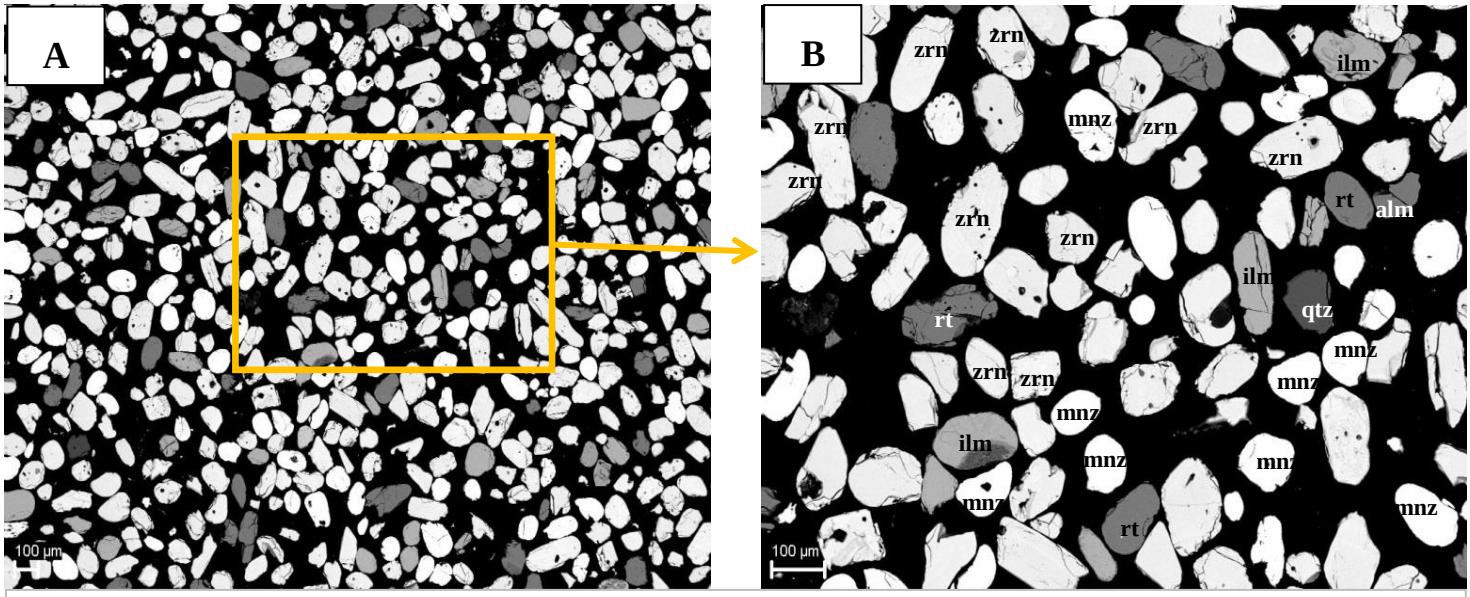


Figure 16: An overview (image A) of the –106µm size fraction illustrating the distribution of several minerals, with selected area in "yellow" presented in image B.

4.2.5. Mineral Chemistry of the tailing feed sample

In order to obtain the mineral chemistry of the REE containing minerals in the feed sample, a total of 365 grains of different minerals were analysed. The EMPA results showed monazite as the most abundant REE mineral in the sample. However, EMPA also succeeded in detecting concentrations of REE in zircon, titanite and almandine. The mineral leucoxene was only identified using EMPA and the results show that this mineral contains detectable REE, as seen in **Table 10**. The results are averaged results of the mineral chemistry of the analysed grains. The detailed results of the analysed 365 grains are presented in **APPENDIX B**.

Table 10: Mineral chemistry (yellow highlighted rows are REE-containing minerals)

Analytes	*MDL*	Epidote	Amphibole 1	Amphibole 2	Amphibole 3	Zircon	Monazite	Titanite	Ilmenite	Rutile	Leucoxene	Hematite	Grossular 1	Grossular 2	Almandine 1	Almandine 2
		n=8	*n=4*	*n=34*	*n=9*	*n=113*	*n=33*	*n=3*	*n=25*	*n=54*	*n=19*	*n=3*	*n=47*	*n=5*	*n=5*	*n=3*
MgO	*0.02*	1.63	27.21	17.34	13.5	-	-	0.02	0.89	<0.1	0.17	0.04	0.05	0.12	9.39	2.29
Al_2O_3	*0.01*	53.13	1.18	2.06	9.52	-	-	2.33	0.11	0.07	0.79	0.30	26.97	19.50	21.53	20.94
SiO_2	*0.02*	27.23	54.09	52.07	47.74	31.48	0.82	29.72	0.27	0.05	1.09	0.34	38.41	38.72	38.59	34.68
P_2O_5	*0.03*	-	-	-	-	-	26.48	0.08	0.14	-	0.06	0.04	0.06	-	-	0.03
CaO	*0.01*	-	2.56	18.50	11.50	-	1.02	27.26	0.04	0.01	0.24	-	23.48	34.08	5.94	1.05
TiO_2	*0.02*	0.50	0.28	0.44	0.97	-	-	36.73	52.79	99.46	82.2	0.21	0.13	0.83	0.08	0.05
MnO	*0.02*	0.32	0.33	0.22	0.3	-	-	0.19	0.71	-	0.21	0.05	0.20	2.08	0.80	16.47
FeO	*0.03*	14.63	14.18	8.09	14.35	-	-	1.56	45.02	0.25	12.81	90.16	10.01	5.40	22.83	20.47
SrO	*0.04*	-	-	-	1.28	-	-	-	-	-	-	-	0.32	-	0.14	0.14
Y_2O_3	*0.04*	-	-	-	-	**0.2**	**1.85**	**0.22**	-	-	**0.05**	-	-	-	-	-
ZrO_2	*0.07*	-	-	-	-	**67.27**	-	**0.08**	-	-	**0.18**	-	-	-	-	-
La_2O_3	*0.1*	-	-	-	-	**0.12**	**14.31**	**0.23**	-	-	-	-	-	-	-	-
Ce_2O_3	*0.09*	-	-	-	-	**0.1**	**29.41**	**0.35**	-	-	-	-	-	-	-	**0.10**
Pr_2O_3	*0.09*	-	-	-	-	**0.12**	**2.99**	-	-	-	-	-	-	-	-	**0.10**
Nd_2O_3	*0.07*	-	-	-	-	**0.1**	**11.88**	**0.31**	-	-	-	-	-	-	-	-
Sm_2O_3	*0.03*	**0.05**	-	-	-	**0.06**	**1.91**	**0.10**	-	-	-	-	-	-	-	**0.04**
Eu_2O_3	*0.03*	**0.05**	-	-	-	**0.06**	-	**0.06**	-	-	-	-	-	-	-	**0.08**
Gd_2O_3	*0.05*	**0.06**	-	-	-	**0.07**	-	**0.09**	-	-	-	-	-	-	-	-
Dy_2O_3	*0.05*	-	-	-	-	**0.07**	**0.49**	**0.10**	-	-	-	-	-	-	-	**3.40**
Ho_2O_3	*0.09*	**0.11**	-	-	-	**0.14**	**0.17**	**0.10**	-	-	-	-	-	-	-	**0.16**
HfO_2	*0.08*	-	-	-	-	-	-	-	-	-	-	-	-	-	-	-
PbO	*0.16*	0.26	-	-	-	-	-	-	-	-	-	-	-	-	-	-
ThO_2	*0.05*	-	-	-	-	0.08	7.54	-	-	-	-	-	-	-	-	-
UO_2	*0.05*	-	-	-	-	0.13	0.38	-	-	-	-	-	-	-	-	-
Total		**97.39**	**99.82**	**98.72**	**96.43**	**98.91**	**99.85**	**98.97**	**99.61**	**99.86**	**97.76**	**91.12**	**99.59**	**100.72**	**99.29**	**99.7**

**n=number of measured grains*
**MDL-minimum detection limit;*
**Grossular1 and Grossular 2 (vary in Ca and Fe amounts)*
NB: "-"= LLD (lower than limit of detection)

4.2.6. Characterisation of REE containing minerals

An integration of different mineralogical techniques was employed and the results showed that apart from monazite and xenotime, there are other minerals originating from this type of deposit that contain REE. Zircon, almandine, titanite and leucoxene showed the presence of REE. However, further REE investigation on titanite, almandine and leucoxene was disregarded due to their proportion in the total sample and the small number of grains that were analysed for their mineral chemistry.

4.2.6.1. The REE species

The minerals listed in **Table 11** were further characterised for their grain size distribution, liberation analysis, deportment and mineral associations. Their normalised proportions in the head sample are given in **Table 11**.

Table 11: Normalised proportions of major REE containing minerals in the feed sample

Mineral	Chemical Formulae	Head Sample	Number of Grains
Monazite	$(Ce,La,Nd,Th)PO_4$	14.4	18871
Xenotime	YPO_4	0.1	2683
Zircon	$ZrSiO_4$.	85.4	38074
Total		100	59628

4.2.6.2. Mineral associations of REE species

Mineral association data is derived from shared boundaries amongst the identified mineral grains. The higher the associated percentage, the greater the degree of boundary-sharing between mineral species. Free surface refers to the perimeter of the particle that is exposed and does not share a grain boundary with any mineral.

Mineral association data shows that monazite and zircon have a high percentage of total free surface. This means that the majority of monazite and zircon are liberated. Xenotime has a free surface of 21.7%, which means most grains of xenotime are associated with other minerals. Such minerals are monazite, zircon, thorite, microcline and traces of iron oxy-hydroxides, epidote and ilmenite **(Table 12)**

Table 12: Mineral associations of REE

Mineral	Xenotime	Monazite	Zircon
Free Surface	21.7	97.0	92.6
Monazite	6.5	0.0	0.1
Xenotime	0.0	0.1	0.3
Zircon	56.9	0.5	0.0
Thorite	3.9	0.1	0.0
Rutile	0.8	1.0	0.2
Ilmenite	1.7	0.0	1.2
Titanite	0.0	0.0	0.0
Leucoxene	0.0	0.0	0.0
Apatite	0.0	0.0	0.3
Almandine	1.7	0.2	1.5
Grossular	0.3	0.1	0.4
Augite	0.1	0.0	0.0
Actinolite	0.0	0.0	0.1
Enstatite	0.1	0.0	0.0
Epidote	1.3	0.0	0.1
Albite	0.3	0.1	0.4
Microcline	3.0	0.1	0.7
Quartz	0.7	0.7	0.8
FeO/OH	1.1	0.2	0.8
Kaolinite	0.0	0.0	0.4
Magnetite_Ti	0.0	0.0	0.1
Total	**100**	**100**	**100**

= significant amounts of association

4.2.6.3. Liberation of REE species

Liberation of minerals is based on liberation by free surface, i.e. the proportion of the particle surface (perimeter in 2D) made up by the mineral of interest. Liberation by free surface plays an important role in leaching and flotation testwork.

The following classes are used to describe liberation:

- **Completely liberated**: (Free) 100% of the surface of the particle
- **80-100% exposed**: >80% and <100% of the free surface of the particle
- **50-80% exposed**: >50% and <=80% of the free surface of the particle
- **20-50% exposed**: >20 and <=50% of the free surface of the particle
- **Locked**: <= 20% of the free surface of the particle

The figure below shows an ideal liberation classification (**Figure 17**). Cropp, (2013) showed the different liberation classes and their degree of liberation in area % and free surface area %.

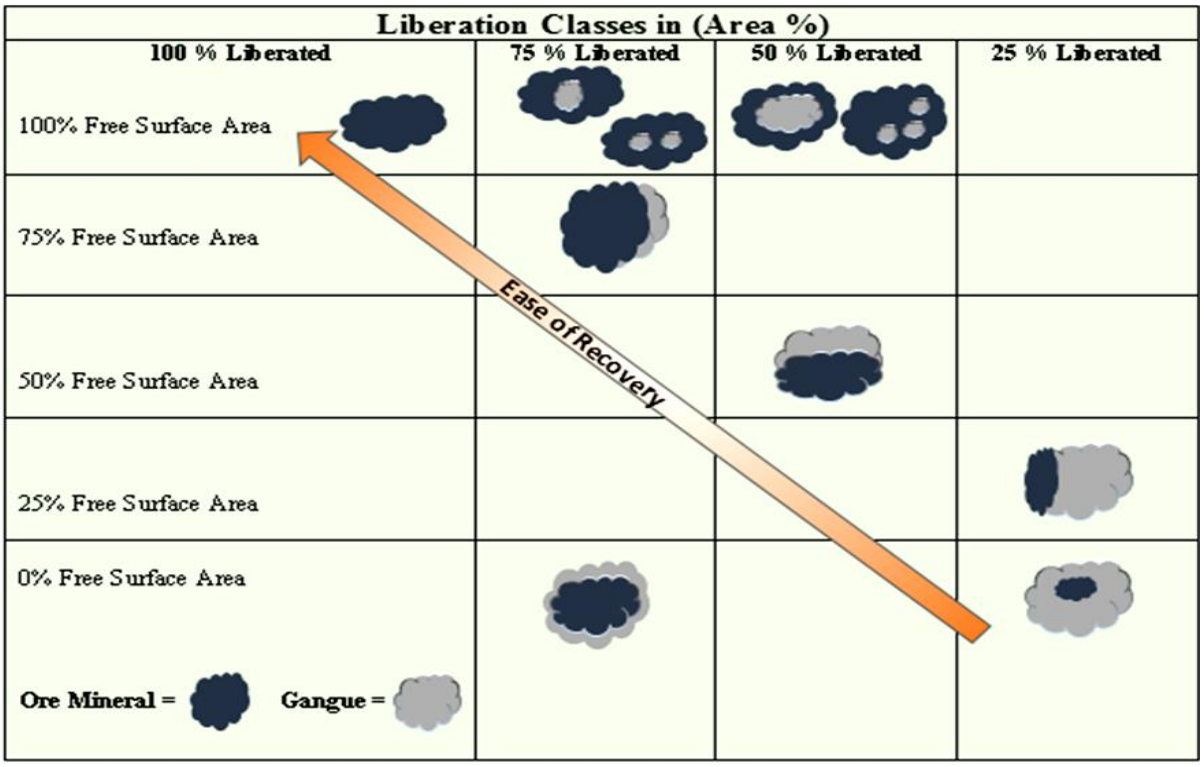


Figure 17: Ideal liberation classes (adapted from Cropp, 2013).

The analysis shows a high percentage of monazite ~91% and ~78% of zircon as liberated (i.e. >80% surface exposure. Completely liberated monazite (i.e. 100% exposed surface) in this case equates to completely liberated monazite in terms of grade, i.e. entire particles are composed of monazite only. Therefore, 91% of monazite reporting to the completely liberated category in terms of surface exposure, will also hold for liberation in terms of grade. Xenotime shows ~39% reporting to the completely liberated category, with 33% reporting to the locked category. The overall liberation results indicate a very good liberation of the abundant REE containing minerals (**Table 13** and **Figure 18**)

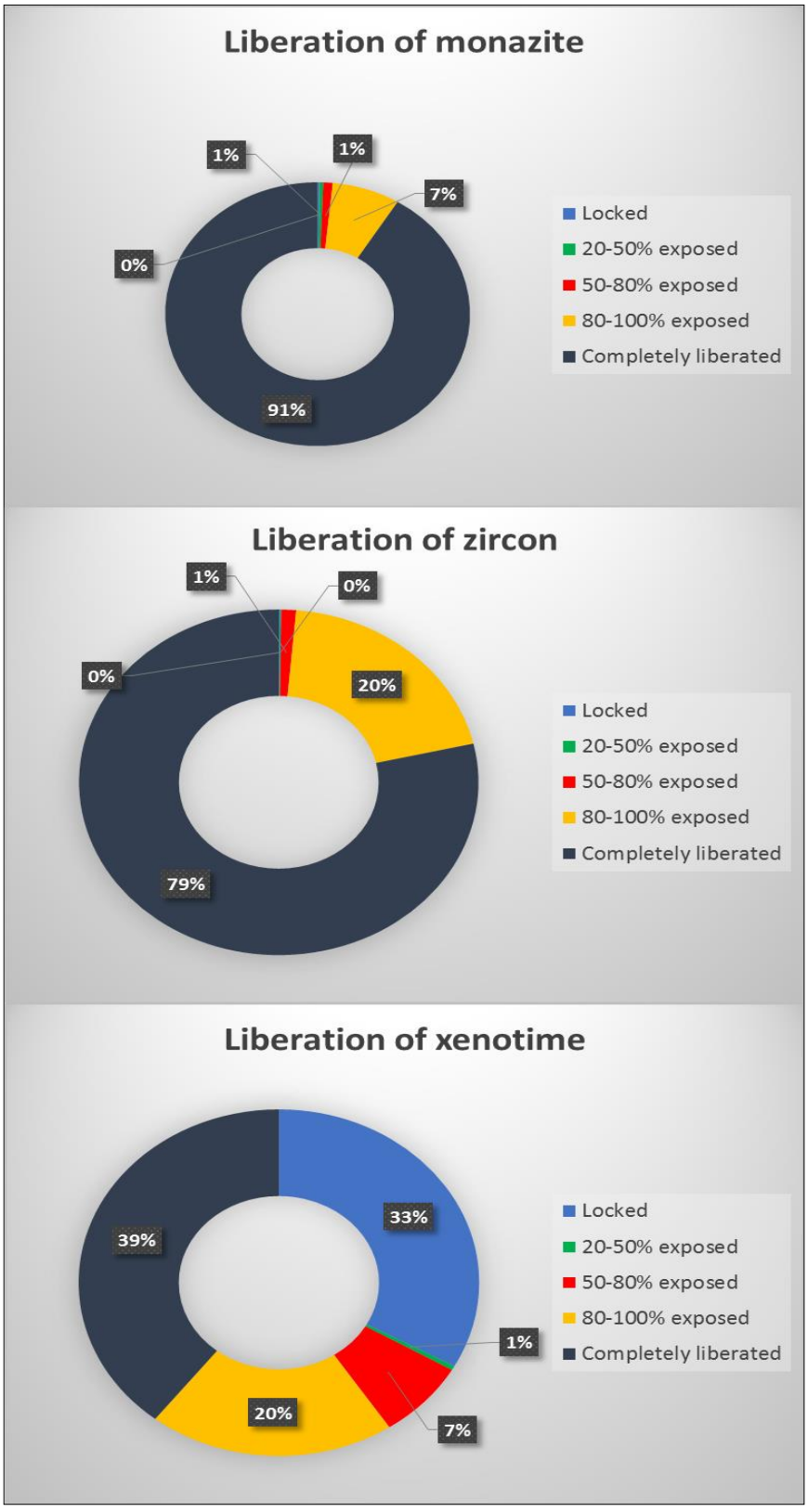


Figure 18: Liberation analysis of REE containing minerals.

Table 13: Liberation analysis of REE containing minerals by free surface %

Liberation category	Monazite	Xenotime	Zircon
Locked	0	33	0
20-50% exposed	0.5	0.5	0.1
50-80% exposed	1	7.3	1.1
80-100% exposed	7.21	19.9	20
Completely liberated	91.2	39.4	78.6
Total	**100**	**100**	**100**

4.2.6.4. Elemental Deportment of REE species

Elemental deportment entails the comprehensive understanding of minerals that contribute to grade, as well as penalty elements that can affect the efficiency of processing or affect the value of the final concentrate or cause environmental concerns with tailings storage.

Mineral/elemental deportment mainly aids in the understanding of which minerals actually contribute to grade, as each mineral is likely to behave differently to comminution, flotation or leaching.

For deportment calculations, the mass percent data for each mineral species is used together with the elemental content in the minerals (EMPA or literature compositions). Deportment calculations are used to give an indication of the relative contribution of the different minerals to the total selected elemental budget of the sample. Deportment indicates which minerals are the dominant contributors of element of interest in the sample.

REE deportment shows that various minerals contain one or more rare earth elements in their structure. Monazite is the main contributor of Ce, La, Nd, Sm and Pr. Zircon mainly contributes Eu, Ho, Gd and amounts of Dy. Zircon, Xenotime and monazite are all contributors of yttrium (**Figure 19** and **Table 14**).

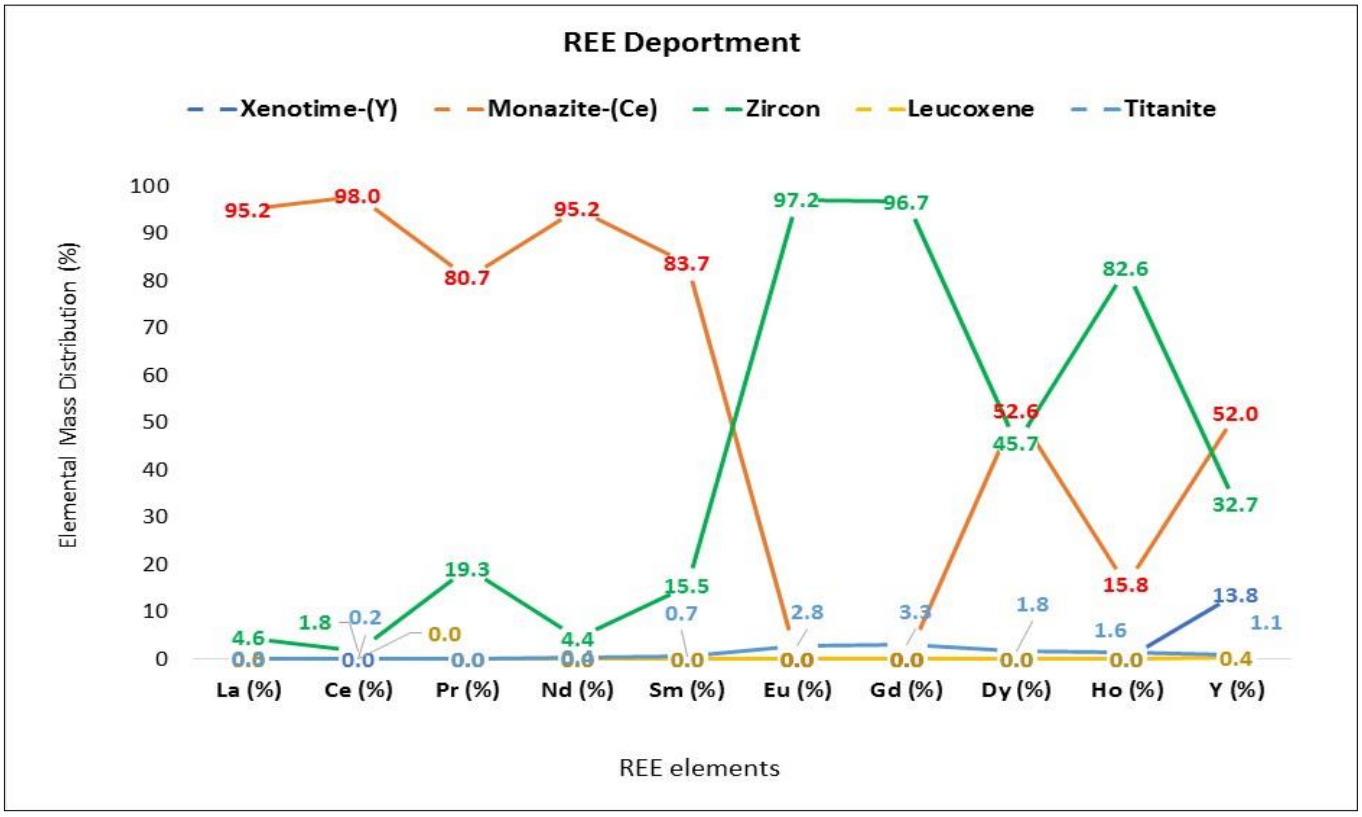


Figure 19: Deportment of REE containing minerals of the bulk sample

Table 14: Deportment of REE containing minerals of the bulk sample.

Mineral	La (%)	Ce (%)	Pr (%)	Nd (%)	Sm (%)	Eu (%)	Gd (%)	Dy (%)	Ho (%)	Y (%)
Xenotime	-	-	-	-	-	-	-	-	-	13.8
Monazite	95.2	98.0	80.7	95.2	83.7	-	-	52.6	15.8	52.0
Zircon	4.6	1.8	19.3	4.4	15.5	97.2	96.7	45.7	82.6	32.7
Leucoxene	-	-	-	-	-	-	-	-	-	0.4
Titanite	0.3	0.2	-	0.4	0.7	2.8	3.3	1.8	1.6	1.1
Total	100	100	100	100	100	100	100	100	100	100

4.2.6.5. Grain size distribution of REE species

Grain sizes are presented in terms of equivalent sphere diameter (ESD), which represents the diameter of a sphere of equal volume to the grain measured. The grain size distribution shows the size classes where most or even less amounts of grains are distributed.

The majority of monazite, zircon and xenotime reports in grain size class –150µm and below. Given their high liberation, and the large number of grains analysed (particularly for zircon and monazite), this shows that a high percentage of this ore is highly concentrated and naturally upgraded in this grain size range for monazite and zircon. The REE containing minerals in this sample are generally fine, with major grains of these REE minerals well distributed at –150µm and below size classes **(Figure 20, Figure 21** and **Figure 22)**

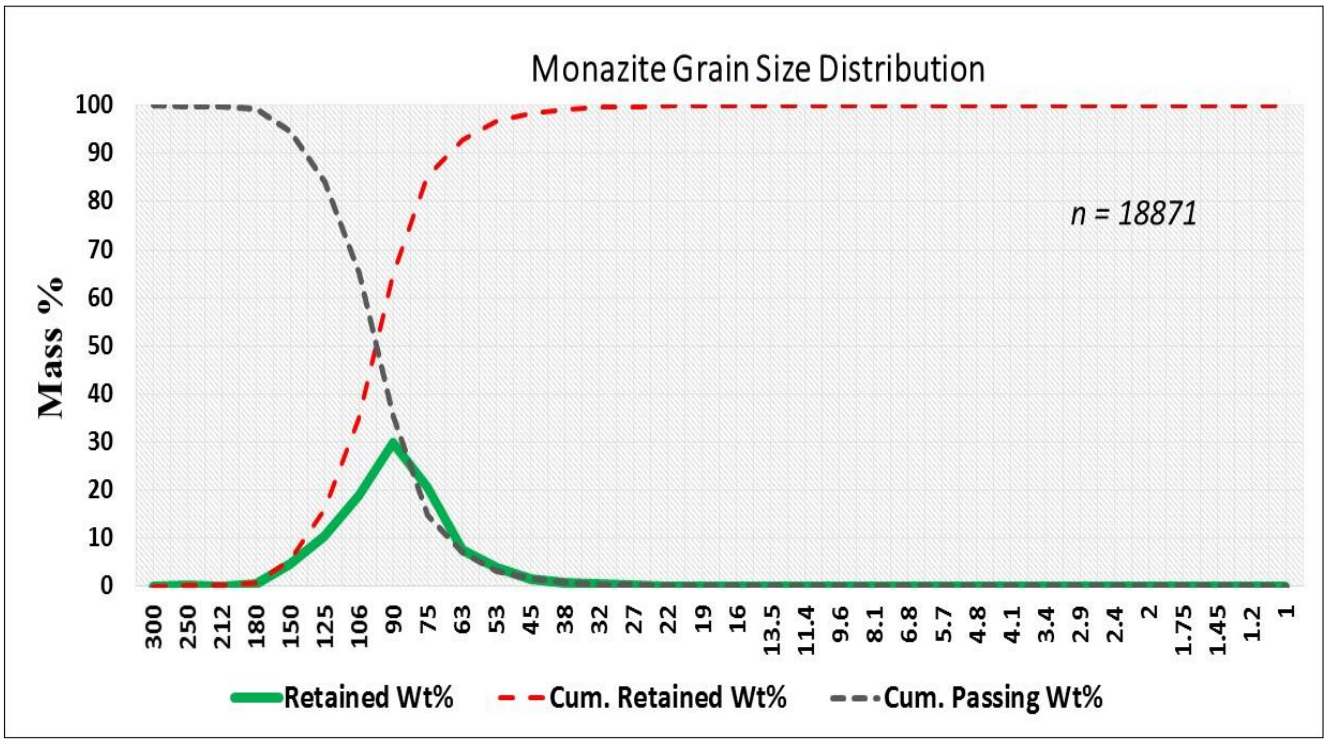


Figure 20: Monazite grain size distribution, *n* = number of grains measured

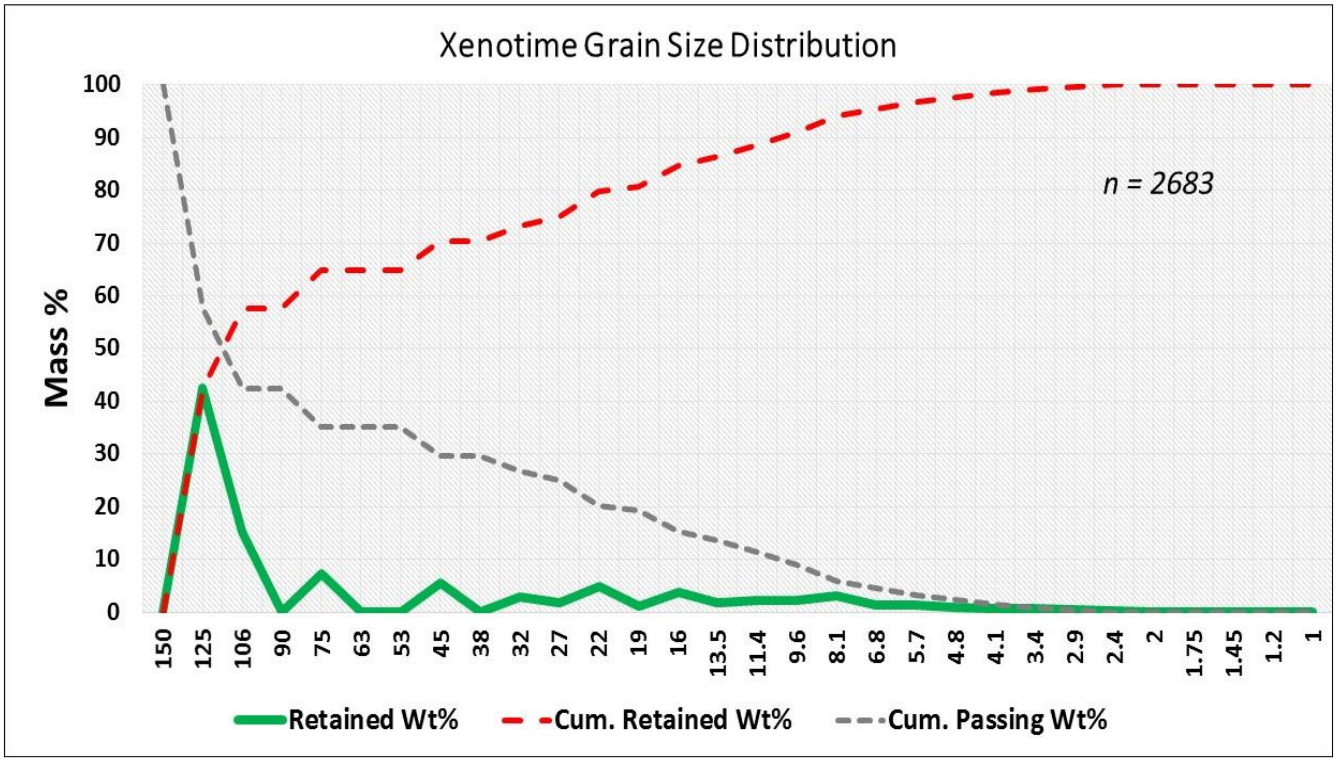


Figure 21: Xenotime grain size distribution, *n* = number of grains measured

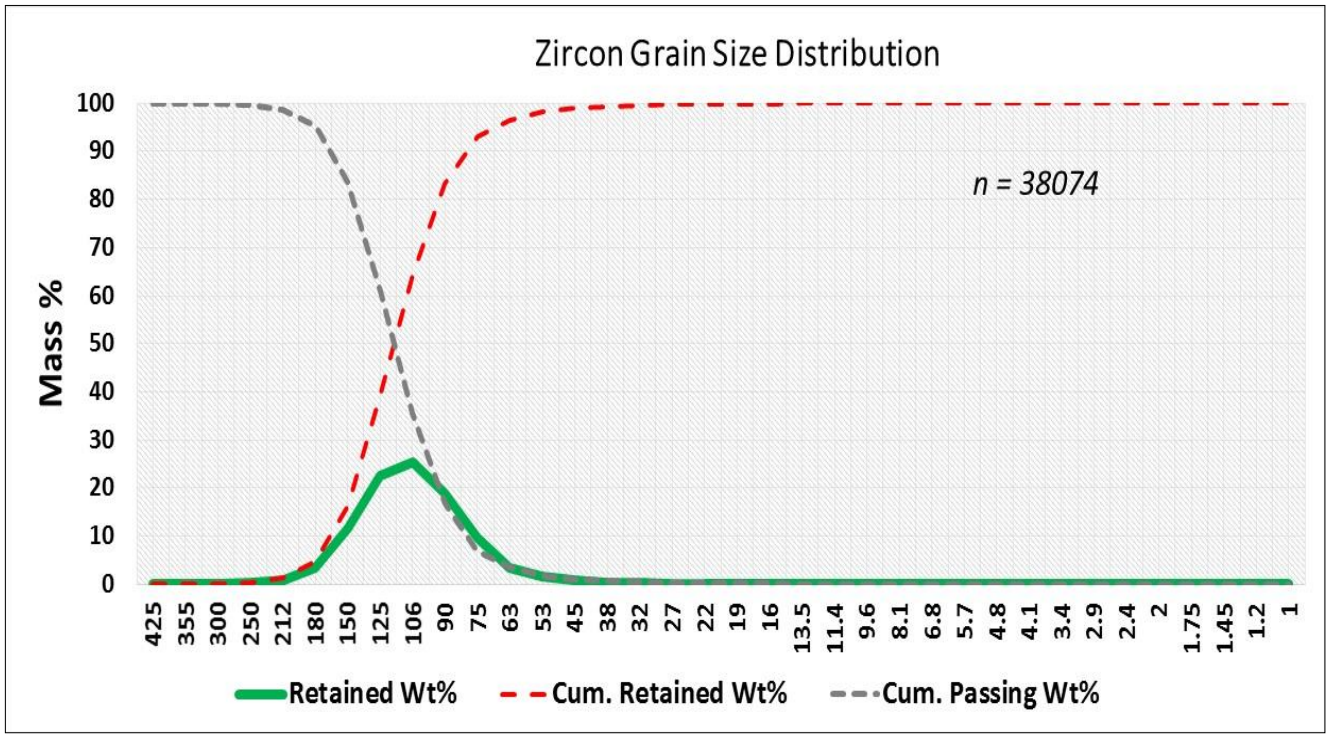


Figure 22*:* Zircon grain size distribution, *n* = number of grains measured

4.3. Summary and discussion

The feed characterisation results showed that a combination of mineralogical tools or techniques is capable of achieving extensive information on the characterisation of the ore. Based on the mineralogical results, epidote and amphibole are the dominant minerals in the sample, with zircon and monazite prevalent in the finer fractions. These minerals and other heavy minerals were investigated for their REE content as a potential resource from an existing placer or beach sand operation.

Based on some of the minerals identified in this sample, the mineral findings correspond with the studies carried out by (Spicer *et al.*, 2008), on the analysis of heavy minerals by quantitative XRD and MLA. In this study and that of (Spicer *et al.* 2008), the mineralogy results show similarities in the minerals detected. Monazite is observed as the prominent REE-bearing mineral. Amongst other techniques employed in this study, EMPA was able to detect REE content in minerals other than monazite. Other studies from literature have showed that REE content is mainly detected by means of LA-ICP-MS (Lehtonen, 2005), where present in trace amounts in minerals. The LA-ICP-MS technique was not used in this case.

Zircon, rutile, garnet (i.e grossular and almandine), ilmenite and quartz were also detected. Epidote and amphibole populate the coarser size fractions (+212µm and –212+150µm) in mineral abundance, whereas the finer size fractions consist mainly of zircon and monazite. Smaller quantities of rutile, amphibole, epidote, ilmenite and garnet were observed in these finer fractions. The abundance of monazite and zircon grains increases with the decrease in size classes, whereas epidote, amphibole and other silicates increase with the increase in size classes.

Quartz is present in trace amounts in this sample. The presence of quartz in trace amounts is typical, as the tailings sample emerged from a series of processing stages in which quartz was removed. Leucoxene was also detected in trace amounts by means of EMPA. Leucoxene is an alteration product of titaniferous minerals, and has also been removed for titania production.

Two types of leucoxene were detected in this study; the ordinary Ti altered leucoxene and the Nb containing leucoxene. Other authors such as Philander and Rozendaal (2009) classified the Nb-Ti altered mineral as ilmenorutile. Ilmenorutile as described by Philander and Rozendaal (2009) comprises significant amounts of Nb (~19%), whereas the mineral classified as Nb leucoxene in this study comprises Nb ranging from 5 to 8 wt. %.

The few grains of leucoxene that were detected with EMPA showed that leucoxene contains yttrium –"a HREE" in its crystal lattice incorporated through substitution of Fe^{3+} or elements with a $^{3+}$ oxidation state. In addition, zircon, titanite and almandine also contain amounts of REE in their crystal lattice; confirmed by means of EMPA. The REE in zircon, titanite and almandine are in a form of HREE and LREE. Other minerals identified by EMPA are rutile, epidote, amphibole; none of these minerals showed any traces of REE.

Studies on Namakwa sands by Philander and Rozendaal (2009) suggested that zircon occurs as three types, namely: -

- Clear (translucent) zircon
- Coloured zircon
- Metamict zircon

Only one type of zircon was identified by its chemical composition and not morphologically in the present study. This type of zircon identified displays multiple concentrations of REE in its crystal lattice. The amounts of REE ranged from 0.05 to 0.16 wt%. However, the theoretical zircon has consistent major element chemistry and a whole range of trace elements that can be incorporated through coupled substitution in the crystal lattice. Hafnium is one of the common substitutions in zircon, (Philander and Rozendaal 2009). In this study zircon did not show any Hf substitutions but that of La, Ho, Ce, Pr, Nd, Sm, Dy, Eu, and Y.

The quantitative mineralogical studies were used to quantify the REE species and their abundance in detail. Though the integration of XRD, Zeiss SEM and EMPA did provide mineralogical information, the MLA was able to show the actual amounts of the REE containing species. The MLA showed that monazite, zircon and xenotime had significant REE amounts compared to almandine, titanite and leucoxene.

Mineral association data showed that monazite and zircon have free surfaces. This means that these minerals are well liberated and therefore there is no need to mill or crush in order to liberate the REE containing minerals from gangue and other minerals. In general, the whole sample showed a very good liberation of zircon and monazite. Very few REE containing grains were associated with gangue, with majority of the gangue minerals such as epidote, amphibole and grossular highly liberated in the coarser size fraction. Numerous grains of xenotime appeared to have been locked in other minerals and reporting to the 20-50% and 50-80% exposed categories. Approximately 33 % of xenotime was locked in other minerals. The overall liberation results indicated a very good liberation of the major REE containing minerals.

In terms of grain size distribution, majority of monazite, zircon and xenotime reports in size class –150µm and below. This shows that a high percentage of this ore is highly concentrated and naturally upgraded in this size class. The REE containing minerals in this sample are generally fine; this is seen through the grains of the major REE minerals well distributed at –150µm.

Zircon and monazite are well liberated, with the majority of these minerals distributed in the–150+106µm and –106µm size fractions. Approximately 50 mass% of the sample constituting the two fractions has concentrated monazite and zircon. The naturally concentrated monazite and zircon in these size fractions showed that this fraction does not require ore upgrading and is amenable to direct leaching.

Though xenotime contained REE, it was disregarded for further hydrometallurgy testwork due to its low amounts in the total sample. Therefore, following the mineralogical findings, the two size fractions (–150+106µm and –106µm) were composited and subjected to hydrometallurgical treatment for REE extraction with monazite and zircon as the main REE target minerals.

5. CHAPTER 5 – CHARACTERISATION OF LEACH FEED AND PRODUCTS

5.1. Introduction

Chapter 5 follows the same format as the previous chapter. It is a continuation of the studies and findings observed in **Chapter 4**. In **chapter 4** it was stated that approximately 50 mass % of the sample reported to the two size fractions (i.e –150+106µm and –106µm), concentrating monazite and zircon (**Table 15**, taken from **Chapter 4**).

The two size fractions: –150+106 µm and –106µm were composited, and a mass of 400 grams (100% passing 45µm) was prepared for hydrometallurgical testwork. The naturally concentrated monazite and zircon in these size fractions showed that this fraction does not require ore upgrading and it is amenable to direct leaching. This chapter presents the results of the testwork performed on the composite fractions "as the leach feed", as well as a mineralogical assessment and chemical analysis of leach products from the different stages of leaching.

Table 15: Previous results of the bulk mineral assemblage of the sample

Mineral groups	Mineral	Chemical Formulae	Head	+212 µm	–212 µm	–150 µm	–106 µm
Mass distribution (in %)			**100**	**8.5**	**40.4**	**34**	**17.1**
REE-containing species	Monazite	$(Ce,La,Nd,Th)PO_4$	5.3	0.2	0.5	3.6	22.1
	Xenotime	YPO_4	<0.1	<0.1	<0.1	0.1	<0.1
	Zircon	$ZrSiO_4$.	31.3	4.7	8.4	45.8	61.6
	Almandine	$Fe_3Al_2Si_3O_{12}$	1.6	3.5	1.5	1.7	0.2
	Grossular	$Ca_3Al_2(SiO_4)_3$	1.2	2.2	1.3	1.2	<0.1
	Titanite	$CaTiSiO_5$	0.9	0.5	1.4	0.9	<0.1
	Thorite	$(Th,U)SiO_4$	0.1	0.1	<0.1	0.2	0.1
	Leucoxene		1.5	0.5	1.4	2.4	0.2
	Leucoxene_Nb		<0.1	<0.1	0.1	<0.1	<0.1

5.2. Chemical and mineralogy data of the REE leaching results

This section describes the chemical data of the composited sample, the mineralogical characterisation and chemical analysis of the leached products.

Table 16 provides the REE chemical analysis of the composite sample. The composite sample shows that the total rare earth element (TREE) content is 5.9%. Cerium, lanthanum and neodymium contribute most to the TREE owing to the abundance of monazite in the composite fraction.

Table 16: The REE Chemical analysis of the composited sample "leach feed"

Elements	Leach feed (in ppm)
Ce	25141
Dy	667
Er	345
Eu	67
Gd	1181
Ho	119
La	12389
Lu	68
Nd	10462
Pr	2693
Sc	30
Sm	1727
Tb	171
Tm	31
Y	3424
Yb	395
TREE in ppm	**58910**
TREE in %	**5.9**

5.2.1. Chemical assay of leach residues and filtrates

The leach residues and leachates (leach filtrates) from the three leaching stages as well as the washing test liquors were chemically analysed for their REE content. The bulk chemical analysis data was used for mass balancing and for extraction efficiency determination. The mass balance is presented in detail in **APPENDIX C.**

5.2.1.1. Chemical assay of leach residues

Representative sub-samples of the ten samples were taken by using the cone and quartering method and were assayed for individual REE. The elemental compositions of the residues are shown in this section. The TREE content of final caustic crack is 3.9% before washing. After washing stages the TREE % improved from 3.9% to 5.4% after repulp wash, and 5.5 % after the second repulp wash. The improvement in TREE% was as a result of the removal of Na entrains from NaOH in the residues (**Table 17).**

Table 17: Elemental composition of caustic cracking residues

Elements	Unit	Final Caustic crack residue	Caustic crack repulp wash 1	Caustic crack repulp wash 2	Caustic crack plug wash 3
Ce	ppm	16499	22810	23647	22967
Dy	ppm	458	622	643	643
Er	ppm	233	332	367	348
Eu	ppm	48.5	61	62	61.8
Gd	ppm	825	1038	1043	1052
Ho	ppm	90	122	126	126
La	ppm	8270	11284	11490	11221
Lu	ppm	47.4	67	71	69
Nd	ppm	6829	9360	9575	9376
Pr	ppm	1761	2420	2531	2446
Sc	ppm	15.7	25.4	29.7	27
Sm	ppm	1152	1509	1577	1542
Tb	ppm	116	148	149	153
Tm	ppm	30.9	44.5	44.7	46
Y	ppm	2360	3365	3509	3477
Yb	ppm	270	391	396	398
TREE in ppm	**ppm**	**390005.5**	**53598.9**	**55260.4**	**53952.8**
TREE in %	**%**	**3.9**	**5.4**	**5.5**	**5.4**

The TREE content of unwashed water leach test was 5.2% before water wash and after the water leach wash 1 test, the residue reading was 5.1% (**Table 18).**

Table 18: Elemental composition of water leach residues

Elements	Unit	Unwashed Water Leach Residue	Water leach Wash 1 Residue
Ce	ppm	22048	21453
Dy	ppm	614	594
Er	ppm	327	308
Eu	ppm	62	61
Gd	ppm	1050	1065
Ho	ppm	117	113
La	ppm	10899	10573
Lu	ppm	65	63
Nd	ppm	9060	8917
Pr	ppm	2349	2296
Sc	ppm	26	24
Sm	ppm	1510	1488
Tb	ppm	151	152
Tm	ppm	40	41
Y	ppm	3278	3076
Yb	ppm	376	361
Total in ppm	**ppm**	**51972**	**50585**
TREE in %	**%**	**5.2**	**5.1**

Table 19 shows the total rare earth content after HCl leaching and the subsequent washing stages. The TREE of the unwashed HCl residue is 3.1%, with varying amounts of TREE in wash test 1, 2 and 3.

Table 19: Elemental composition of HCl leach residues

Elements	Unit	HCl leach unwashed residue	HCl leach washed residue 1	HCl leach washed residue 2	HCl leach washed residue 3
Ce	ppm	13065	11955	10031	11294
Dy	ppm	476	489	442	468
Er	ppm	263	267	256	267
Eu	ppm	45	43	37.4	41
Gd	ppm	694	678	579	648
Ho	ppm	96	98	91	95
La	ppm	5400	4624	3633	4365
Lu	ppm	57	59	56	58
Nd	ppm	5225	4709	3866	4462
Pr	ppm	1351	1221	1016	1162
Sc	ppm	12.22	11	7.8	10.8
Sm	ppm	1004	951	811	915
Tb	ppm	110	116	103	108
Tm	ppm	36.7	38.3	36.4	37.5
Y	ppm	2426	2499	2340	2302
Yb	ppm	321	332	315	325
Total in ppm	**ppm**	30581.9	**28090.3**	**23620.6**	**26558.3**
TREE in %	**%**	**3.06**	**2.8**	**2.4**	**2.7**

5.2.1.2. Chemical assay of the leachates

A total of 12 filtrates or leachates were chemically analysed and the data obtained from chemical analysis was used for mass balance calculations and to obtain the extraction efficiencies and accountability information. Detailed results are presented in **APPENDIX C.**

The caustic cracking filtrates and water leach TREE % content is zero since the main aim of caustic cracking was to convert REE containing minerals into hydroxides. The chemistry and mineralogy of the residues did show that monazite was successfully converted into hydroxides by means of cracking the phosphate ion, similarly with water leaching test (**Table 20** and **Table 21**)

Table 20: Elemental composition of caustic (NaOH) cracking filtrate

Elements	Units	Caustic crack Final Filtrate	Caustic crack wash 1	Caustic crack wash 2	Caustic crack wash 3	Combined caustic crack wash
Ce	ppm	<0.1	<0.1	<0.1	<0.1	<0.1
Dy	ppm	<0.1	<0.1	<0.1	<0.1	<0.1
Er	ppm	<0.1	<0.1	<0.1	<0.1	<0.1
Eu	ppm	<0.1	<0.1	<0.1	<0.1	<0.1
Gd	ppm	<0.1	<0.1	<0.1	<0.1	<0.1
Ho	ppm	<0.1	<0.1	<0.1	<0.1	<0.1
La	ppm	<0.1	<0.1	<0.1	<0.1	<0.1
Lu	ppm	<0.1	<0.1	<0.1	<0.1	<0.1
Nd	ppm	<0.1	<0.1	<0.1	<0.1	<0.1
Pr	ppm	<0.1	<0.1	<0.1	<0.1	<0.1
Sc	ppm	<0.1	<0.1	<0.1	<0.1	<0.1
Sm	ppm	<0.1	<0.1	<0.1	<0.1	<0.1
Tb	ppm	<0.1	<0.1	<0.1	<0.1	<0.1
Tm	ppm	<0.1	<0.1	<0.1	<0.1	<0.1
Y	ppm	<0.1	<0.1	<0.1	<0.1	<0.1
Yb	ppm	<0.1	<0.1	<0.1	<0.1	<0.1
TREE %	**%**	**<0.1**	**<0.1**	**<0.1**	**<0.1**	**<0.1**

**<0.1= below detection limit (since this leaching stage was not aimed at dissolving REE)*

Table 21: Elemental composition of water leach filtrate

Elements	Units	water leach wash 1	Water leach Final filtrate
Ce	ppm	<0.1	<0.1
Dy	ppm	<0.1	<0.1
Er	ppm	<0.1	<0.1
Eu	ppm	<0.1	<0.1
Gd	ppm	<0.1	<0.1
Ho	ppm	<0.1	<0.1
La	ppm	<0.1	<0.1
Lu	ppm	<0.1	<0.1
Nd	ppm	<0.1	<0.1
Pr	ppm	<0.1	<0.1
Sc	ppm	<0.1	<0.1
Sm	ppm	<0.1	<0.1
Tb	ppm	<0.1	<0.1
Tm	ppm	<0.1	<0.1
Y	ppm	<0.1	<0.1
Yb	ppm	<0.1	<0.1
TREE %	**%**	**<0.1**	**<0.1**

**<0.1= below detection limit (since this leaching stage was not aimed at dissolving REE)*

The HCl leaching stage was aimed at dissolving the REE into the solution. The analysed leachates showed that there is a total of 0.67% TREE in the pregnant solution (PLS). The combined wash liquor from the HCl leaching test showed that the TREE% is 0.02 (

Table 22).

However, the mass balance was calculated using TREE that dissolved after the HCl leaching test, as shown in **APPENDIX D**.

Elements	HCl leach final filtrate (PLS)	HCl leach wash 1	HCl leach wash 2	HCl leach wash 3	HCl leach combined wash
Ce	**2842**	220	5.12	3.02	**82**
Dy	44.3	3.7	<0,10	0.47	1.65
Er	9.97	1.52	<0,10	0.93	1.14
Eu	6.04	0.47	<0,10	<0,10	0.183
Gd	117	9.06	0.23	<0,10	3.21
Ho	7.13	1.03	<0,10	<0,10	0.721
La	**1678**	139	4.21	1.26	51.3
Lu	2.36	0.142	<0,10	<0,10	0.031
Nd	**1270**	94.4	1.45	0.55	35.4
Pr	323	25	<0,10	<0,10	10.2
Sc	2.08	0.178	<0,10	<0,10	0.071
Sm	170	12.7	0.163	<0,10	4.81
Tb	11.4	0.879	<0,10	<0,10	0.32
Tm	0.86	0.042	<0,10	<0,10	<0,10
Y	232	19.2	<0,10	<0,10	7.3
Yb	14.4	1.12	<0,10	<0,10	0.41
TREE in ppm	**6730.54**	**528.44**	**11.17**	**6.23**	**198.75**
TRE in %	**0.67**	**0.05**	**<0.01**	**<0.01**	**0.02**

Table 22: Elemental composition of HCl selective leaching.

**Elements highlighted in red are hosted by monazite and its products*

5.2.2. Mineralogical characterisation of REE leach residues

The mineralogical characterisation was undertaken on a total of ten residues. These included the residues from each individual leaching test and the washing stages. Owing to the nature of the residues, it should be noted that SEM-EDS analyses were conducted on stub mounts of the residues, not on polished sections. The data are therefore viewed in a qualitative light, for comparative purposes.

5.2.2.1. Mineralogy of caustic (NaOH) cracking residues

The mineralogy of the caustic cracking residues is presented on the next page with BSE images taken to illustrate elemental compositions of the sample after it was treated with NaOH.

The NaOH cracking was carried out at different time intervals at a constant temperature of 140̊ °C. The NaOH crack residues were studied and the findings showed that the phosphate ion was successfully cracked from the monazite, likely into trisodium phosphate and Ce, La, Nd(OH), as shown by this reaction:

$$\mathbf{(REE, Th, U)PO_4 + NaOH \rightarrow (RE, Th, U)OH + Na_3PO_4} \qquad \mathbf{5.1}$$

However, the zircon grains did not appear to have reacted with NaOH (see **Figure 23**) as seen on NaOH crack BSE images on grains number 3 and 5).

Subsequent to NaOH cracking, the residues were washed three times in order to remove the entrained NaOH solution prior to water leaching and HCl leaching. The two repulp washing results of the residue show a general decrease in sodium (Na) content related to NaOH, in contrast to the Na content of the unwashed NaOH cracked residue (**Table 23**).

The zircon grains did not show any form of reaction with NaOH; observed by high Zr and Si values, very similar to the original and theoretical values of zircon composition. (**Figure 23**). The third wash, which was the plug wash, was aimed to further remove NaOH solution entrained in the residue. After the third wash, the residue appeared to have the same or unchanged effects as the two repulp washes. The removal of NaOH across three washes yielded similar results in terms of Na content (**Table 23**).

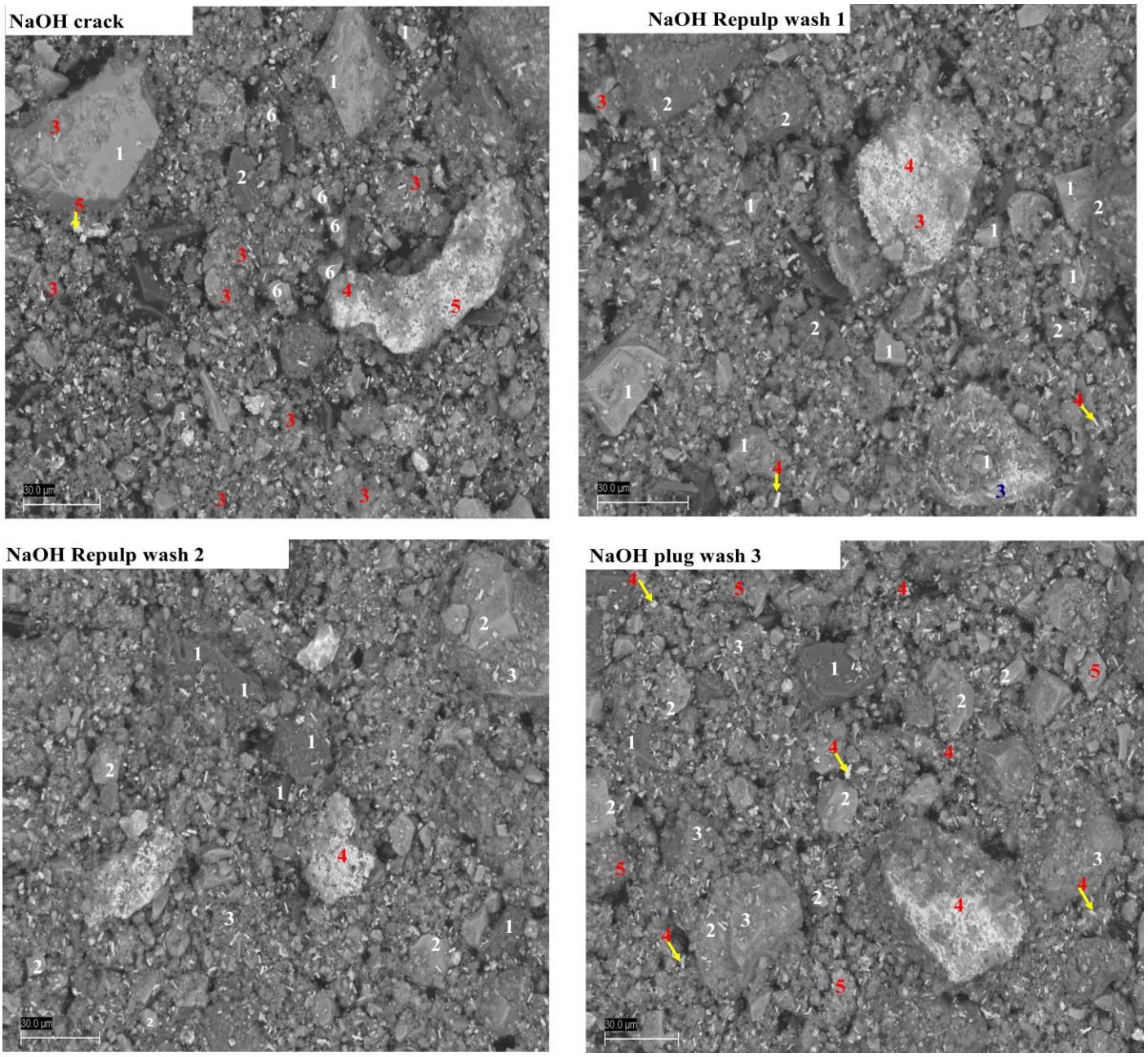


Figure 23: BSE images of residues from caustic cracking and washing tests; the numbered labels represent the analysed points for which average compositions are given in **Table 23**.

Table 23: Averaged chemical compositions from the analysed points of residues from caustic cracking and washing tests (wt %) on **Figure 23**. *Note: No phosphorus was detected.*

Samp	Anal	O	Na	Mg	Al	Si	Ca	Ti	Fe	Sr	Zr	La	Ce	Nd	Eu	Th	Com
NaO	1	19	13	1	1	3	2	8	3		8						Oxide
NaO	2	21	34	1		1	1	6	3		3		4				Oxide
NaO	3	28	5			10		1			40				0		Unrea
NaO	4	38	1	18	1	19	1	1	7								Silica
NaO	5	27	4			10		2			38						Unrea
NaO	6	21	6			4	1	10	4		17						Oxide
NaO	7	16	10			1	0	5	3		3	8	17	7		3	Crack
NaO	8	25	5		5	8	4	3	12		3	2	4	2		0	Crack
NaO	9	9				1					1	13	25	8		4	Crack
NaO	10	12	5			1					1	15	26	8		5	Crack
NaO	1	32				13					50						Unrea
NaO	2	38	2	9	7	17	9	2	5								Silica
NaO	3	23	9	1	0	3	2	17	7		7						Oxide
NaO	4	18	8	1		3	1	7	4	0	6		9	4		3	Crack
NaO	5	14	6			4	0				2	8	17	9		8	Crack
NaO	6	31				12		2			46						Unrea
NaO	1	30	1			11		3			43				1		Unrea
NaO	2	38	3			1	1	50	5		2						Oxide
NaO	3	20	7	1		2	1	10	5		5	9	13	5		3	Crack
NaO	4	13	5			2	0		2		2	15	22	6		4	Crack
NaO	1	39		6	12	16	8		10								Silica
NaO	2	28	1			10		1	1		41						Unrea
NaO	3	26	4	0		7	1	7	4		27						oxide
NaO	4	14	3			2		2			4	12	23	9		4	Crack

5.2.2.2. Mineralogy of water (H_2O) leach residues

The water leach test was carried out at 60 °C for 4 hours. The mineralogy result shows that the REE containing phases are compounds containing a mixture of Ce, La and Th with Al, Mg, Si, Ca and Fe (**Figure 24** and **Table 24**).

The zircon grains also remained unreacted from this procedure; this is expected since zircon failed to react at a higher temperature of 140 °C with NaOH. The SEM analysis confirmed the presence of Eu in some of the zircon grains.

The water leach residue and its repulp wash residue showed no notable differences, except a slight decrease of Na in the washed residues (**Table 24**).

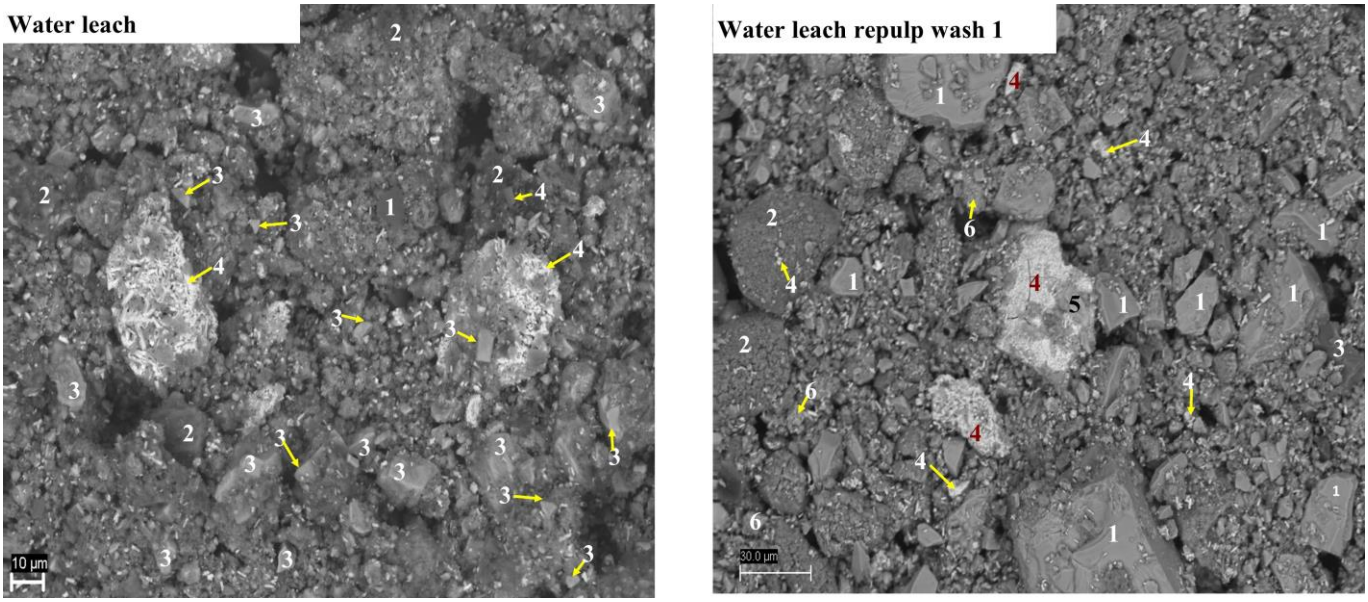


Figure 24: BSE images of residues from water leaching and washing tests; the numbered labels represent the analysed points for which average compositions are given in **Table 24**.

Table 24: Averaged chemical compositions from the analysed points of water leaching and washing test residue (wt %) on **Figure 24**. *Note: no phosphorus was detected*.

Sample	Analysed	O	Na	Mg	Al	Si	Ca	Ti	Fe	Sr	Zr	La	Ce	Nd	Eu	Th	Comments
Water Leach	1	40		14	1	22	4	1	10								Silicate
Water Leach	2	27				11		1			42						Unreacted zircon
Water Leach	3	24	5	0	0	5	1	12	6		14		2				Oxide
Water Leach	4	13	2		0	1		2				14	29	9		6	Cracked
Water Leach repulp Wash	1	23				9					36						Unreacted zircon
Water Leach repulp Wash	2	29	7	1	0.	2	2	29	8		4						Oxide
Water Leach repulp Wash	3	24	1		7	8	10	3	5		3						Oxide
Water Leach repulp Wash	4	21	2		0	5	0	3	1		4		8	5		6	Oxide
Water Leach repulp Wash	5	25				10		1			38				0		Unreacted zircon
Water Leach repulp Wash	6	25	4	1	0	7	1	8	3		22		3			2	Oxide

5.2.2.3. Mineralogy of selective (HCl) leaching residues

The final water leach repulp washed residue was subjected to HCl leaching for 4 hours, at a pH of 3 under ambient temperature and varying redox potential. The HCl leach and its subsequent washes were successful in removing remnant Na from the water washed residue. A decrease was observed in La, Nd, and Ce content, relative to the first two stages (**Table 23** and **Table 24**), indicating successful removal of the filtrate by the HCl leaching. Concentrations of Th were high compared to the Th concentrations in residues of the first two leaching stages. Some of the REE containing phases also showed associations with Al, Si, Ca, Mg and Fe compounds (shown in **Figure 25** and **Table 25**).

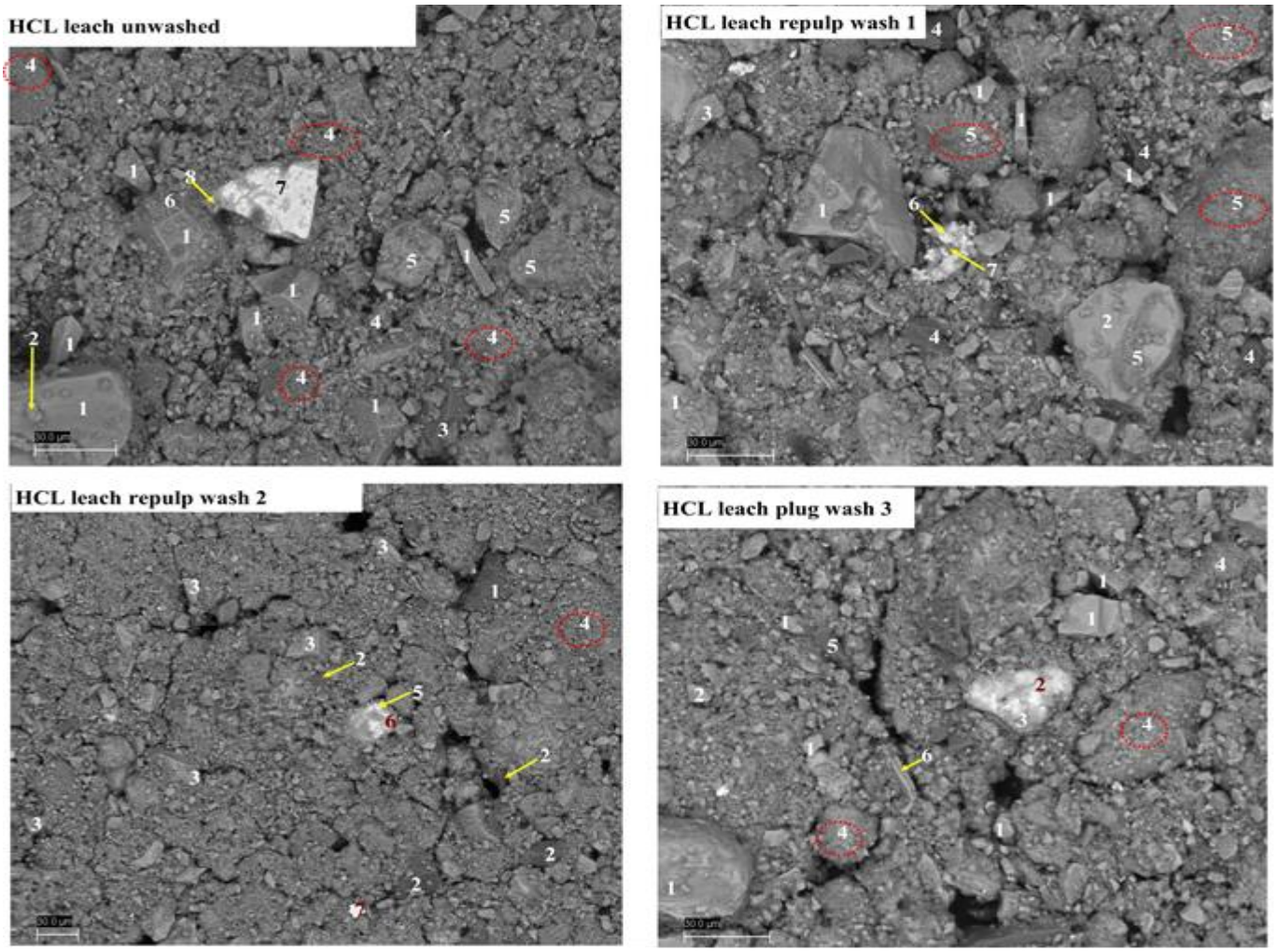


Figure 25: BSE images of residues from HCl leaching and washing tests; the numbered labels represent the analysed points for which average compositions are given in **Table 25**. The circled labelling indicates fine grained phases.

Table 25: Averaged chemical compositions from the analysed points of HCl leaching and washing test residues (wt %) on **Figure 25**. *Note no phosphorus was detected*.

Sample	Analysed	O	Na	Mg	Al	Si	Cl	Ca	Ti	Fe	Zr	La	Ce	Nd	Th	Comments
HCl leach unwashed	1	23				9					36					Unreacted zircon
HCl leach unwashed	2	24				7	1	0	7	3	27					Oxide
HCl leach unwashed	3	34			12	14		15		7						Silicate
HCl leach unwashed	4	23	1		1	4	1	0	16	6	12				1	Oxide
HCl leach unwashed	5	23		0	0	7	1	0	5	3	27		2			Oxide
HCl leach unwashed	6	14	0	1	0	3	1	0	2	1	5		3	2	43	Oxide
HCL leach unwashed	7	12	0	0	0	2	1	0	1	1	4		3	2	43	Oxide
HCl leach unwashed	8	21	1	1	0	4	1	0	11	6	10		4	2	13	Oxide
HCl leach wash 1	1	27		0	0	8			9	7	27					Oxide
HCl leach wash 1	2	25				9			2	1	36					Unreacted zircon
HCl leach wash 1	3	24				8			4	2	33					Unreacted zircon
HCl leach wash 1	4	38			14	15		15		8						Silicate
HCl leach wash 1	5	24				2			23	17	4				0	Oxide
HCl leach wash 1	6	20				1		0		1		9	17	6	3	Cracked monazite
HCl leach wash 1	7	18				3		0		2		8	14	6	3	Cracked monazite
HCl leach wash 2	1	39		10	1	21		12	1	7						Silicate
HCl leach wash 2	2	30			9	11		17		9						Oxide
HCl leach wash 2	3	25				10					39					Unreacted zircon
HCl leach wash 2	4	22				5			16	8	13				1	Oxide
HCl leach wash 2	5	13				2			5	3	4		17		11	Cracked Monazite
HCl leach wash 2	6	12				2			5	2	5		13		11	Cracked monazite
HCl leach wash 2	7	16				3			6	3	8		4		31	Cracked monazite
HCl leach wash 3	1	25				10					39					Unreacted Zircon
HCl leach wash 3	2	18			0	4		0	3	2	9	4	8	3	24	Cracked monazite
HCl leach wash 3	3	18				3			9	5	7		7		18	Cracked monazite
HCl leach wash 3	4	23				6			11	5	20				1	Oxide
HCl leach wash 3	5	28			7	9		12	5	8	2					Oxide
HCl leach wash 3	6	29				11			4	2	39					Unreacted zircon

5.2.3. Extraction Efficiency

The detailed mass balance, calculations and extraction efficiencies are presented in

APPENDIX C and **APPENDIX D**. **Table 26** shows the summary of REE extraction. The TREE leach efficiency is 55%, indicating that 55% of REE dissolved, thus showing a good extraction since the samples did not undergo any stages of ore upgrading to concentrate the sample prior to leaching.

Dissolution took place during HCl leaching. The extraction summary results are mainly focused on HCl leach since NaOH cracking and water leach aided in breaking down of phosphate ion prior to HCl leaching.

Table 26: Summary of REE extraction

Test description	NaOH cracking	Water leach	HCl leach
Temperature, °C	144	61	21.4
Mass loss, % (m/m)	6	0	15
TREE concentration, mg/L	0	0	6731
TREE leach efficiency, %	0%	0%	**55%**
Total Acid added, kg/t solids	n/a	n/a	213
Total Acid Consumption, kg/t solids	n/a	n/a	213

5.3. Summary and discussion

In this section, one of the objectives was to explore possible ways of extracting REE by introducing mineralogical characterisation of the ore before embarking on any REE extraction processes. Detailed mineralogical investigation showed that the two smaller size fractions of the initial sample were naturally concentrated in monazite and zircon; two major carriers of REE, and were amenable to direct leaching. This shows the value of introducing mineralogical characterisation of the ore, before embarking on any REE extraction processes, which can have a great significance in cost cutting.

Subsequent to hydrometallurgy testwork, the two composited size fractions showed that after NaOH cracking of monazite, the phosphate ion of monazite was successfully removed. Although NaOH is highly reactive with monazite, the three washing tests showed that the NaOH did not react with zircon.

The unreacted zircon demonstrated that the NaOH leaching temperature is sufficient for phosphate ion cracking but not for the silica within the zircon structure ($ZrSiO_4$), as evident by the consistent ratio of Zr: Si in the EDS analyses, see **APPENDIX E: calculated Zr/SI ratio**. During the NaOH cracking process, it was anticipated that the NaOH will decrease with each wash; however, both plug and the two repulp washed residues returned similar phase chemistries, based on mineralogical observations of Na content.

The water leaching test of the residue from cracking advanced the removal of NaOH solution that initially reacted with the sample, likely converting the cracked monazite into hydroxides. The SEM images and **EDS** (energy dispersive X-Ray Spectroscopy) analysis also showed that the REE containing phases were also associated with a mixture of Al, Si, Ca and Fe compound. The residues from selective HCl leaching and washing show that remnant Na from NaOH was entirely removed during this leaching stage.

The decrease in REE content of phases from the second to the third stage (i.e. water leach to HCl leach) indicated that REE dissolution by HCl took place. This was also confirmed by chemical analysis.

The chemical analysis of REE on both residues and leachates aided in undertaking the mass balance, extraction efficiencies and the accountability calculations in the HCl leaching test. The TREE leach efficiency and accountability was calculated according to all the REEs determined. However, in this study, the extraction efficiency of 55% represent that of TREE calculated according to the **Feed solids "in**" that of the required mass of dry solids prior to HCl leaching and the **leach residue "out**" presented in **APPENDIX D**.

An extraction efficiency of 55% is good since the samples did not undergo any stages of ore upgrading to concentrate the sample prior to leaching. In conclusion, since zircon did not react under the same conditions as monazite, zircon was further and separately investigated for REE extraction. The results are discussed in the next Chapter.

6. CHAPTER 6 – CHARACTERISATION OF ZIRCON

6.1. Introduction

As described in Chapters 4 and 5, the naturally upgraded –150µm fraction was subjected to three stages of hydrometallurgy testing, namely; caustic cracking, water leaching and HCl leaching. Caustic cracking is the decomposition of REE using NaOH solution, with the aim to break down the phosphate ion of monazite. The mineralogical examination of the residues from different leach stages showed that monazite was successfully cracked and the REE were released to solution in the final leaching stage. Zircon was not as reactive under the conditions used, and REE release was not expected from this mineral.

As a result of zircon not reacting under the same conditions as monazite, further investigations were conducted on the zircon sample. This chapter sums up the work that was carried out in order to explore REE yields from zircon. The work involved the decomposition of zircon prior to leaching testwork.

Zircon was targeted as the alternative resource of REE, since EMPA data showed that zircon contains fewer REE in its crystal lattice and this REE are different from the REE in monazite. However, zircon is one of the prominent minerals originating from the beach placer deposit. Zircon is a valuable mineral used as a raw material in various industries including foundry, ceramics and refractories (Ruble and Heuer 1984).

Zircon is one of the most stable chemical compounds due to the strong bond between zirconia and silica in its molecule. Therefore, any extraction for zirconium metal or other useful zirconium compounds must start with the breakdown of such bonds. The breakdown of zircon using the alkali fusion method is a well-known technique and can be more favourable than using traditional chlorination. There are few commercial valuable methods to break down zircon. The common methods are discussed below.

6.1.1. Alkali fusion

It is well known that zircon is decomposed at high temperature in reducing media. The decomposition temperature, however, is lowered when the silicate is mixed with fluxing agents such as NaOH, Na_2CO_3 and CaO+MgO (El-Barawy *et al*., 2000) The degree of decomposition depends on parameters such as particle size of zircon, alkali/zircon molar ratio and temperature (Biswas *et al*., 2010). By careful control of the process parameters, the following reaction products are obtained with zircon decomposition either with NaOH or Na_2CO_3;

$$\mathbf{ZrO_2.SiO_2 + 4NaOH \rightarrow Na_2ZrO_3 + Na_2SiO_3 + 2H_2O} \qquad \mathbf{6.1}$$

Or

$$\mathbf{ZrSiO_4 + 2Na_2CO_3 \rightarrow Na_2ZrO_3 + Na_2SiO_3 + 2CO_2}$$

Subsequent to alkali fusion during leaching, hydrolysis of sodium silicate (**Na_2SiO_3**) and sodium zirconate (**Na_2ZrO_3**) takes place (Abdel-Rehim, 2005). The impure hydrated zirconia is dissolved in concentrated HCl, HNO_3 or H_2SO_4 at 80 ^oC for obtaining a zirconyl chloride, nitrate or sulfate solution, respectively (Biswas *et al*., 2010; Abdel-Rehim, 2005). These solutions are then purified either by precipitation as basic zirconium sulfate or by crystallization as the corresponding zirconium salt.

6.1.2. Lime fusion technique

Lime fusion is conducted when a mixture of different proportions of $ZrSiO_4$, and calcium oxide is heated at various temperatures. The products; calcium zirconium silicate, calcium zirconate and calcium silicate are formed:

$$\mathbf{ZrO_2.SiO_2 + CaO \rightarrow CaZrSiO_5} \qquad \mathbf{6.2}$$

Or

$$\mathbf{ZrO_2.SiO_2 + CaO \rightarrow ZrO_2 + CaSiO_3} \qquad \mathbf{6.3}$$

Subsequent to lime fusion, the reaction (**6.3**) is amenable to HCl leaching at 90 ^0C accompanied by caustic leaching at 15 ^0C (Manhique *et al*., 2003).

6.1.3. Plasma decomposition technique

This process involves decomposing of zircon particles using a stable argon plasma reactor at a temperature ranging from 600–1500 ^{0}C. The dissociation of zircon takes place by oxidizing zircon, i.e. ZrO_2 and SiO_2 (Syamaprasad *et al*., 1993). The degree of dissociation depends on a number of process parameters, e.g. the particle size of zircon, flow rate of argon gas, arc current, feed rate, etc. The decomposed mass is treated with NaOH or H_2SO_4.

6.1.4. Thermal dissociation technique

The dissociation of zircon takes place in an arc furnace or an electric reactor, heated at high temperature above 1750 ^{0}C (Syamaprasad *et al*., 1993) accompanied by rapid cooling. The dissociation process aims to convert the heated zircon into oxides, represented by the chemical reaction below:

$$\mathbf{ZrSiO_4 \rightarrow ZrO_2 + SiO_2\ (gas)} \qquad \mathbf{6.4}$$

ZrO_2 and **SiO_2** are recovered separately

In order to break down the zircon, the alkali fusion method was used for this testwork. The choice of the method was based on the available and reliable method to dissociate Zircon at Mintek analytical laboratory.

6.2. Experimental procedures

6.2.1. Alkali fusion

A representative portion of the similar naturally upgraded –150+106µm and –106µm composite sample milled to 45µm passing 100% was fused using NaOH, with lithium tetraborate as the flux (**Figure 26**).

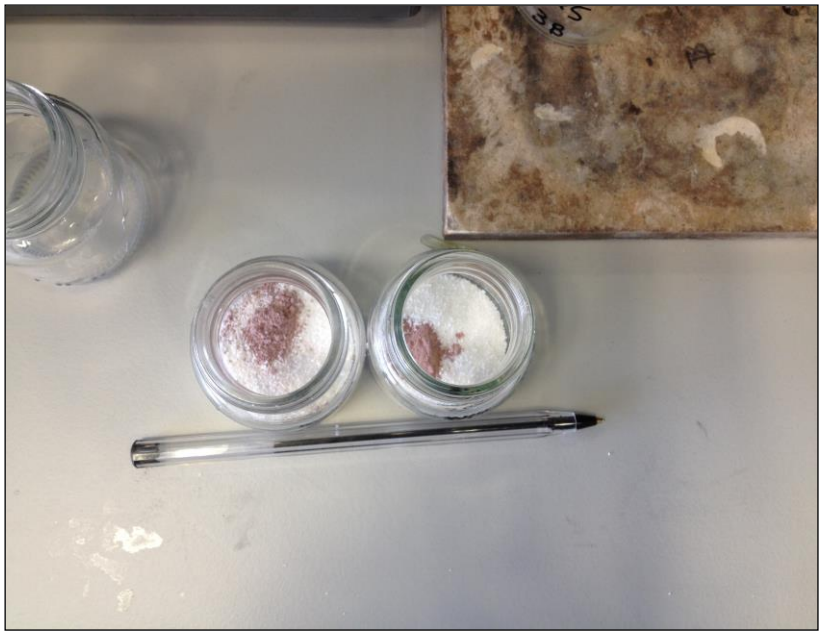


Figure 26: A photograph showing the sample mixture before alkali fusion.

In alkaline fusion, 10 grams of zircon concentrate were mixed with various amounts of lithium tetraborate flux in a platinum boat, which was then heated for different time periods in a muffle furnace or a tubular furnace, at 900 ^{0}C. With the fusion method, a weighed amount of NaOH and zircon concentrate was placed in two separate platinum crucibles and pre-heated to the required temperature in a muffle furnace. After 5 minutes, they were mixed within the furnace to start fusion under static conditions. As soon as the mixing was complete, the time of fusion was counted. A total of 10 fused zircon beads were produced prior to hydrometallurgical testwork. The 10 zircon beads were later pulverised, and a quantity of 67 grams was produced.

6.2.2. Chemical analysis

A representative portion of the pulverised zircon bead was analysed using ICP-OES, described in **Chapter 3**.

6.2.3. Hydrometallurgy tests

The HCl leaching test was carried out in order to dissolve REE present in the sample, subsequent to alkali fusion of the zircon sample:

The projected reaction was as follows:

$$Na_2ZrSiO_4\,(solid) + 4HCl\,(aq) \rightarrow 2NaCl\,(aq) + ZrCl_2\,(aq) + H_2SiO_3\,(gel) + H_2O \qquad 6.5$$

The solids (60g) were slurried with deionised water to 20% solids (m/m) in a 1L thermoplastic coated glass reactor. The reactor was equipped with an overhead stirrer with a thermoplastic coated impeller, thermocouple and also pH and Eh meter. The operating parameters such as temperature, redox potential (Eh) and pH were recorded half-hourly. A concentrated HCl acid (32% m/m) was added at timely intervals to control the pH of the mixture at the value of 3.

On completion of the test, the slurry was filtered by means of vacuum filtration. The filtered wet solids mass, volume and mass of filtrate were recorded. The wet solids were washed three times with two re-pulping washes and one plug wash using deionised water. The washed solids were dried in an oven at 50°C. The dried solids were then homogenized and a representative sample was taken using a cone and quartering technique for mineralogical and chemical assessment (**Table 27**).

Table 27: Experimental conditions of selective leaching test

Parameter	**Target**
Temperature	60 ^{o}C
Residence time	4 hours
Target pH	3
Target Eh	variable mV
Solids content	20% (m/m)
Grind Size	45µm
Feed Data:	**Target**
Required mass of dry feed solids	60 g
Solids content	20 % (m/m)
Mass of DI water	240 g
Reagents concentration	**Target**
HCl concentration	32.0 %

**DI water- deionised water*

6.2.4. Mineralogical characterisation of the zircon rich sample

6.2.4.1. Sample preparation

The dry aliquot of the fused zircon leach residue was prepared for mineralogical investigation, to assess the breakdown of zircon and to evaluate the leachability of the sample. A sub-sample was pulverised for X-Ray Diffraction (XRD) and other sub-samples were prepared into normal polished sections for scanning electron microscopy (SEM) analysis.

6.2.4.2. X-Ray Diffraction analysis

X-Ray powder diffraction was used for phase identification of the crystalline minerals and to provide information on the bulk mineralogy of the sample. Pulverized samples were analysed using a Bruker D8 Advance diffractometer. A Co Kα radiation, a 2θ scan range of 5-80º, a step size of 0.02º 2θ, and a counting time of 3 s per step were employed. Note that only crystalline minerals present in mass percentage greater than ~3% are detected by this method.

6.2.4.3. Scanning Electron Microscopy analysis

Polished sections were prepared for examination using the Zeiss EVO MA1 scanning electron microscopy, equipped with quantitative energy dispersive spectrometry (EDS). The SEM was used to identify the phases present in the leached residues as well as to verify the possibility of zircon breakdown.

6.3. Results

This section entails the results from the HCl leaching test and the mineralogical characterisation of leached residues of the fused zircon sample.

6.3.1. HCl leaching targets

Table 28 shows the targeted and actual readings recorded during the HCl leaching test. The recorded information on the log sheet shows that the sample was indeed fused with alkali, not acid. This is shown by the high pH reading of 10.9 at a duration of 0 hours. At 0 hours 100ml of HCl was added, with the aim to reach a targeted pH of 3.

The pH only dropped after 116 ml of HCl acid were added to the slurried fused zircon sample. A volume of 16 ml was later added from a duration of 0.5 hours to the duration of 3 hours. However, only a slight change was noticed in the actual pH; this resulted in the termination of the test before it reached 4 hours residence time, due to the high acid consumption.

Table 28: Leaching conditions of REE extraction from zircon rich sample

Time, hours	**Solution Temp,^{oC}**	**pH of solution**	**Eh of** solution, mV(vs Ag/AgCl)	**Volume of** HCl added, mL
0	19.4	10.9	-39.5	
0.5	21.6	4.1	423.88	35
1	21.9	3.6	528.13	9
1.5	21.9	3.52	551.5	6
2	21.9	2.84		2
2.5	21.6	3.048	524.13	1
3	21.5	3.084	508	2
3.5	21.4	3.054	518.25	1
4	21.4	3.054	519.88	0.5
Total	**21.4**	**3.3**	**441.8**	**56.5**

6.3.2. Minerals and phase compositions

The XRD was conducted on the sample obtained after the test was terminated. The fused residue sample showed that the sample has 100 mass % of sassolite-$B(OH)_3$ mineral (as shown in **Figure 27**. The presence of sassoite could have been a result of the lithium tetraborate used as the flux. The XRD did not show any form of REE or zirconium minerals present within the residue.

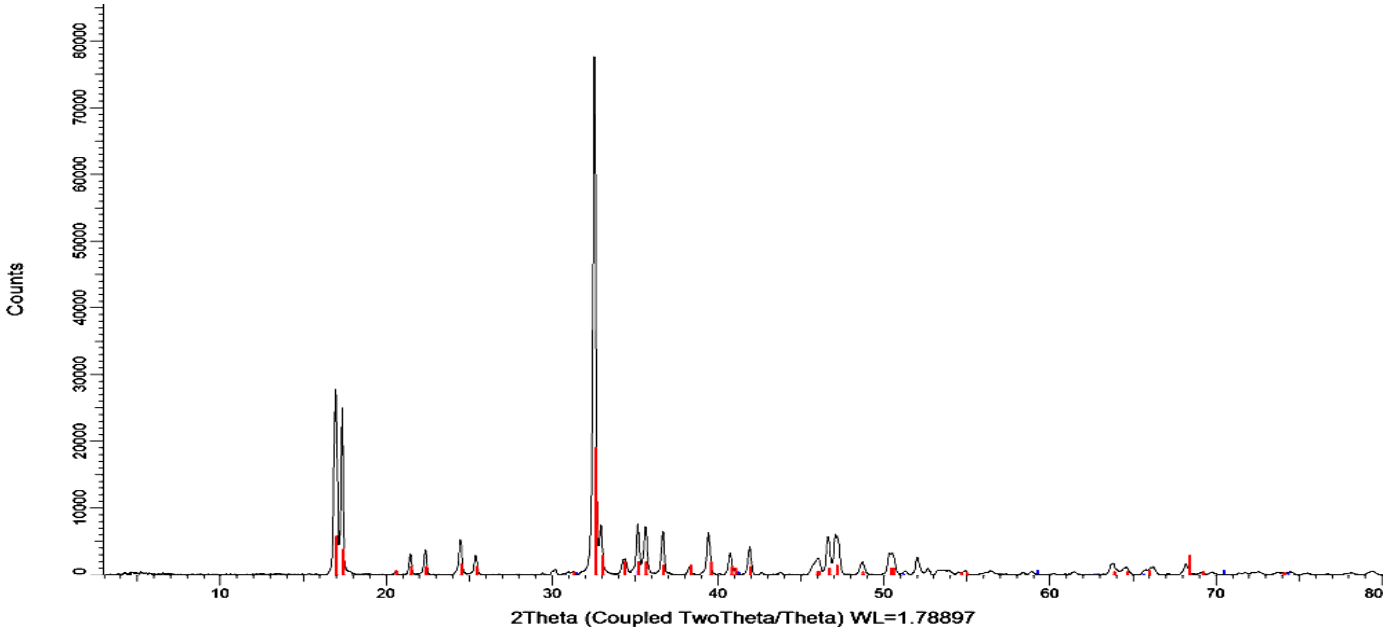


Figure 27: The XRD spectra of the leached fused zircon.

No minerals or phases were reported from the SEM analysis due to difficulties encountered during mounting of the polished sections. The residue sample was more of a gel sample and had difficulty in settling when mixed with epoxy resin. The sample also had a tendency of swelling when mounted or prepared on a stub for analysis. For this reason, only data from XRD could be presented in this report.

6.4. Summary and discussion

The extraction of REE in zircon was terminated since the method of extracting REE from an alkaline fused zircon is very expensive. This contradicted with the purpose of this study, which is aimed at processing REE in an effective manner. The following listed points resulted in the termination of the extraction of REE from zircon.

- This study showed that the breaking down of zircon composition prior to REE extraction was not economical.

- The test required high energy usage and high amounts of acid for REE dissolution, which is in contradiction with the main objective of the research project of processing REE in the most effective method. Zircon had to be fused at 900 ^{o}C temperature conditions in order to dissociate the zircon structure before leaching.

- High acid consumption: An average of 196 grams of HCl solution was used to leach 60 grams of solids at a ratio of 1:3. The combination of high energy usage and high acid consumption resulted in the termination of the test before it reached 4 hours residence time.

7. CHAPTER 7 – CONCLUSIONS AND RECOMMENDATIONS

7.1. Conclusions

7.1.1. Introduction

The process mineralogy and extraction of rare earth elements from a beach placer deposit was addressed in the study. The main objective of this project was to investigate the cost-effective processing route for the extraction of rare earth elements from alternative sources. The study focused on the following:

- To assess if conducting mineralogical characterisation prior to processing route selection can serve as economical decision-making tool.
- To explore other additional REE resources apart from monazite.

7.1.2. The value of mineralogy

In order to address the research objectives, the tailing sample from an existing heavy mineral beach placer deposit currently being mined for titanium and iron was mineralogically explored for an additional and alternative REE resource. This involved the study of monazite and other heavy minerals from a tailing sample from a Ti operation for their REE content. The mineral monazite was investigated and other minerals such as leucoxene, zircon and garnets were investigated as an additional REE resource from an existing placer or beach sand operation, currently being mined for ilmenite and rutile in titanium production.

In the Ti production plants, monazite, garnet, zircon and leucoxene are known to report to the tailings stream. Hence an opportunity was seen to investigate REE from the tailings streams as a by-product of the existing titanium production operation, and also as a means of maximising the potential of REE as an additional resource.

Monazite, a REE phosphate mineral, and other heavy minerals such as zircon, xenotime, almandine (garnets) leucoxene and titanite were identified as REE containing species. The amount of REE in these other heavy minerals was identified by the use of EMPA – a technique used to classify the mineral chemistry.

The research objectives were well addressed in this study. The mineralogical investigation did show that apart from monazite, there are other heavy minerals that contain REE. This was observed through electron microprobe. An integration of XRD, SEM, EMPA and MLA demonstrated that a combination of these techniques can be used to achieve a specific goal.

It was however, impossible for a single mineralogical technique to quantify in terms of abundance and to demonstrate that REE are present in monazite, xenotime and other heavy minerals (i.e. zircon, titanite, leucoxene). For instance, XRD analysis only showed the gangue minerals and amounts of monazite and other heavy minerals. The MLA provided a systematic quantitative information of the entire sample and REE species. Additionally, MLA also provided the list of minerals that were below the detection limit of XRD. Though MLA provided the quantitative data of the mineral present in the sample, EMPA provided the mineral chemistry of the REE containing minerals. Due to this holistic mineralogical approach, other alternative REE resources such as zircon, titanite and leucoxene were identified.

7.1.3. Role of mineralogy in selection of metallurgical process

The mineralogy by size also showed the distinction of minerals distribution within the four size fractions (i.e. +212 µm, –212+150 µm, –150+106 µm and –106 µm). The mineralogy results derived from the AutoSEM analysis showed that the sample consists of monazite, zircon, amphibole, diopside, augite, epidote, rutile, quartz, leucoxene, titanite and almandine. Monazite and zircon were the chief REE-containing minerals. The mineralogy of the sample varied per size fraction. The coarser fractions (+212µm and –212+150µm) were dominated by epidote, followed by minor amounts of diopside, augite, and amphibole. Mineralogical variations were more evident in the two smallest size fractions (–150+106µm and –106µm), which contained the majority of the zircon, rutile, and monazite and which combined constituted approximately 50 mass%.

As a result of these findings, the (–150+106µm and –106µm) fractions were composited for the next stage of metallurgy studies. The main REE-bearing minerals, monazite and zircon, were preferentially concentrated in the finer (–150µm) fractions, which constituted about 50 mass % of the sample and the composite sample was subjected to direct leaching.

Through mineralogical investigation, a flowsheet was established to treat the composited sample through the alkaline (NaOH) route. Mineralogy showed that both major REE containing minerals (i.e monazite and zircon) require alkaline cracking of the phosphate ion and silica ion.

However, the two REE species, monazite and zircon, did not fully react in the same leaching conditions. It was found that the silica ion of zircon required a high temperature of greater than 650ºC to dissociate the SiO_4^{2-} ion, whereas the phosphate ion of monazite was successfully cracked at 140ºC. The findings showed that the two minerals can only be treated separately and not simultaneously. In addition, the extraction of REE in zircon proved to be very uneconomical. When zircon is fused using alkali, it tends to consume higher amounts of HCl during dissolution stages. From the studies, the consumed quantities of acid versus the mass of the alkali fused zircon was at a ratio of **3:1.**

In conclusion, a combination of mineralogical techniques proved that conducting mineralogy beforehand is of good value. It also showed that mineralogy should be highly considered as a decision-making tool so as to cut down on unnecessary costs associated with processes that may not be necessary in designing a flowsheet, demonstrated by **Figure 28** (estimated analysis cost break down).

The estimated cost break down showed mineralogy testwork cost at ~ZAR 25 000, ore upgrading at ZAR 40 000 and leaching ZAR 50 000. Based on this study, the information on the figure below demonstrates that approximately ZAR 40 000 was spared by conducting mineralogy upfront rather than later when problems are encountered within the plant.

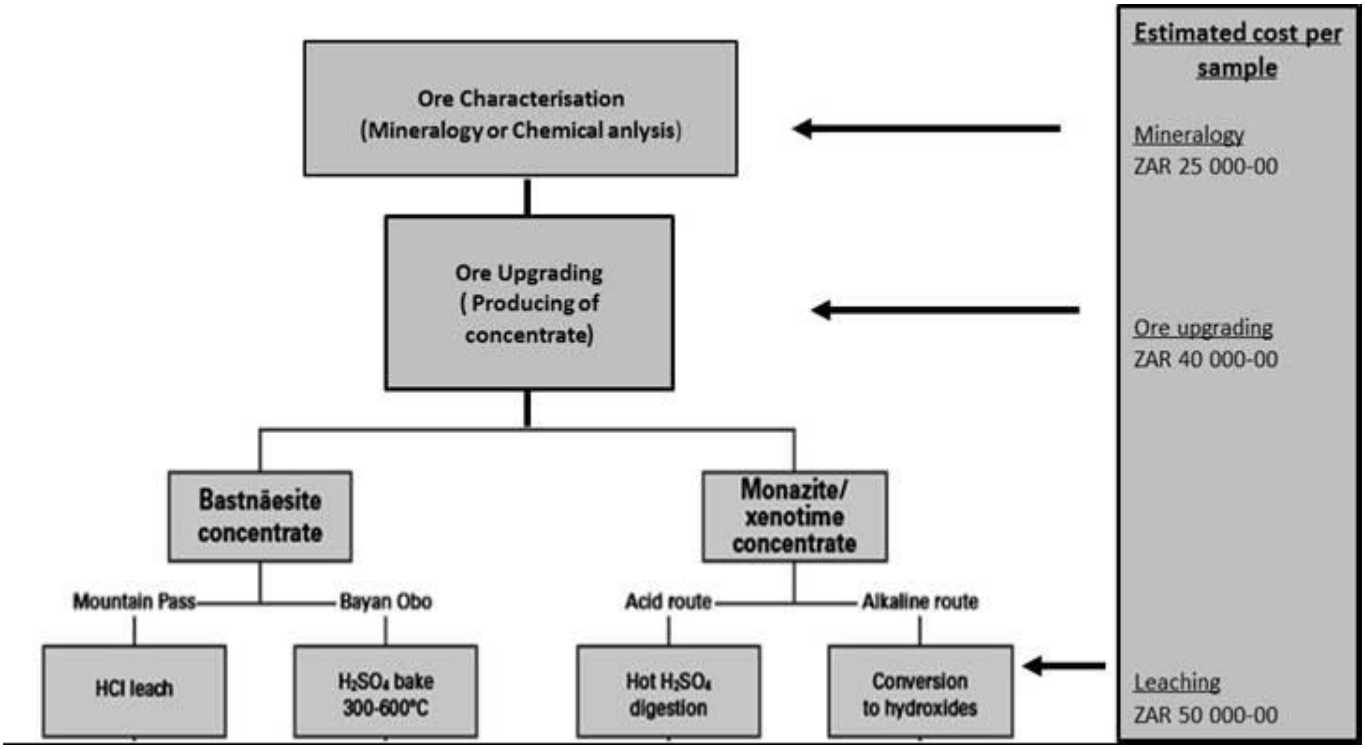


Figure 28: Estimated cost analysis

Through detailed mineralogical studies, certain stages of ore beneficiation in order to produce a concentrate prior leaching testwork were bypassed. It was observed in this study that the ore was naturally upgraded in the (–150+106µm and –106µm) size fractions. The composited fractions were directly leached and an extraction efficiency of 55% was achieved. Considering that the ore did not undergo any other beneficiation stages for further upgrading, the study showed good extraction efficiency. An extraction higher than 55 % could have been achieved if the ore was upgraded further, owing to highly liberated monazite. The presence of zircon, oxide minerals like rutile and silicate minerals in the leach concentrate could have impacted the extraction efficiency, by limiting REE dissolution.

In addition, alternative REE-containing minerals were explored and identified for possible REE extraction, such as the mineral zircon. The zircon rich material did not undergo complete extraction; the test was terminated due to the high consumption of leach solution in the processing of zircon, which carried a possibility of being uneconomical.

7.2. Recommendations and further work

Other REE studies, conducted by Mintek, have shown an extraction efficiency of 90% in the same type of placer deposit origin ore. The 90% extraction efficiency with other REE projects at Mintek were achieved by means of using physical separation methods and froth flotation methods to produce a monazite rich leaching concentrate. However, in the case of this study, the extraction efficiency obtained was 55%, without any prior physical separation or froth flotation methods being employed to produce a monazite rich concentrate for leaching. In order to achieve a similar 90% extraction efficiency, the ore must first be screened to –150µm, then a physical separation method must be considered to reduce gangue presence, as well as zircon in the initial stages of leaching, since the zircon did not react under the same conditions as monazite during caustic cracking.

As the demand for REE continues to grow and the number of REE producers increase, further work and a better and different approach can be investigated to extract REE in zircon from a zircon-rich geological deposit; bearing in mind that there is no accessible data available on the extraction of REE from zircon.

REFERENCES

Abdel-Rehim A.M. (2005) A new technique for extracting zirconium from Egyptian zircon concentrate Alexandria University, Egypt. *International Journal of Mineral processing*. **76**, 234– 243

Alam, M.A., Zuga, L., and Pecht, M.G. (2012) Economics of rare earth elements in ceramic capacitors, Center for Advanced Life Cycle Engineering (CALCE), University of Maryland, College Park, *Ceramics International*, **38,** 6091–6098

Barbosa, J. P., Ribeiro, R. A. and Cunha, O. G. C. (2001) Alkaline leaching of a xenotime, pp. 451-456

Binnemans, K., Jones, P.T., Blanpain, B., Van Gerven, T., Yang, Y., Walton, A., and Buchert, M. (2013) Recycling of rare earths: a critical review. *Journal of Cleaner Production*, **51,** 1-22

Biswas, R.K., Habib, M.A., Karmakar, A.K., and Islam, M.R. (2010) A novel method for processing of Bangladeshi zircon: Part I: Baking, and fusion with NaOH. *Hydrometallurgy* **103**, 124–129

Boss, B.C and Freeden. (2004) Concepts, Instrumentation and Techniques in Inductively Coupled Plasma Optical Emission Spectrometry, Third Edition, *PerkinElmer Life and Analytical Sciences*, Printed I USA, p.120

British Geological survey. (2011) *Rare earth element*; Natural Environment Research Council

Bruker axis (2001) Introduction to Powder X-Ray Diffraction, *History Basic Principles*, Bruker, *Presentation*, p.38

Castor, S.B and Hedrick, J.B. (2006) Rare earth elements. Industrial Minerals Volume, **7th** edition. *Society for mining, Metallurgy, and Exploration*, Littleton, CO, pp. 769-792

Charalampides, G. and Vatalis, K.I. (2015) Global Production Estimation of Rare Earth Elements and Their Environmental Impacts on Soils. *Journal of Geoscience and Environment Protection*, **3**, 66-73

Chegwidden, J., and Kingsnorth, D.J. (2002) Rare earths supply and demand. *A European market focus. Industrial minerals*, pp. 52-61

Chen, Z. (2011) Global rare earth resources and scenarios of future rare earth industry, *Journal of Rare Earths***, 29**, 1-6

Chi, R., and Wang, D. (1996) Rare earth ore processing and extraction technology. *Science Publishing Company*, Beijing, 305-332

Chi, R., Xu, S., Zhu, G., Xu, J., Qiu, X. (2001) Beneficiation of rare earth ore in China. In Light Metals 2001: *Technical Sessions at the 130th TMS Annual Meeting. TMS Aluminium Committee, New Orleans,* pp. 1159–1165

Cropp. A. (2013) http://www.minassist.com.au/blog/liberation-and-free-surface-area-in-the-float-feed/

Cropp, A. (2013) What is Process Mineralogy?http://www.minassist.com.au/blog/what-is-process-mineralogy/

Cropp, A. F., Goodall, W. R. and Bradshaw, D. J. (2013) The influence of textural variation and gangue mineralogy on recovery of copper by flotation from porphyry ore: a review. *Proceedings of the 2nd, AusIMM International Geometallurgy Conference 2013,* 30 September-2 October 2013, Brisbane, 279-291

Dixit, S.G and Biswas, A.K., (2008) Minerals beneficiation – pH dependence of the flotation and adsorption properties of some beach sand minerals. AIME Trans

Du, X. and Graedel, T. E. (2011) Global in-use stocks of the rare earth elements: A first estimate. American Chemical Society. *Environ. Sci. Technol.* **45**, 4096-4101

El-Barawy, K.A., El Tawil, S.Z., and Francis, A.A. (2000) Alkali Fusion of Zircon Sand. *Transaction of the Institute of Mining and Metallurgical Sect. C,* **109**, 49–56.

Fatherly, N., O'Neill, M., and Glemza, A. (2008) Formerly used sites remedial action program (FUSRAP) W.R. Grace Feasibility Study (FS) Alternative Development Process Challenges and Successes, WM Conference, Phoenix, AZ.

Fernelius, W.C. (1946) Inorganic Syntheses, first ed. McGraw-Hill Inc., New York, USA, (**vol. II**), 38-43

Ferron, C. J and Bulatovic, S.M. (1991) Beneficiation of Rare Earth Oxide Minerals. *Materials Science Forum*. Trans Tech Publications, Switzerland

Goonan, T. G. (2011) Rare Earth Elements—End Use and Recyclability. U.S. Geological Survey Scientific *Investigations Report 2011-5094*, **15**. Retrieved from http://pubs.usgs.gov/sir/2011/5094/.

Gordon, J. (2011) Analysis: Underwater rare earths likely a pipe dream. Reuters.com. July 6. Retrieved from http://www.reuters.com/article/2011/07/06/us-rareearths-underwater-idUSTRE7655M320110706

Grauch, R., and Mariano, A. (2008) Ion-adsorption Type Lanthanide Deposits. *SME conference,* Salt Lake City

Gu, Y. (2003) Automated Scanning Electron Microscope Based Mineral Liberation Analysis: An Introduction to JKMRC/FEI Mineral Liberation Analyser. *Journal of Minerals and Materials Characterisation and Engineering*, **2(1)**, 33–41.

Gupta, C.K. (2003) *Chemical Metallurgy: Principles and Practice.* WILEY-VCH Verlag GmbH & Co. KGaA, Weinheim, **ISBN**: 3-527-30376-6, p.824

Gupta, C. K. and Krishnamurthy, N. (2005) *Extractive Metallurgy of Rare Earths*. Boca Raton London New York Washington, D.C., p. 502

Gupta, C.K. and Krishnamurthy, N. (1992) Extractive metallurgy of rare earths. *International Materials Reviews* **37 (5)**, 197–248

Guy, P.J., Bruckard, W.J. and Vaisey, M.J. (2000) Beneficiation of Mt Weld rare earth oxides by gravity concentration, flotation, and magnetic separation. In: *Seventh Mill Operators' Conference. AusIMM*, Kalgoorlie, pp.197-205

Habashi, F. (1997). *Handbook of extractive metallurgy*, Vol. III. Wiley-VCH, Weinheim, Germany, p. 2427

Habib, K and Wenzel, H. (2014) Exploring rare earths supply constraints for the emerging clean energy technologies and the role of recycling, *Journal of cleaner production*, **84**, 348-359

Haxel, G.B., Hedrick, J.B. and Orris. G.J. (2002) *Rare Earth Elements—Critical Resources for High Technology.* Fact sheet 087-02. Reston, VA: USGS

Helmenstine, A.M (2017) https://www.thoughtco.com/rare-earth-properties-606661

Hoatson, D.M., Jareth, S and Miezitis, Y. (2011) *The major rare earth element deposits of Australia: geological setting, exploration, and resources*. Geoscience Australia, pp.204

Hou, X and Jones, B.T. (2000) Inductively Coupled Plasma/Optical Emission Spectrometry *Encyclopedia of Analytical Chemistry,* R.A. Meyers (Ed.) John Wiley & Sons Ltd, Chichester, pp. 9468-9485

http://www.kaiserbottomfish.com/s/Education.asp?ReportID=362761

IAMGOLD (2012) *Rare Earth Elements 101*
https://www.scribd.com/document/112339862/Rare-Earth-Elements-101-April-2012

Jackson, W.D. and Christiansen, G. (1993) International Strategic Minerals Inventory Summary Report—Rare Earth Oxides, *U.S. Geological Survey Circular* 930-N, U.S. Geological Survey, Map Distribution, Denver CO, p. 69

Jacoby, M. and Jiang, J. (2010) Securing the supply of rare earths. *Chem Eng. News* **88**, 9-12

Jordens, A., Cheng, Y.P., and Waters, K.E. (2013) A review of the beneficiation of rare earth element bearing minerals. *Minerals Engineering*, **41**, 97–114

Kanazawa, T., and Kamitani, M. (2006) Rare earth minerals and resources in the world. *Alloys and compounds, Vol* **408 -412**. pp.1339-1343

Kim, E., and Osseo-Asare, K. (2012) Aqueous stability of thorium and rare earth metals in monazite hydrometallurgy: Eh-pH diagrams for the systems Th–, Ce–, La–, Nd– (PO_4)–(SO_4)–H_2O at 25℃. *Hydrometallurgy,* **113–114**, 67–78

Kim, W., Bae, I., Chae, S. and Shin, H. (2009) Mechanochemical decomposition of monazite to assist the extraction of rare earth elements. *Jr.Alloys Comp*. 486, 610-614

Kogel, J., Trivedi, N.C., Baker, J.M and Krukowsk, S.T. (2006) *Industrial minerals and rocks: Commodities, Markets and Uses*, 7th edition.SME, Society for Mining, Metallurgy and Exploration Inc. pp. 1568

Koltun, P and Tharumarajah, A. (2014) Life Cycle Impact of Rare Earth Elements. *CSIRO Process Science and Engineering, ISBN Metallurgy*, Vol 2014, Article ID 907536, Received 19 December 2013; Published 4 May 2014, p. 10

Krumholtz, P. (1957) Brazilian practice for monazite treatment. Rare Earth, Bombay

Kul, M., Topkaya, Y. and Karakaya, I. (2008) Rare earth double sulfates from preconcentrated bastnaesite. *Hydrometallurgy*, **93**, 129–135

Kumari, A., Panda, R., Jha, M.K., Kumar, J.R., and Lee, J.Y. (2015) Process development to recover rare earth metals from monazite mineral: A review, *Minerals Engineering*, **79,** 102-115

Lastra, L, (2007) Seven practical application cases of liberation analysis. *Mineral Processing*, **84**, 337-347

Lehtonen, M. (2005) Rare earth elements characteristics of pyrope garnets from Kaavi-Kuopi kimberlites-implications for mantle metasomatism. *Bulletin of geological society of Finland*, **77**, 31-47

Levkowitz, L., and Beauchamp-Mustafaga, N. (2010) China's rare earths industry and its role in the international market. U*.S.–China Economic and Security Review Commission*, 3November.From: ⟨www.uscc.gov/researchpapers/2011/RareEarthsBackgrounderFINAL.pdf⟩

Long, K.R and Bradley, S. (2010) *The principal rare earth elements deposits of the United States –A summary of domestic deposits and a global perspective*. USGS Scientific Investigation Report 2010-5220, Reston, Virginia. Retrieved from http://pubs.usgs.gov/sir/2010/5220/.

Lotter, N.O. (2011) Modern Process Mineralogy: An integrated multi-disciplined approach to flowsheeting. *Minerals Engineering*, **24**, 1229-1237

Lotter, N.O., Kormos, L.J., Oliviera, J., Fragomeni, D. and Whiteman, E. (2011) Modern Process Mineralogy: Two case studies. *Minerals Engineering*, **24**, 638-650

Manhique, A., Kwela, Z., and Foeke, W.W. (2003) De wet process for the beneficiation of zircon: optimization of the alkali fusion step. *Industrial and Engineering Chemistry Research* **42**, 777-783

Massari, S., and Ruberti, M. (2013) Rare earth elements as critical raw materials: Focus on international markets and future strategies, *Resources Policy*, **23**, 36-48

Meerson, G.A. (1957) Alkaline leaching of monazite. *Atom. Energy* **3 (9**), 259-264

Meloy, T.G. (1990) Textural Transforms - Definition and Use. Particle Technology, 2"d World Congress, Kyoto, 1990. *Sot. Powder Tech*, Japan, **Vol. I**, 248-256

Montgomery, M. (2011) Rare earths recycling enter the new reality. IB times.com. February 23. Retrieved from http://www.ibtimes.com/articles/115379/20110223/rare-earth-recycling-enter-the-new-reality.htm

Morrison, W.M., and Tang, R. (2012) China's Rare Earth Industry and Export Regime: Economic and Trade Implications for the United States, *Congressional Research Service*, April 30, 2012 https://fas.org/sgp/crs/row/R42510.pdf

Naumov, A V. (2008) Review of the world market of rare earth metals. *Russian Journal of Non-Ferrous Metals*, **49 (1)**, 14–22

Orris, G. J. and Grauch R. I. (2002) Rare earth element mines, deposits, and occurrences. *U.S. Geological Survey, Open-File Report 02-189*, Version 1.0. Retrieved from http://pubs.usgs.gov/of/2002/of02-189/

Pavez, O., and Peres, A.E.C. (1993) Flotation of monazite–zircon–rutile with sodium oleate and hydroxamates. XVIII *International Mineral Processing Congress*, **4**, 1007–1012

Pavez, O., and Peres, A.E.C. (1994) Technical note bench scale flotation of a Brazilian monazite ore. *Minerals Engineering*, **7 (12),** 561-1564

Peelman, S Yang, Y., Sietsma, J., and Sun, Z.H.I. (2014) Leaching of rare earth elements: past and present. Department of Materials Science and Engineering, Delft University of Technology, Mekelweg 2, 2628 CD Delft, The Netherlands: *1st European Rare Earth Resources Conference*|Milos|04-07/09/2014, pp. 446-456

Perez-Barnuevo, L., Pirard, E., and Castroviejo, R. (2013) Automated characterisation of intergrowth textures in mineral particles. *Minerals Engineering*. **52**, 136-142

Philander, C., and Rozendaal, A. (2009) Mineral intricacies of the Namakwa Sands mineral resource. *The 7th International Heavy Minerals Conference 'What next', The Southern African Institute of Mining and Metallurgy*, SAIMM, pp. 99–106

Rabie, K.A., Abdel-Wahaab, S.M., Mahmoud, K.F., Hussein, A.E.M., Abd El-Fatah, A.I.L., (2013) Monazite–uranium separation and purification applying oxalic–nitrate–TBP extraction. *Arab Journal of Nuclear Science and Applications*, **46** (**1**), 30–42

Rao, N.S and Misra, S. (2009) Source monazite sand in southern Orissa beach placer, eastern India, *Journal Geological Society of India*, **74**, 357-362

Rare Earth Elements (2012): *A Review of Production, Processing, Recycling, and Associated Environmental Issues*, EPA 600/R-12/572 | December 2012 | www.epa.gov/ord EPA/600/R-12/572, December 2012, Revised

Robb, L. (2005) *Introduction of Ore-forming processes*. 550 Swanston Street, Carlton, Victoria 3053, Australia. p. 386

Ruble, M., and Heuer, MA.H. (1984) Phase Transformation in ZrO_2-containing Ceramics. II. The Martensitic Reaction in t-ZrO_2. *American Ceramic Society, Columbus, OH*, **12**, 14–32

Sappin, A.A and Beaudoin, G. (2015) Rare earth elements in Québec, Canada: Main deposit types and their economic potential. In: Simandl, G.J. and Neetz, M., (Eds.), *Symposium on Strategic and Critical Materials Proceedings, November 13-14, 2015, Victoria, British Columbia. British Columbia Ministry of Energy and Mines, British Columbia Geological Survey Paper*, 2015-3, pp 265-273

Schweitzer, G.K and Pesterfield, L.L. (2010) *The aqueous chemistry of the elements* published by Oxford University Press, Inc. New York. p. 431

Seaman, J. (2010) Rare Earth sand Clean Energy: *Analyzing China's upper hand* http://www.iaea.org/inis/collection/NCLCollectionStore/_Public/42/052/42052647.pdf

Sengupta, D and Van Gosen, B.S. (2016) Placer-Type Rare Earth Element Deposits, Chapter 4, Department of Geology and Geophysics, Indian Institute of Technology, Society of Economic Geologists, Inc. Reviews in *Economic Geology*, **18**, 81-100

Shepherd, M.S. (1990) Eneabba heavy mineral sand placers, in Geology of the Mineral Deposits of Australia and Papua New Guinea (Ed. F.E. Hughes), *The Australasian Institute of Mining and Metallurgy*: Melbourne, pp. 1591-1594

Smythe, D.M., Lombard, A. and Coetzee, L.L. (2013) Rare Earth Element deportment studies utilising QEMSCAN technology, *Minerals Engineering*, **52**, 52-61

Spedding, F.H. (1975) Contributions of the rare earths to science and technology. *In: Symposium on the Effects of Rare Earths on the Properties of Metals and Alloys.ASM, Cincinnati*, pp. 1–11

Spicer, E., Verryn, S M C. and Deysel, K. (2008) Analysis of Heavy Mineral Sands by Quantitative X-Ray Powder Diffraction and Mineral Liberation Analyser – Implications for Process Control, *ICAM 2008 - Ninth International Congress for Applied Mineralogy*,165-172

Sulaiman, M.Y. (1991) An overview of the rare-earth mineral processing industry in Malaysia. *Mater. Sci. Forum,* **70–72**, 389-396

Syamaprasad, U., Bhattacharjee, S., Galgali, R.K., Mohanty, B.C., (1993). Zirconia ceramics by thermal plasma, *Trans. Ind. Ceram. Soc*. **52**, 35–46

Szumigala, D.J., and Werdon, M.B. (2011) Rare-Earth Elements: A brief overview including uses, worldwide resources, and known occurrences in Alaska: *Alaska Division of Geological & Geophysical Surveys Information Circular 61*, 1-15

Tabuchi, H. (2010) Japan Recycles Minerals From Used Electronics, *The New York Times*, October 5 Retrieved from: http://www.nytimes.com/2010/10/05/business/global/05recycle.html

Thompson, W., Lombard, A., Santiago, E., and Singh, A. (2011) Mineralogical studies in assisting beneficiation of rare earth element minerals from carbonatite deposits. *10th international congress for applied mineralogy, ICAM Conference*, pp. 668-672

tnahistoryoftechnology.com http://tnahistoryoftechnology.wikispaces.com/Rare+Earth+Metals

Tse, P. (2011) China‘s rare earth industry: U.S. *Geological Survey Open-File report* **2011-1042,** https://pubs.usgs.gov/of/2011/1042/of2011-1042.pdf, 1-15

Tyler, R.M and Minnitt, R.C.A. (2004) A review of sub-Saharan heavy mineral sand deposits: implications for new projects in southern Africa, *The Journal of The South African Institute of Mining and Metallurgy* (SAIMM), March 2004, pp. 89-99

Tyler, G. (2004) Rare earth elements in soil and plant systems-a review. *Plant and Soil*, **267**, 1191-2004

U.S. Geological Survey. (2011) Rare earths, Mineral Commodity Summaries, 2 p., available at http://minerals.usgs.gov/minerals/pubs/commodity/rare_earths/mcs-2011-raree.pdf

USGS, United States Geological Survey (2004) https://minerals.usgs.gov/minerals/pubs/mcs/2004/mcs2004.pdf U.S. Department of the Interior U.S. Geological Survey MINERAL COMMODITY SUMMARIES 2004

Van Gosen B.S., Fey, D.L., Shah, A.K., Verplanck, P.L. and Hoefen, T.M. (2010) Deposit Model for Heavy-Mineral Sands in Coastal Environments. *Mineral Deposit Models for Resource Assessment*. Scientific Investigations Report 2010, U.S. Department of the Interior, U.S. Geological Survey

Van Rahden, H.V.R. (1979) The role of the mineralogist in the minerals industry, SAIMM, December 1979, pp. 509-512

Verbaan, N., Bradley, K., Brown, J., Mackie, S. (2015) A review of hydrometallurgical flowsheets considered in current REE projects. In: Simandl, G.J. and Neetz, M., (Eds.), *Symposium on Strategic and Critical Materials Proceedings. British Columbia Ministry of Energy and Mines*, British Columbia Geological Survey Paper, **3**, 147-162

Welt, M.A., Brooklyn, N.Y. and Smutz, M. (1958) Method of processing monazite sand, **9**, 505-510

Wills, B.A. (2006) *Will's Mineral Processing Technology: An Introduction to the Practical Aspects of Ore Treatment and Mineral Recovery* (7th edition). Butterworth-Heinemann, Oxford, p.444

Wübbeke, J. (2013) Rare earth elements in China: Policies and narratives of reinventing an industry, *Resource Policy*, **38**, 384 -394

Zhang, J., and Lincoln, F.J. (1994) The decomposition of monazite by mechanical milling with calcium oxide and calcium chloride. *Alloys and Compounds*, **205**, 69–75

Zhang, J., and Edwards, C. (2012) A review of rare earth mineral processing technology. In: *44th Annual Meeting of the Canadian Mineral Processors*. CIM, Ottawa, pp. 79–102

APPENDIX A: ELEMENTAL MAPS

The elemental maps and the elemental compositions of minerals identified in each size fraction are below.

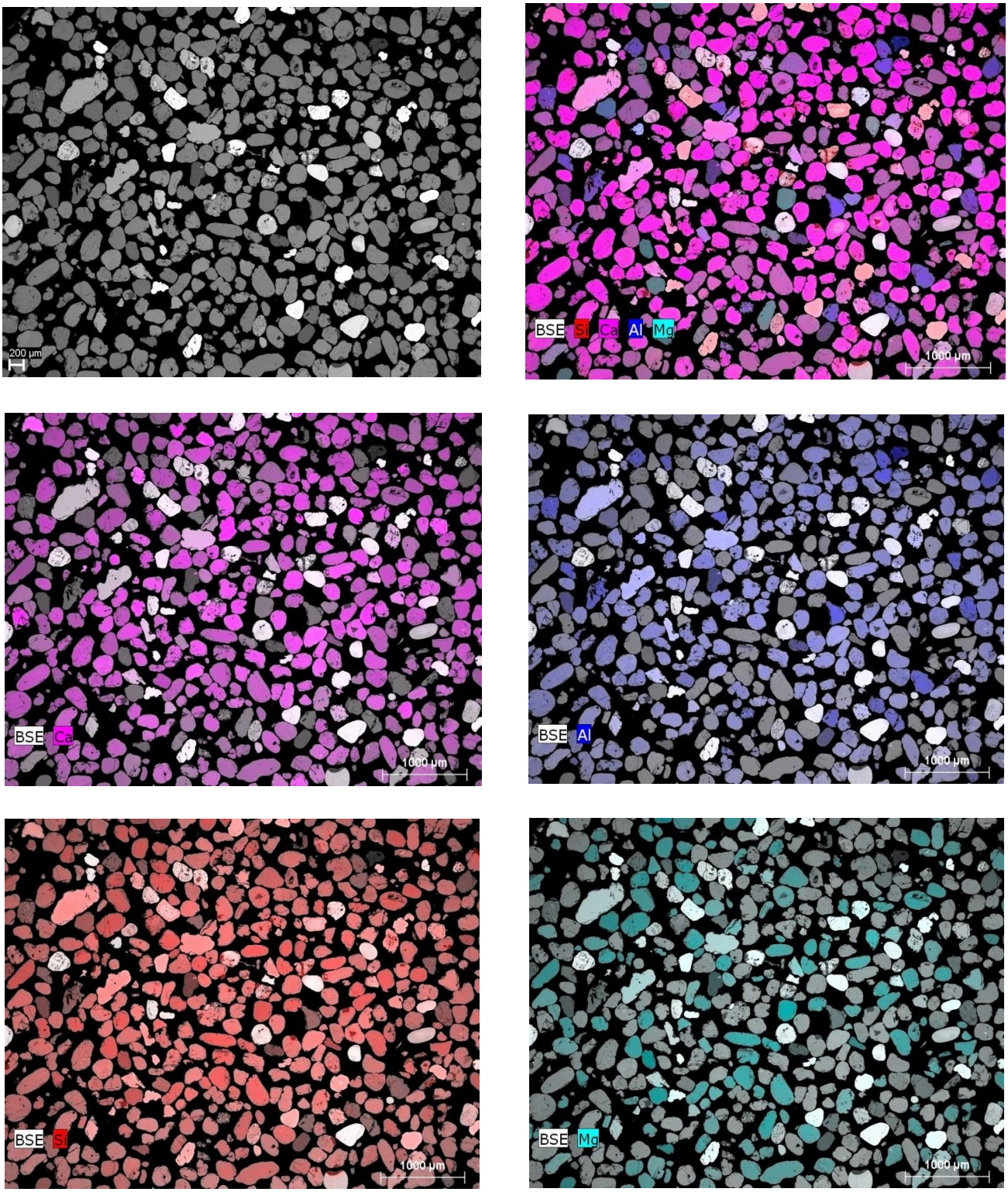


Figure A.1: BSE image, multiple and individual elemental maps showing the occurrence of specific mapped elements of +212 µm size fraction.

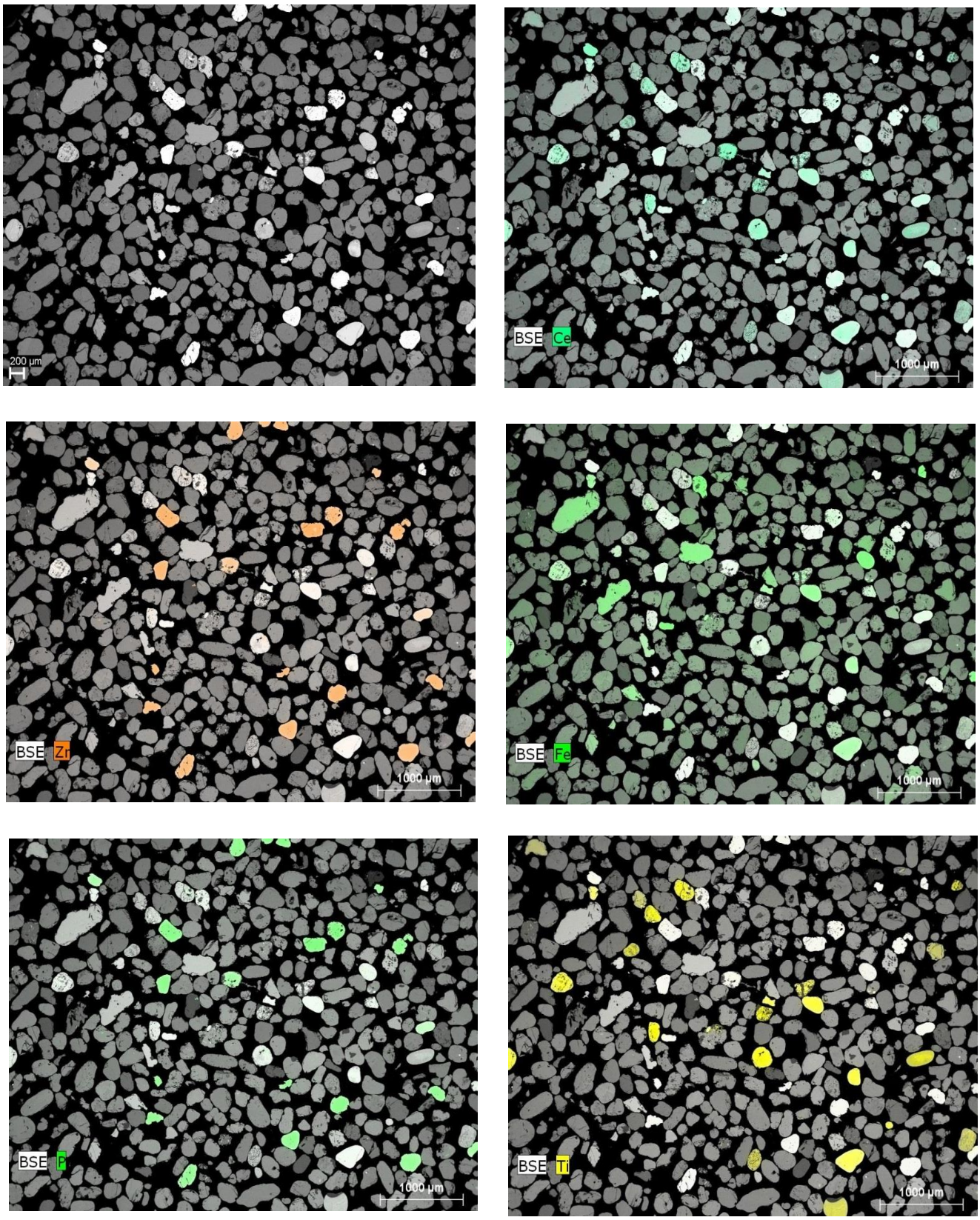


Figure A.2: BSE image and individual elemental maps showing the occurrence of specific mapped elements of +212 µm size fraction.

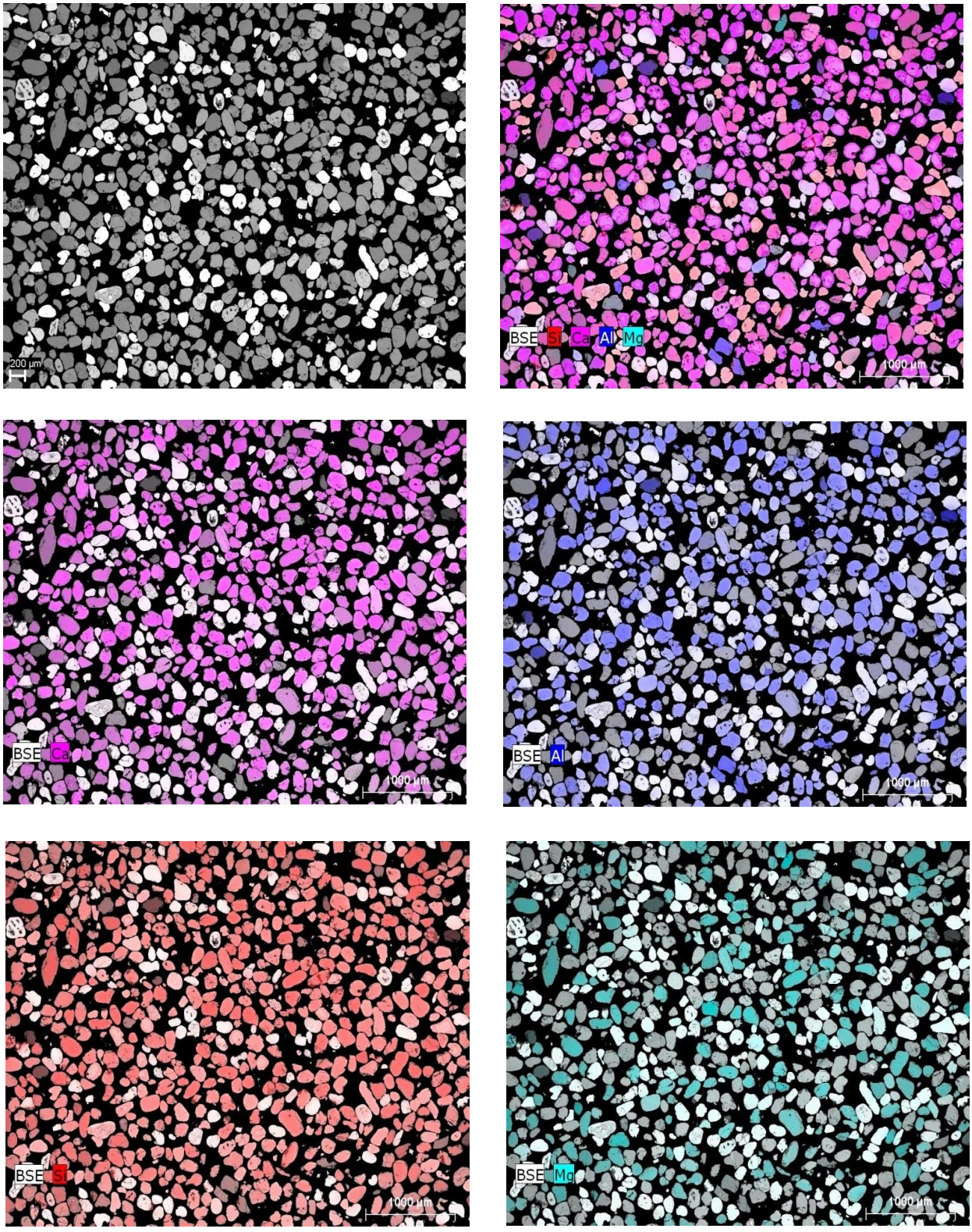


Figure A.3: BSE image, multiple and individual elemental maps showing the occurrence of specific mapped elements of –212+150 µm size fraction.

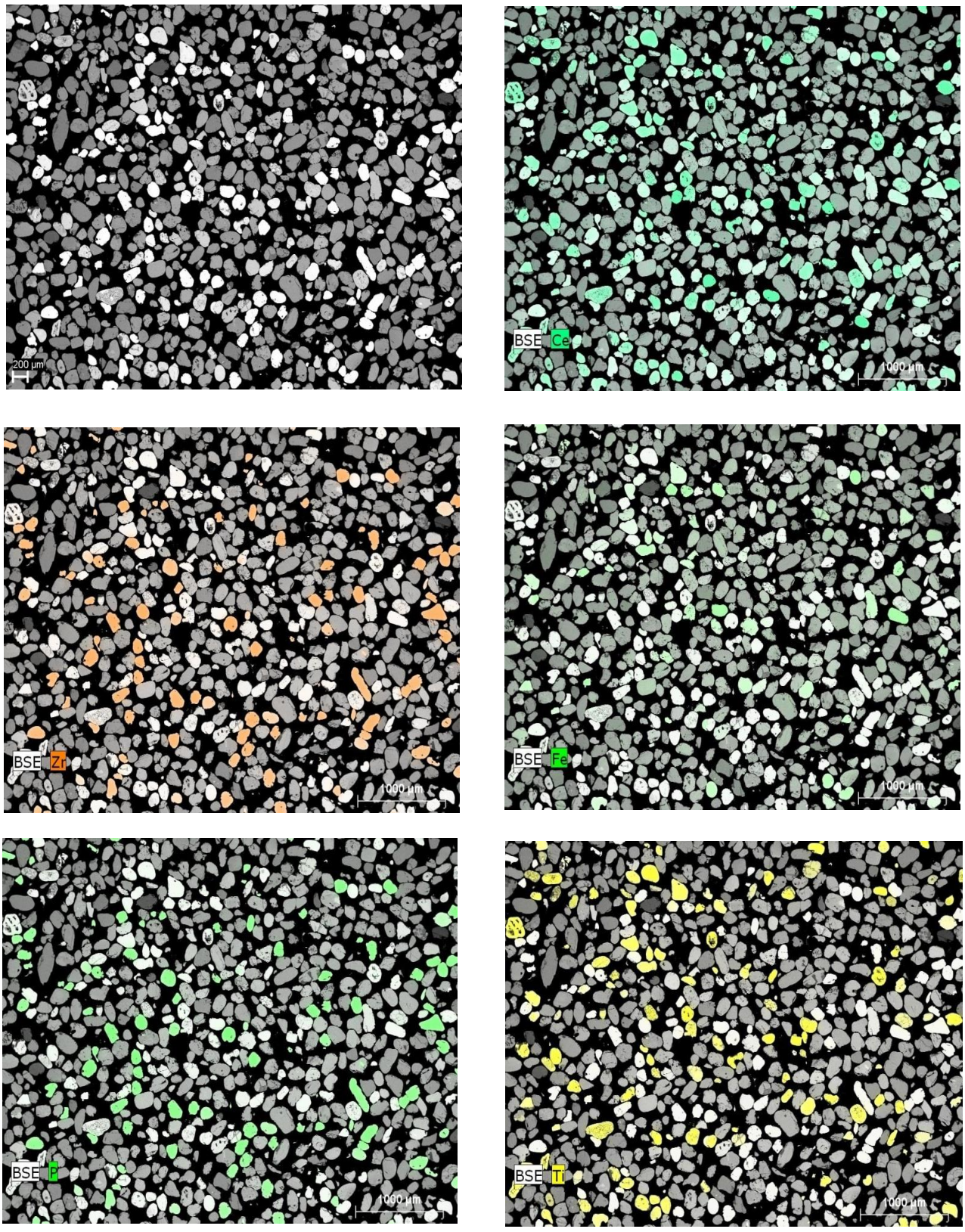


Figure A.4: BSE image and individual elemental maps showing the occurrence of specific mapped elements of –212+150 µm size fraction.

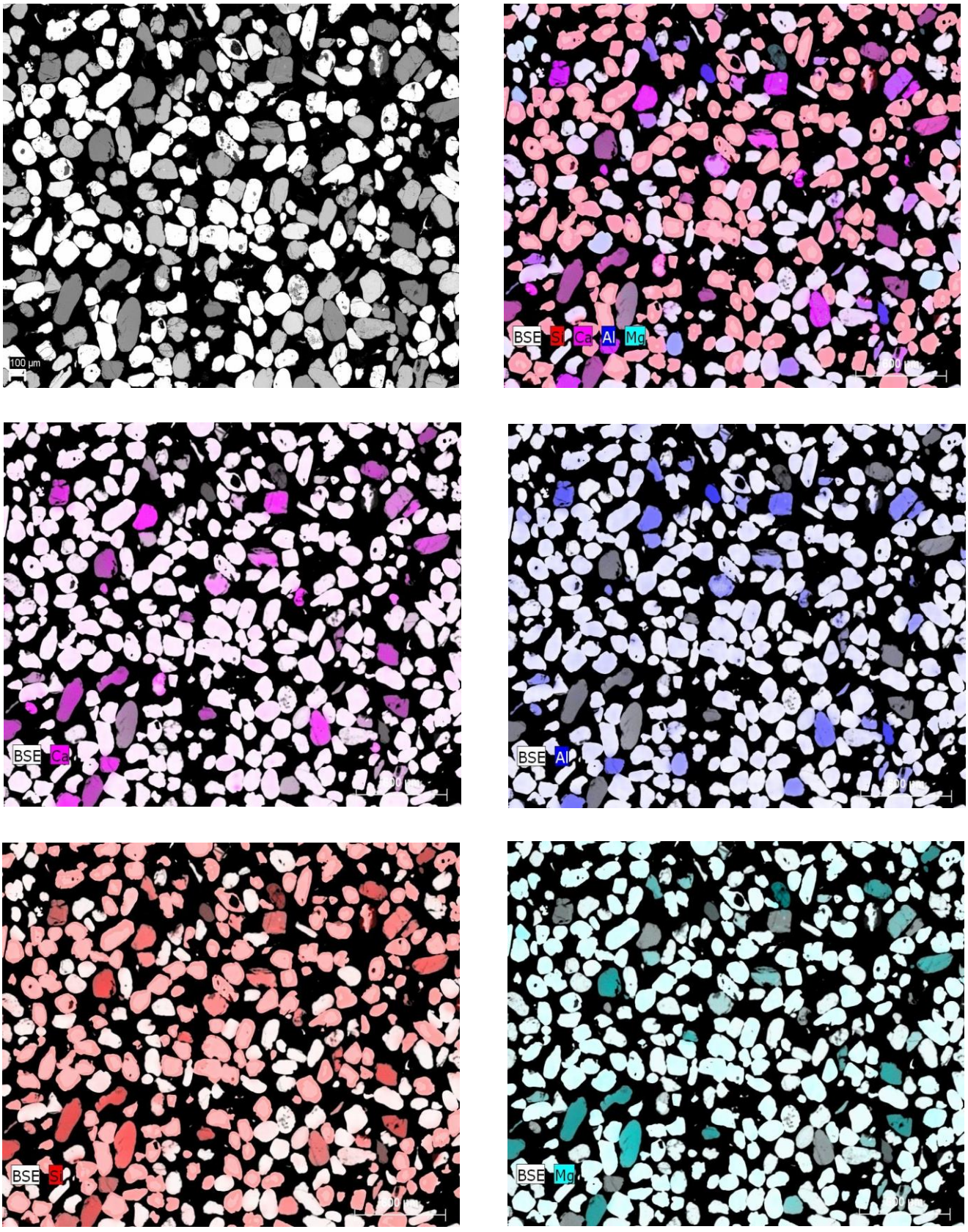


Figure A.5: BSE image, multiple and individual elemental maps showing the occurrence of specific mapped elements of –150+106 µm size fraction.

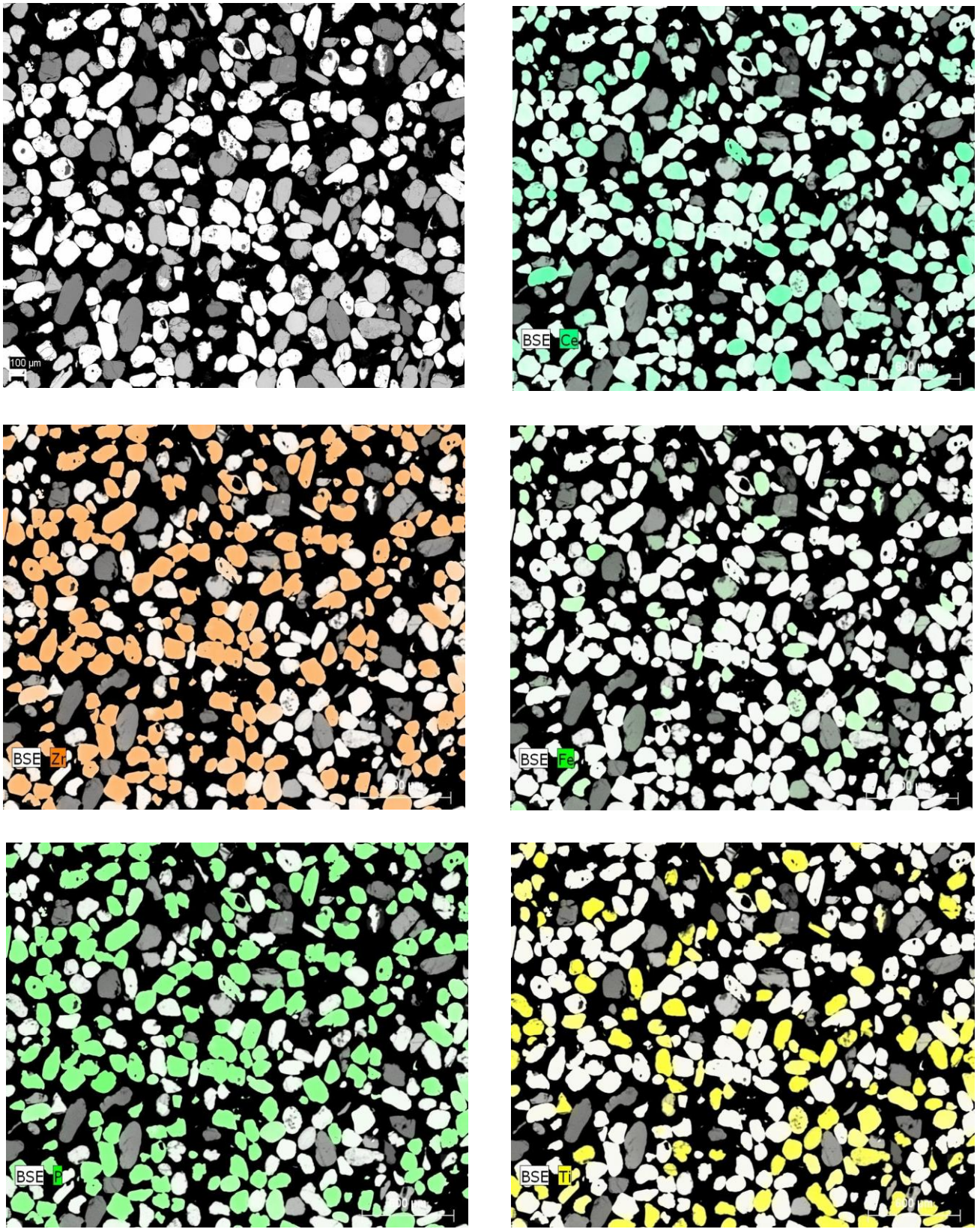


Figure A.6: BSE image and individual elemental maps showing the occurrence of specific mapped elements of –150+106 µm size fraction.

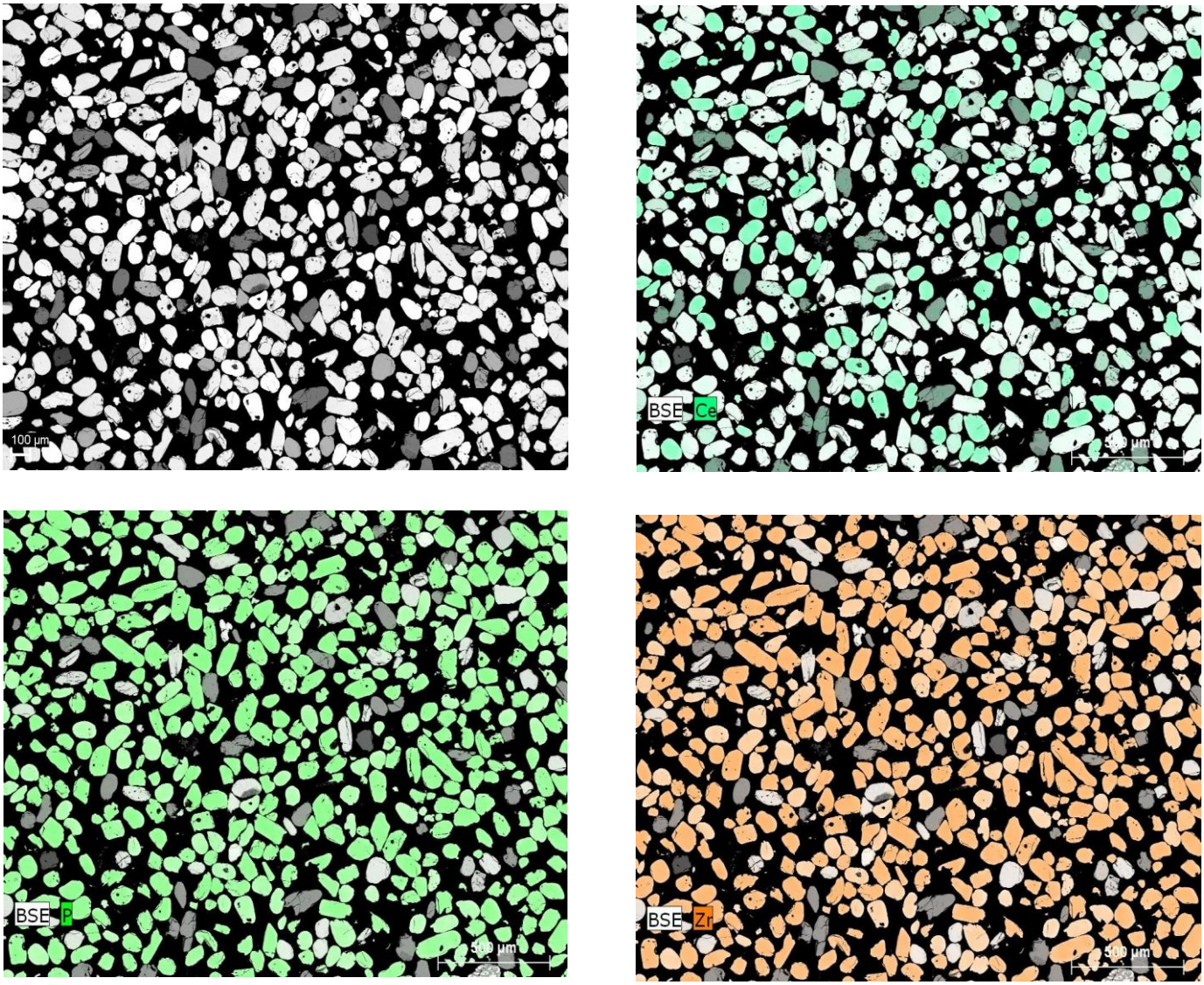


Figure A.7: BSE image and individual elemental maps showing the occurrence of specific mapped elements of –106 µm size fraction.

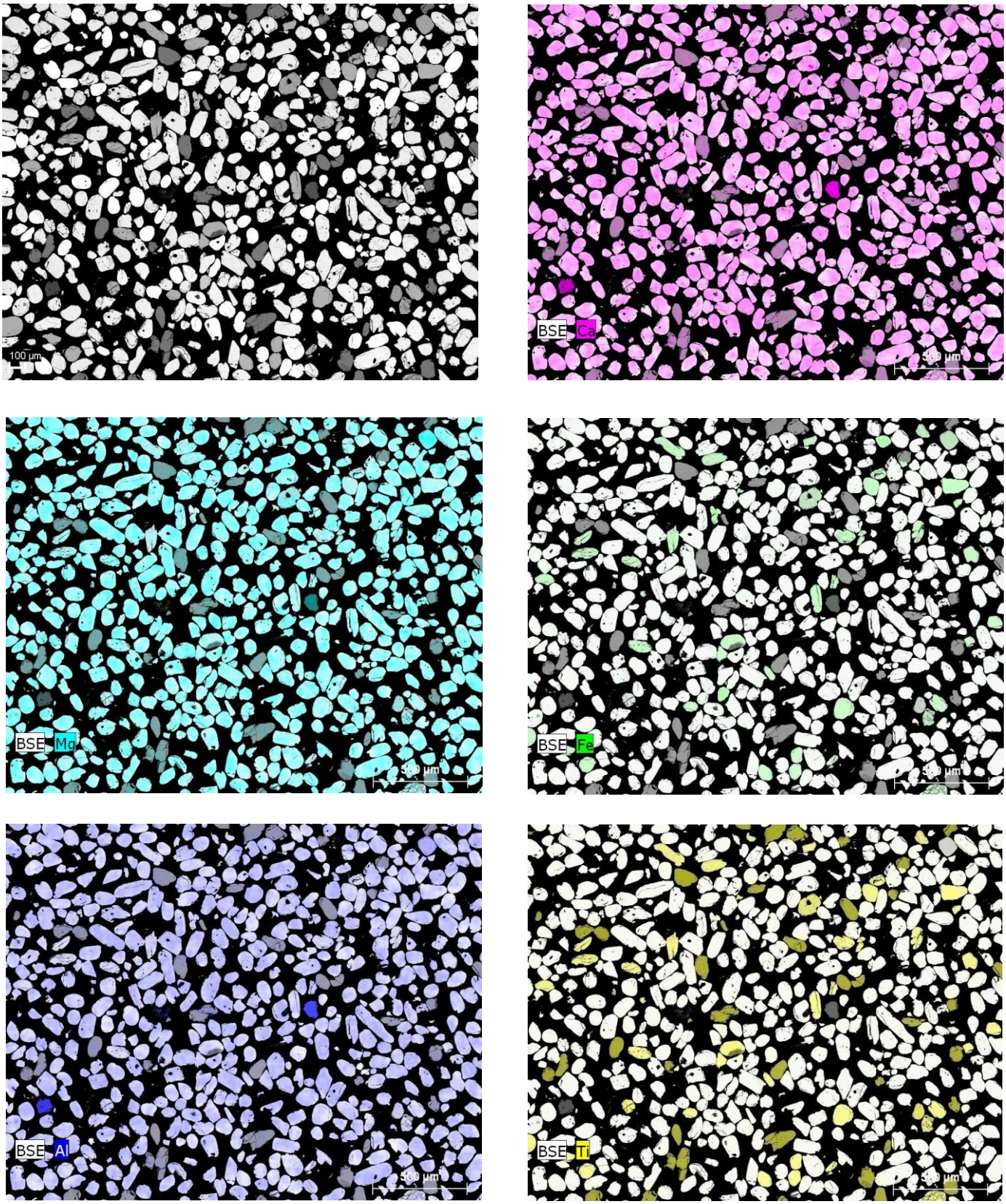


Figure A.8: BSE image and individual elemental maps showing the occurrence of specific mapped elements of –106 µm size fraction.

APPENDIX B: EMPA DATA

The detailed EMPA data is presented tables below:

Table B.1: EMPA data of amphibole and other silicate minerals

Analytes	MgO	Al_2O_3	SiO_2	CaO	TiO_2	MnO	FeO	Sm_2O_3	Eu_2O_3	Gd_2O_3	Ho_2O_3	PbO		
LLD	0.02	0.01	0.02	0.01	0.02	0.02	0.03	0.03	0.03	0.05	0.09	0.16		
Grain. No.	MgO	Al_2O_3	SiO_2	CaO	TiO_2	MnO	FeO	Sm_2O_3	Eu_2O_3	Gd_2O_3	Ho_2O_3	PbO	Total	Mineral name
1	2.24	53.10	27.34	-	0.38	0.21	14.22	-	0.05	-	0.11	-	97.64	Silicate
2	1.34	53.75	27.64	-	0.52	0.04	14.92	-	-	-	-	-	98.22	Silicate
3	1.43	53.01	27.04	-	0.53	-	15.04	-	-	-	-	-	97.04	silicate
4	2.26	53.19	27.54	-	0.61	1.00	11.27	0.04	-	-	-	0.26	96.16	Silicate
5	1.92	52.91	26.92	-	0.60	0.27	14.46	-	-	-	-	-	97.07	Silicate
6	1.88	52.80	26.71	-	0.59	0.09	15.12	-	-	-	-	-	97.19	Silicate
7	1.00	52.57	27.19	-	0.40	-	16.31	0.06	-	0.06	-	-	97.58	Silicate
8	0.97	53.72	27.49	-	0.40	-	15.68	-	-	-	-	-	98.26	silicate
9	28.82	1.16	55.14	2.18	0.37	0.29	12.62	-	-	-	-	-	100.59	amphibole
10	21.49	0.87	52.36	3.72	0.35	0.45	20.67	-	-	-	-	-	99.91	amphibole
11	30.46	1.37	54.86	2.03	0.15	0.29	10.68	-	-	-	-	-	99.84	amphibole
12	28.06	1.34	54.00	2.30	0.23	0.29	12.74	-	-	-	-	-	98.96	amphibole

Table B.2: EMPA data of epidote

Analytes	MgO	Al_2O_3	SiO_2	CaO	TiO_2	MnO	FeO		
LLD	0.02	0.01	0.02	0.01	0.02	0.02	0.03		
Grain No.	MgO	Al_2O_3	SiO_2	CaO	TiO_2	MnO	FeO	Total	Mineral name
13	17.00	3.24	51.60	18.62	0.69	0.22	7.78	99.15	Epidote
14	17.08	2.85	51.50	18.67	0.57	0.21	7.77	98.65	Epidote
15	18.09	1.96	51.57	18.63	0.40	0.24	7.44	98.32	Epidote
16	17.54	3.00	51.75	17.73	0.42	0.21	7.26	97.91	Epidote
17	17.79	2.49	52.16	17.30	0.49	0.26	8.13	98.62	Epidote
18	16.42	1.88	51.76	17.29	0.56	0.28	10.95	99.14	Epidote
19	17.04	2.48	51.74	20.07	0.36	0.17	6.22	98.07	Epidote
20	16.57	1.30	52.40	17.36	0.51	0.31	11.16	99.61	Epidote
21	17.05	2.75	51.51	18.85	0.43	0.18	6.79	97.55	Epidote
22	18.48	1.77	52.18	17.71	0.30	0.21	7.69	98.34	Epidote
23	18.28	1.87	52.59	18.21	0.26	0.17	6.87	98.27	Epidote
24	17.98	1.43	52.10	18.47	0.34	0.26	8.45	99.02	Epidote
25	18.17	1.35	51.53	17.67	0.34	0.28	8.74	98.07	Epidote
26	17.72	1.90	52.37	17.72	0.42	0.23	8.80	99.16	Epidote
27	18.05	2.24	52.86	17.80	0.38	0.19	7.25	98.77	Epidote
28	16.93	1.56	52.07	19.47	0.46	0.22	8.13	98.82	Epidote
29	16.48	2.44	51.83	19.32	0.42	0.21	7.86	98.55	Epidote
30	18.02	1.57	52.39	18.39	0.32	0.20	7.11	98.00	Epidote
31	17.73	1.67	52.02	18.67	0.37	0.21	7.83	98.49	Epidote
32	17.43	1.37	53.13	19.02	0.41	0.22	8.34	99.94	Epidote
33	16.48	1.84	51.78	18.68	0.54	0.22	9.61	99.16	Epidote
34	16.99	1.79	52.18	19.11	0.38	0.21	8.12	98.77	Epidote
35	16.64	1.13	52.58	17.00	0.55	0.33	11.81	100.04	Epidote
36	17.05	2.26	52.74	19.94	0.34	0.14	6.01	98.49	Epidote
37	16.13	2.37	51.69	19.31	0.56	0.18	8.24	98.48	Epidote
38	15.26	1.55	51.31	17.31	0.66	0.30	12.48	98.87	Epidote
39	16.79	2.71	51.24	19.94	0.50	0.19	6.92	98.30	Epidote
40	17.51	2.08	51.87	19.11	0.37	0.19	6.78	97.91	Epidote
41	17.28	2.43	52.37	20.30	0.48	0.17	6.36	99.40	Epidote
42	17.83	1.95	52.65	18.50	0.40	0.22	7.07	98.63	Epidote
43	18.35	2.04	52.57	19.14	0.34	0.19	7.16	99.80	Epidote
44	17.67	2.52	51.48	18.11	0.49	0.19	7.29	97.75	Epidote
45	17.50	2.04	52.13	18.16	0.35	0.25	8.19	98.62	Epidote
46	18.16	2.21	52.77	17.45	0.43	0.22	8.43	99.67	Epidote

Table B.3: EMPA data of other silicate minerals

Analytes	MgO	Al_2O_3	SiO_2	P_2O_5	CaO	TiO_2	MnO	FeO	SrO		
LLD	0.02	0.01	0.02	0.03	0.01	0.02	0.02	0.03	0.04		
Grain No.	MgO	Al_2O_3	SiO_2	P_2O_5	CaO	TiO_2	MnO	FeO	SrO	Total	Mineral name
47	18.04	2.59	50.83	-	18.14	0.51	0.19	6.43	-	96.74	CaFeMgAlSiO+Na
48	9.92	11.45	42.30	-	11.41	1.10	0.27	17.55	-	94.00	CaFeMgAlSiO+Na
49	16.14	8.51	47.84	-	11.28	0.99	0.19	10.08	-	95.03	CaFeAlSiO
50	5.75	10.10	40.58	-	10.55	2.18	0.38	24.85	-	94.40	CaFeMgAlSiO+Na
51	24.94	0.65	53.23	-	4.16	0.16	0.34	15.32	-	98.81	FeCaAlSiO
52	10.42	9.33	46.12	-	9.97	1.06	0.39	19.12	-	96.40	CaFeMgAlSiO+Na
53	11.58	11.22	44.29	-	11.83	0.99	0.32	15.82	-	96.04	CaFeMgAlSiO+Na
54	11.24	13.18	44.13	-	11.14	0.78	0.28	14.54	-	95.30	CaFeMgAlSiO+Na
55	-	18.67	60.32	-	15.05	-	0.37	5.44	1.28	101.13	CaAlSiO

Table B.4: EMPA data of zircon

Analytes	SiO_2	Y_2O_3	ZrO_2	Ce_2O_3	Pr_2O_3	Sm_2O_3	Eu_2O_3	Gd_2O_3	Dy_2O_3	Ho_2O_3	ThO_2	UO_2		
LLD	0.02	0.04	0.07	0.09	0.09	0.03	0.03	0.05	0.05	0.09	0.05	0.05		
Grain No.	SiO_2	Y_2O_3	ZrO_2	Ce_2O_3	Pr_2O_3	Sm_2O_3	Eu_2O_3	Gd_2O_3	Dy_2O_3	Ho_2O_3	ThO_2	UO_2	Total	Mineral name
56	31.52	-	67.15	0.09	-	0.07	-	-	0.07	-	-	-	98.90	zircon
57	30.97	-	67.50	-	-	0.04	-	0.06	-	-	-	-	98.57	zircon
58	31.25	-	67.77	-	-	-	-	-	-	0.16	-	-	99.18	zircon
59	31.60	-	67.48	-	-	-	-	-	-	-	-	-	99.08	zircon
60	31.35	-	67.30	-	0.16	0.08	0.05	0.06	-	-	0.05	-	99.04	zircon
61	31.58	-	66.65	-	-	-	-	-	-	-	0.09	0.08	98.40	zircon
62	30.94	-	67.80	-	-	-	-	-	-	-	0.07	-	98.81	zircon
63	31.40	-	67.46	-	-	-	-	0.05	-	-	-	-	98.91	zircon
64	31.48	-	67.56	-	0.10	-	-	-	-	-	-	-	99.14	zircon
65	31.55	-	67.49	-	-	-	0.09	-	0.08	-	-	-	99.21	zircon

Table B.5: EMPA data of zircon

Analytes	SiO_2	ZrO_2	La_2O_3	Ce_2O_3	Pr_2O_3	Nd_2O_3	Sm_2O_3	Eu_2O_3	Gd_2O_3	Dy_2O_3	ThO_2	UO_2		
LLD	0.02	0.07	0.10	0.09	0.09	0.07	0.03	0.03	0.05	0.05	0.05	0.05		
Grain No.	SiO_2	ZrO_2	La_2O_3	Ce_2O_3	Pr_2O_3	Nd_2O_3	Sm_2O_3	Eu_2O_3	Gd_2O_3	Dy_2O_3	ThO_2	UO_2	Total	Mineral name
66	31.62	67.15	0.11	0.11	-	-	0.06	0.05	-	-	-	0.06	99.16	zircon
67	31.57	66.86	-	-	-	0.08	-	-	-	-	-	-	98.51	zircon
68	31.47	67.49	-	-	-	-	-	-	-	-	0.06	-	99.02	zircon
69	32.05	67.11	0.13	-	-	-	-	-	-	0.10	-	-	99.39	zircon
70	33.41	66.38	-	-	-	-	0.04	0.11	-	0.07	0.07	-	100.08	zircon
71	31.07	68.13	-	-	-	-	-	-	-	-	-	-	99.20	zircon
72	31.44	67.74	-	-	0.16	0.10	-	-	-	0.12	-	-	99.55	zircon
73	32.14	66.69	-	-	-	-	-	-	-	0.06	-	-	98.89	zircon
74	31.92	66.36	-	-	-	-	-	-	0.05	0.09	-	-	98.43	zircon

Table B.6: EMPA data of zircon

Analytes	SiO_2	Y_2O_3	ZrO_2	La_2O_3	Pr_2O_3	Nd_2O_3	Sm_2O_3	Eu_2O_3	Gd_2O_3	Dy_2O_3	Ho_2O_3	ThO_2	UO_2		
LLD	0.02	0.04	0.07	0.10	0.09	0.07	0.03	0.03	0.05	0.05	0.09	0.05	0.05		
Grain No.	SiO_2	Y_2O_3	ZrO_2	La_2O_3	Pr_2O_3	Nd_2O_3	Sm_2O_3	Eu_2O_3	Gd_2O_3	Dy_2O_3	Ho_2O_3	ThO_2	UO_2	Total	Mineral name
75	32.22	0.07	67.04	-	-	0.11	-	-	-	-	-	0.06	-	99.50	zircon
76	32.17	-	66.90	-	-	-	-	-	-	-	-	-	0.05	99.12	zircon
77	31.59	-	67.82	-	-	0.14	-	-	-	-	-	0.10	0.07	99.72	zircon
78	31.66	-	67.92	-	-	-	-	0.07	0.06	-	-	-	-	99.71	zircon
79	31.14	-	68.19	-	-	-	0.06	-	0.09	0.05	-	-	-	99.52	zircon
80	31.50	-	67.37	-	-	-	-	-	-	0.09	-	-	-	98.95	zircon
81	31.44	-	67.37	-	0.10	-	0.09	-	0.09	0.09	-	-	-	99.17	zircon
82	31.32	-	67.33	-	-	-	-	-	-	-	-	-	-	98.65	zircon
83	30.83	-	67.77	-	-	-	0.05	-	-	0.08	-	-	-	98.72	zircon
84	32.76	-	66.35	-	-	-	-	-	-	-	-	-	-	99.11	zircon
85	31.47	-	67.55	0.11	0.10	-	-	-	-	-	0.13	-	-	99.36	zircon
86	31.10	-	67.93	-	-	-	-	-	-	0.07	0.20	-	-	99.30	zircon
87	31.02	-	67.38	-	-	-	-	-	-	-	-	0.06	-	98.46	zircon
88	31.87	-	66.56	-	-	-	-	-	-	0.07	-	-	-	98.50	zircon
89	31.78	-	67.15	-	-	-	-	-	-	0.05	-	-	-	98.99	zircon
90	31.55	-	66.92	-	-	-	0.08	-	-	-	-	-	-	98.56	zircon
91	31.61	-	66.86	-	-	-	0.06	-	-	-	-	-	-	98.53	zircon
92	31.85	-	66.97	-	-	-	-	-	-	-	-	-	-	98.82	zircon
93	31.41	-	67.16	-	-	-	-	-	-	-	-	-	-	98.56	zircon
94	31.63	-	66.77	-	-	-	-	-	-	-	-	0.05	-	98.45	zircon
95	31.59	-	67.43	-	-	-	-	-	-	-	-	0.12	0.09	99.22	zircon
96	31.38	-	68.41	-	-	-	-	-	-	-	-	0.07	-	99.86	zircon
97	31.45	-	67.11	-	-	-	0.06	-	-	-	-	-	0.22	98.84	zircon
98	30.67	-	68.43	-	-	0.11	0.10	-	-	0.06	-	-	-	99.37	zircon
99	32.07	-	66.87	-	-	0.11	0.04	0.05	-	-	-	-	-	99.14	zircon
100	32.08	-	66.58	-	-	-	-	-	-	0.08	0.16	-	-	98.90	zircon

Table B.7: EMPA data of zircon

Analytes	SiO_2	Y_2O_3	ZrO_2	La_2O_3	Ce_2O_3	Pr_2O_3	Nd_2O_3	Sm_2O_3	Eu_2O_3	Gd_2O_3	Dy_2O_3	Ho_2O_3	ThO_2	UO_2		
LLD	0.02	0.04	0.07	0.10	0.09	0.09	0.07	0.03	0.03	0.05	0.05	0.09	0.05	0.05		
Grain No.	SiO_2	Y_2O_3	ZrO_2	La_2O_3	Ce_2O_3	Pr_2O_3	Nd_2O_3	Sm_2O_3	Eu_2O_3	Gd_2O_3	Dy_2O_3	Ho_2O_3	ThO_2	UO_2	Total	Mineral name
101	31.53	-	67.47	-	0.11	0.12	-	0.04	0.04	0.15	0.06	0.18	-	-	99.70	zircon
102	31.65	-	67.47	-	-	-	-	-	-	-	0.09	-	-	-	99.20	zircon
103	32.27	-	67.49	-	-	-	-	-	0.05	-	0.11	0.11	-	-	100.02	zircon
104	32.06	-	67.74	-	-	-	-	0.05	-	-	-	-	0.05	-	99.91	zircon
105	31.48	-	67.48	-	-	-	-	-	0.07	-	0.10	-	-	-	99.13	zircon
106	30.39	-	68.11	-	0.10	-	-	-	0.08	-	-	-	-	-	98.69	zircon
107	32.09	-	66.46	-	-	0.11	-	-	-	-	0.06	-	0.08	0.08	98.88	zircon
108	31.10	-	68.30	0.12	-	-	-	-	-	-	-	-	-	-	99.52	zircon
109	32.13	-	66.81	-	-	-	-	-	0.05	0.06	-	0.13	-	-	99.19	zircon
110	31.42	0.09	67.30	-	-	-	0.09	-	0.06	-	-	-	-	-	98.96	zircon
111	31.29	-	66.59	-	-	-	-	-	-	-	-	-	-	-	97.88	zircon
112	31.45	-	67.37	-	0.09	-	-	-	-	-	-	-	-	-	98.91	zircon
113	32.24	-	66.48	-	-	-	-	-	-	-	0.05	0.13	-	0.29	99.18	zircon
114	31.71	-	67.23	-	-	-	-	-	-	-	-	-	-	-	98.94	zircon
115	32.11	-	65.13	-	-	0.14	0.11	0.06	-	-	0.08	-	-	-	97.64	zircon
116	31.96	-	67.12	-	-	-	-	-	-	-	0.09	-	-	-	99.17	zircon
117	30.98	-	66.97	-	-	-	0.10	-	-	-	0.17	-	0.07	0.14	98.45	zircon
118	31.47	-	67.38	-	-	-	-	-	-	-	-	-	0.08	-	98.93	zircon
119	31.69	-	66.09	-	-	-	-	-	-	-	-	-	0.12	0.40	98.30	zircon
120	31.15	-	67.30	-	-	-	-	-	-	-	-	-	-	-	98.45	zircon
121	31.24	-	67.45	-	-	-	-	-	-	-	-	-	-	-	98.68	zircon
122	31.36	-	66.84	-	-	-	-	-	-	-	0.05	-	-	-	98.25	zircon
123	31.19	0.19	67.36	-	-	-	-	-	-	-	-	-	-	-	98.73	zircon
124	31.17	-	67.65	-	-	-	-	-	-	-	-	0.16	-	-	98.98	zircon
125	31.92	-	66.63	-	-	0.12	-	-	-	-	0.05	-	-	-	98.71	zircon
126	30.81	0.43	67.58	-	-	-	-	-	-	-	-	-	-	-	98.83	zircon
127	31.88	-	67.58	-	-	-	-	-	-	-	-	-	-	-	99.46	zircon
128	31.12	0.04	66.93	-	-	-	-	-	-	-	-	-	0.12	-	98.22	zircon
129	30.85	0.30	67.58	-	-	-	-	-	-	-	-	-	0.13	0.26	99.12	zircon
130	31.24	-	67.24	-	-	-	-	-	-	-	-	-	-	-	98.49	zircon

Table B.8: EMPA data of zircon

Analytes	SiO_2	Y_2O_3	ZrO_2	La_2O_3	Ce_2O_3	Pr_2O_3	Nd_2O_3	$Sm2O_3$	Eu_2O_3	Gd_2O_3	Dy_2O_3	Ho_2O_3	ThO_2	UO_2		
LLD	0.02	0.04	0.07	0.10	0.09	0.09	0.07	0.03	0.03	0.05	0.05	0.09	0.05	0.05		
Grain No.	SiO_2	Y_2O_3	ZrO_2	La_2O_3	Ce_2O_3	Pr_2O_3	Nd_2O_3	$Sm2O_3$	Eu_2O_3	Gd_2O_3	Dy_2O_3	Ho_2O_3	ThO_2	UO_2	Total	Mineral name
131	30.38	-	68.20	-	-	-	-	-	-	-	-	-	-	-	98.58	zircon
132	31.14	-	68.10	-	-	-	-	-	-	-	-	-	-	-	99.24	zircon
133	31.29	-	67.30	0.12	-	0.15	-	-	-	-	-	-	0.06	0.06	98.98	zircon
134	31.20	-	67.67	-	-	-	-	-	-	-	-	-	-	-	98.87	zircon
135	31.38	-	67.28	-	-	-	-	-	-	-	0.10	-	-	-	98.75	zircon
136	31.63	-	66.81	-	-	0.13	-	-	-	-	-	-	-	-	98.56	zircon
137	31.34	-	66.92	-	-	-	0.09	-	-	-	0.07	-	0.11	-	98.54	zircon
138	31.50	-	67.66	-	0.09	-	-	-	-	-	-	0.14	-	-	99.39	zircon
139	30.92	-	67.47	-	-	-	-	-	-	-	0.06	-	-	0.06	98.50	zircon
140	31.42	-	67.17	-	-	-	-	-	-	-	-	-	-	-	98.59	zircon
141	31.62	-	66.94	-	-	0.15	-	0.08	-	-	-	0.09	-	-	98.88	zircon
142	31.84	-	66.62	-	-	-	-	-	-	-	-	0.13	-	-	98.59	zircon
143	31.17	-	66.68	-	-	0.10	-	-	-	-	-	-	-	-	97.95	zircon
144	30.90	-	67.49	-	-	-	-	-	-	-	-	-	-	-	98.39	zircon
145	31.06	0.34	67.86	-	-	-	-	-	-	-	-	-	-	-	99.26	zircon
146	31.42	-	67.14	-	-	-	-	0.05	-	-	-	-	-	-	98.60	zircon
147	32.00	-	66.46	-	0.10	-	-	-	-	-	-	-	-	-	98.57	zircon
148	31.27	-	67.95	-	-	-	-	0.06	-	-	0.05	-	-	-	99.33	zircon
149	31.07	-	67.44	-	-	-	-	-	-	-	-	0.15	-	-	98.66	zircon
150	32.13	-	66.84	-	-	0.11	-	-	-	-	0.05	-	0.12	-	99.26	zircon
151	31.52	0.04	66.86	0.13	-	-	-	-	-	-	-	-	0.05	-	98.60	zircon
152	31.90	-	66.69	-	-	-	-	-	-	-	0.06	-	-	0.09	98.74	zircon
153	31.53	-	67.64	-	-	0.11	-	-	-	-	-	-	-	-	99.28	zircon
154	31.25	-	67.05	-	-	-	-	-	-	-	-	-	-	-	98.30	zircon
155	31.17	-	67.81	-	-	-	-	0.07	-	-	-	-	-	-	99.05	zircon
156	30.57	-	67.76	-	0.10	-	-	-	-	-	0.06	0.11	-	-	98.60	zircon

Table B.9: EMPA data of zircon

Analytes	SiO_2	Y_2O_3	ZrO_2	Nd_2O_3	Sm_2O_3	Dy_2O_3	Ho_2O_3	ThO_2	UO_2		
LLD	0.02	0.04	0.07	0.07	0.03	0.05	0.09	0.05	0.05		
Grain No.	SiO_2	Y_2O_3	ZrO_2	Nd_2O_3	Sm_2O_3	Dy_2O_3	Ho_2O_3	ThO_2	UO_2	Total	Mineral name
157	31.37	-	67.37	-	0.05	-	-	-	-	98.79	zircon
158	31.51	-	66.96	-	0.07	0.05	-	-	-	98.59	zircon
159	31.37	-	67.16	-	0.05	-	-	0.07	-	98.64	zircon
160	31.74	-	66.49	-	-	-	-	-	0.07	98.30	zircon
161	32.00	0.31	66.99	0.08	-	-	-	0.15	0.12	99.65	zircon
162	31.67	-	67.23	-	0.04	0.05	-	0.05	-	99.04	zircon
163	31.20	-	67.21	-	0.05	0.08	-	0.10	-	98.64	zircon
164	31.70	-	67.68	-	-	-	-	-	-	99.38	zircon
165	31.12	-	67.76	-	-	-	0.12	-	-	99.00	zircon
166	31.15	-	67.75	-	-	0.06	-	-	-	98.96	zircon
167	30.54	-	67.87	-	-	-	-	-	-	98.40	zircon
168	31.08	-	67.35	-	-	-	-	0.05	-	98.48	zircon

Table B.10: EMPA data of monazite

Analytes	F	SiO_2	P_2O5	CaO	Y_2O_3	La_2O_3	Ce_2O_3	Pr_2O_3	Nd_2O_3	Sm_2O_3	Dy_2O_3	Ho_2O_3	ThO_2	UO_2		
LLD	0.04	0.02	0.03	0.01	0.04	0.10	0.09	0.09	0.07	0.03	0.05	0.09	0.05	0.05		
Grain No.	F	SiO_2	P_2O5	CaO	Y_2O_3	La_2O_3	Ce_2O_3	Pr_2O_3	Nd_2O_3	Sm_2O_3	Dy_2O_3	Ho_2O_3	ThO_2	UO_2	Total	Mineral name
169	0.8246	1.00	25.87	1.07	4.85	14.33	28.00	2.74	9.70	1.61	0.57	0.19	6.75	0.11	97.62	monazite
170	0.8208	1.02	26.62	1.11	2.15	13.47	28.04	3.00	11.59	1.90	0.52	-	9.03	0.24	99.51	monazite
171	0.8835	0.91	27.37	1.21	2.17	13.37	28.16	3.05	12.68	2.29	0.48	-	7.54	0.16	100.28	monazite
172	0.8531	0.80	26.97	1.21	1.37	15.39	29.58	2.72	10.42	1.54	0.38	-	8.76	0.27	100.27	monazite
173	0.8285	1.07	26.26	0.75	0.22	18.07	31.70	2.64	8.97	0.85	0.12	0.17	7.95	-	99.60	monazite
174	0.8007	1.10	25.67	0.87	-	15.53	31.47	2.99	11.06	1.38	-	-	8.70	0.21	99.79	monazite
175	0.9849	0.13	28.72	1.74	3.49	13.08	26.94	2.75	10.58	2.22	1.02	-	7.62	0.52	99.80	monazite
176	0.8955	0.56	26.40	1.45	0.46	13.60	29.63	3.46	12.11	1.94	0.22	0.12	8.72	0.57	100.13	monazite
177	0.8377	1.67	24.44	1.78	-	9.04	25.97	3.49	15.61	2.19	0.07	-	15.03	0.18	100.31	monazite
178	0.8105	0.79	26.68	0.77	0.60	16.16	31.51	2.83	10.90	1.29	0.29	-	7.00	0.08	99.71	monazite
179	0.9078	0.94	27.36	1.52	2.29	10.56	25.77	3.22	13.23	2.65	0.76	-	10.46	0.38	100.05	monazite
180	0.8251	0.47	27.21	0.31	1.04	19.31	33.91	2.78	9.85	1.20	0.22	0.20	2.81	0.15	100.29	monazite
181	0.8767	1.07	26.08	1.18	1.42	14.20	28.75	2.85	10.75	1.66	0.49	-	10.13	0.11	99.57	monazite
182	0.9326	0.43	27.59	0.98	1.11	13.26	30.08	3.24	13.50	2.46	0.56	-	5.68	0.40	100.21	monazite
183	0.8966	0.40	27.37	0.91	2.99	16.07	30.91	2.68	9.55	1.36	0.63	-	6.04	0.17	99.98	monazite
184	0.78	3.48	22.07	1.18	3.50	10.33	22.34	2.66	9.62	2.01	0.84	0.22	17.78	1.40	98.23	monazite
185	0.7916	1.85	23.50	0.30	2.00	15.53	31.25	2.82	11.37	1.73	0.53	0.10	8.13	0.35	100.25	monazite
186	0.783	1.27	25.25	0.34	0.79	15.94	31.84	2.89	11.10	1.78	0.57	0.14	6.73	0.21	99.64	monazite
187	0.8484	0.71	26.39	0.90	0.23	11.70	29.28	3.46	16.43	2.70	0.31	-	7.03	0.05	100.01	monazite
188	0.8317	1.23	25.86	0.74	1.45	14.32	29.87	3.01	11.70	1.76	0.49	0.23	8.08	0.56	100.14	monazite
189	0.8743	0.26	27.89	0.85	2.85	14.00	29.31	3.14	12.87	2.12	0.75	0.17	4.02	1.16	100.25	monazite
190	0.8201	0.35	27.01	0.52	0.50	19.12	34.22	3.01	9.93	1.07	0.11	-	3.37	0.16	100.19	monazite
191	0.8152	0.34	27.46	0.46	0.88	16.70	32.57	3.03	12.64	1.58	0.36	-	2.87	0.25	99.94	monazite
192	0.9141	1.24	26.69	0.96	5.96	10.22	24.81	2.98	12.53	2.80	1.26	-	8.18	1.30	99.82	monazite
193	0.9167	1.14	26.60	1.32	3.52	12.05	26.25	2.60	11.77	2.30	0.80	-	10.20	0.27	99.71	monazite
194	0.8823	0.75	26.91	0.73	2.40	13.48	29.46	3.06	12.97	2.14	0.60	-	6.33	0.32	100.02	monazite
195	0.8178	0.60	26.20	0.87	0.32	20.88	32.06	2.61	8.51	0.71	0.12	-	6.10	0.22	100.02	monazite
196	0.8752	0.30	27.42	0.98	1.32	13.26	29.55	3.12	14.55	2.58	0.51	-	5.45	0.29	100.21	monazite
197	0.8661	0.09	27.97	1.09	1.64	13.49	29.17	3.10	14.02	2.44	0.55	-	4.79	0.60	99.82	monazite
198	0.8862	0.51	27.56	1.61	1.21	13.64	29.06	2.93	11.44	1.98	0.42	-	8.60	0.22	100.08	monazite
199	0.8078	0.22	27.00	0.78	0.69	14.45	32.07	3.48	13.93	1.67	0.18	-	4.36	0.26	99.90	monazite
200	0.8828	0.17	25.35	1.36	0.58	15.57	30.25	3.44	13.37	2.38	0.24	-	6.19	0.53	100.31	monazite
201	0.9408	0.31	26.09	1.67	3.45	12.22	26.74	2.85	12.73	2.63	0.80	-	8.37	0.52	99.30	monazite

Table B.11: EMPA data of titanite

Analytes	MgO	Al_2O_3	SiO_2	P_2O_5	CaO	TiO_2	MnO	FeO	Y_2O_3	ZrO_2	La_2O_3	Ce_2O_3	Nd_2O_3	Sm_2O_3	Eu_2O_3	Gd_2O_3	Dy_2O_3	Ho_2O_3		
LLD	0.02	0.01	0.02	0.03	0.01	0.02	0.02	0.03	0.04	0.07	0.10	0.09	0.07	0.03	0.03	0.05	0.05	0.09		
Grain No.	MgO	Al_2O_3	SiO_2	P_2O_5	CaO	TiO_2	MnO	FeO	Y_2O_3	ZrO_2	La_2O_3	Ce_2O_3	Nd_2O_3	Sm_2O_3	Eu_2O_3	Gd_2O_3	Dy_2O_3	Ho_2O_3	Total	Mineral name
202	-	2.09	29.33	-	26.93	36.63	0.25	1.63	0.27	0.08	0.30	0.54	0.53	0.11	0.05	0.11	0.14	-	98.97	titanite
203	0.02	3.05	30.12	0.08	27.13	36.05	0.18	1.55	0.17	-	-	-	0.27	0.10	0.07	0.07	0.06	0.10	99.02	titanite
204	0.02	1.84	29.71	-	27.73	37.52	0.14	1.48	-	-	0.17	0.16	0.14	-	-	-	-	-	98.92	titanite

Table B.12: EMPA data of ilmenite

Analytes	MgO	Al_2O_3	SiO_2	P_2O_5	CaO	TiO_2	MnO	FeO		
LLD	0.02	0.01	0.02	0.03	0.01	0.02	0.02	0.03		
Grain No.	MgO	Al_2O_3	SiO_2	P_2O_5	CaO	TiO_2	MnO	FeO	Total	Mineral name
205	0.85	0.19	-	-	-	53.58	0.30	44.67	99.59	ilmenite
206	0.95	-	2.27	-	0.05	52.25	0.39	42.56	98.47	ilmenite
207	1.16	0.12	-	-	-	52.53	0.37	45.09	99.27	ilmenite
208	2.98	0.20	0.04	-	-	50.96	0.39	44.66	99.24	ilmenite
209	1.08	0.07	0.03	-	-	54.22	0.44	43.09	98.93	ilmenite
210	0.05	0.30	0.40	0.14	0.06	54.32	0.43	43.95	99.66	ilmenite
211	1.30	0.04	0.05	-	0.02	55.30	0.31	42.23	99.24	ilmenite
212	0.69	0.12	-	-	-	54.73	0.27	43.41	99.21	ilmenite
213	-	0.07	0.06	-	0.02	56.41	0.78	41.80	99.14	ilmenite
214	0.64	0.05	-	-	-	52.17	0.46	46.65	99.96	ilmenite
215	2.19	0.18	0.02	-	-	50.19	0.44	46.87	99.90	ilmenite
216	0.37	0.08	0.03	-	-	52.76	0.57	45.98	99.80	ilmenite
217	0.11	0.07	0.06	-	0.11	51.14	2.82	45.58	99.88	ilmenite
218	1.08	0.15	0.04	-	0.03	55.88	0.57	42.46	100.21	ilmenite
219	0.35	0.08	-	-	-	51.42	0.68	47.85	100.38	ilmenite
220	1.57	0.13	0.05	-	0.02	52.89	0.42	44.55	99.62	ilmenite
221	0.03	0.03	-	-	-	51.16	2.13	46.68	100.03	ilmenite
222	1.14	0.10	-	-	-	51.05	0.46	47.07	99.81	ilmenite
223	0.47	0.05	-	-	-	49.78	0.59	48.63	99.52	ilmenite
224	1.37	0.04	-	-	-	53.59	0.45	44.42	99.88	ilmenite
225	0.37	0.42	0.51	-	0.04	55.31	1.52	41.33	99.49	ilmenite
226	0.07	0.01	0.02	-	-	53.91	1.05	44.61	99.68	ilmenite
227	0.76	0.06	-	-	-	51.88	0.42	46.84	99.97	ilmenite
228	1.01	0.05	-	-	-	51.12	0.54	46.77	99.49	ilmenite
229	-	0.01	-	-	-	51.14	1.04	47.82	100.01	ilmenite

Table B.13: EMPA data of rutile

Analytes	F	MgO	Al_2O_3	SiO_2	P_2O_5	CaO	TiO_2	MnO	FeO		
LLD	0.04	0.02	0.01	0.02	0.03	0.01	0.02	0.02	0.03		
Grain No.	F	MgO	Al_2O_3	SiO_2	P_2O_5	CaO	TiO_2	MnO	FeO	Total	Mineral name
230	0	0.00	0.05	0.00	0.00	0.01	99.48	0.00	0.02	99.56	rutile
231	0.0001	0.00	0.04	0.00	0.00	0.02	99.02	0.00	0.01	99.09	rutile
232	0	0.00	0.14	0.12	0.00	0.02	98.88	0.03	0.41	99.60	rutile
233	0	0.00	0.05	0.02	0.00	0.00	99.86	0.01	0.09	100.04	rutile
234	0	0.00	0.04	0.01	0.02	0.00	99.66	0.02	0.07	99.82	rutile
235	0	0.00	0.05	0.01	0.00	0.00	100.03	0.00	0.00	100.09	rutile
236	0	0.00	0.03	0.02	0.01	0.01	99.72	0.00	0.07	99.86	rutile
237	0	0.00	0.04	0.03	0.00	0.00	99.78	0.00	0.06	99.90	rutile
238	0	0.00	0.04	0.01	0.00	0.00	99.95	0.00	0.04	100.05	rutile
239	0	0.00	0.04	0.03	0.00	0.00	99.85	0.00	0.06	99.98	rutile
240	0.0189	0.00	0.03	0.05	0.00	0.02	99.73	0.00	0.13	99.98	rutile
241	0.007	0.01	0.09	0.13	0.00	0.02	97.21	0.02	1.36	98.85	rutile
242	0	0.00	0.04	0.05	0.00	0.00	99.73	0.00	0.31	100.13	rutile
243	0	0.00	0.04	0.01	0.00	0.01	99.35	0.00	0.22	99.64	rutile
244	0	0.00	0.08	0.01	0.00	0.00	99.70	0.00	0.16	99.95	rutile
245	0	0.00	0.04	0.03	0.00	0.02	98.06	0.02	0.64	98.80	rutile
246	0	0.00	0.04	0.01	0.00	0.00	99.70	0.01	0.16	99.92	rutile
247	0	0.00	0.04	0.06	0.00	0.04	99.65	0.00	0.12	99.91	rutile
248	0	0.00	0.02	0.01	0.02	0.00	99.74	0.02	0.02	99.83	rutile
249	0	0.00	0.03	0.02	0.00	0.01	99.73	0.01	0.20	99.99	rutile
250	0	0.00	0.06	0.01	0.00	0.02	99.82	0.00	0.08	99.99	rutile
251	0	0.00	0.04	0.06	0.00	0.01	99.48	0.00	0.17	99.75	rutile
252	0	0.00	0.06	0.00	0.01	0.00	99.91	0.00	0.13	100.13	rutile
253	0	0.00	0.06	0.03	0.00	0.00	99.23	0.02	0.37	99.70	rutile
254	0	0.00	0.06	0.04	0.01	0.01	99.63	0.00	0.19	99.95	rutile
255	0	0.00	0.06	0.00	0.00	0.00	99.69	0.02	0.25	100.02	rutile
256	0.0158	0.00	0.09	0.16	0.03	0.03	99.66	0.02	0.28	100.28	rutile
257	0	0.00	0.08	0.11	0.00	0.04	99.32	0.03	0.44	100.03	rutile
258	0	0.00	0.19	0.12	0.01	0.05	98.89	0.00	0.51	99.77	rutile
259	0	0.00	0.10	0.10	0.00	0.02	99.57	0.03	0.19	100.00	rutile
260	0	0.00	0.06	0.04	0.00	0.04	99.75	0.01	0.24	100.13	rutile
261	0	0.00	0.02	0.01	0.00	0.00	99.75	0.00	0.20	99.99	rutile
262	0	0.00	0.08	0.02	0.00	0.01	99.56	0.00	0.14	99.82	rutile
263	0	0.00	0.07	0.00	0.01	0.00	99.26	0.01	0.29	99.65	rutile
264	0	0.00	0.43	0.35	0.00	0.00	98.58	0.03	0.45	99.83	rutile
265	0	0.00	0.06	0.01	0.00	0.01	99.57	0.00	0.28	99.93	rutile
266	0	0.00	0.06	0.01	0.00	0.00	99.90	0.00	0.19	100.16	rutile

Table B.14: EMPA data of rutile

Analytes	Al_2O_3	SiO_2	P_2O_5	CaO	TiO_2	MnO	FeO		
LLD	0.01	0.02	0.03	0.01	0.02	0.02	0.03		
Grain No.	Al_2O_3	SiO_2	P_2O_5	CaO	TiO_2	MnO	FeO	Total	Mineral name
267	0.06	0.02	0.01	0.01	100.00	0.02	0.02	100.13	rutile
268	0.05	0.00	0.00	0.01	99.52	0.00	0.26	99.84	rutile
269	0.07	0.17	0.00	0.06	99.59	0.00	0.21	100.10	rutile
270	0.09	0.03	0.00	0.01	99.48	0.00	0.43	100.04	rutile
271	0.10	0.07	0.03	0.01	99.16	0.00	0.87	100.23	rutile
272	0.04	0.03	0.00	0.00	99.16	0.00	0.15	99.40	rutile
273	0.03	0.06	0.00	0.05	99.71	0.01	0.16	100.02	rutile
274	0.03	0.06	0.00	0.00	99.87	0.00	0.19	100.17	rutile
275	0.10	0.03	0.00	0.01	99.77	0.01	0.22	100.15	rutile
276	0.05	0.08	0.00	0.00	99.52	0.00	0.20	99.85	rutile
277	0.12	0.02	0.00	0.00	98.60	0.00	0.78	99.52	rutile
278	0.31	0.50	0.00	0.01	98.54	0.00	0.41	99.78	rutile
279	0.06	0.01	0.00	0.01	99.78	0.00	0.13	99.98	rutile
280	0.05	0.03	0.02	0.00	99.57	0.02	0.62	100.31	rutile
281	0.08	0.06	0.00	0.00	99.24	0.00	0.40	99.79	rutile
282	0.05	0.01	0.00	0.00	99.13	0.00	0.07	99.26	rutile
283	0.01	0.03	0.00	0.01	99.88	0.00	0.04	99.97	rutile

Table B.15: EMPA data of leucoxene and hematite

Analytes	F	MgO	Al_2O_3	SiO_2	P_2O_5	CaO	TiO_2	MnO	FeO	SrO	Y_2O_3	ZrO_2		
LLD	0.04	0.02	0.01	0.02	0.03	0.01	0.02	0.02	0.03	0.04	0.04	0.07		
Grain No.	F	MgO	Al_2O_3	SiO_2	P_2O_5	CaO	TiO_2	MnO	FeO	SrO	Y_2O_3	ZrO_2	Total	Mineral name
284	0	0.00	0.11	0.01	0.00	0.01	90.22	0.00	3.30	0.00	-	0.23	93.89	leucoxene
285	0.004	0.01	0.47	0.29	0.03	0.03	93.69	0.03	5.84	0.01	-	0.11	100.50	leucoxene
286	0	0.19	0.66	3.81	0.01	3.38	73.27	0.10	15.38	0.04	-	0.00	96.83	leucoxene
287	0.0023	0.08	1.47	2.02	0.11	0.16	74.48	0.02	17.77	0.01	-	0.04	96.16	leucoxene
288	0	0.01	0.02	0.02	0.02	0.01	57.23	0.74	40.49	0.00	-	0.00	98.55	leucoxene
289	0.0146	0.00	0.17	0.37	0.01	0.10	94.13	0.01	8.11	0.01	-	0.13	103.06	leucoxene
290	0.0214	0.02	1.09	0.59	0.32	0.20	86.75	1.49	9.97	0.00	-	0.05	100.51	leucoxene
291	0.0212	0.07	2.78	0.53	0.28	0.16	75.00	0.20	18.93	0.05	-	0.08	98.09	leucoxene
292	0	0.05	1.74	2.12	0.00	0.05	93.86	0.00	2.38	0.06	-	1.11	101.37	leucoxene
293	0	0.02	0.34	0.04	0.00	0.02	85.11	0.04	6.18	0.00	-	0.11	91.87	leucoxene
294	0	0.07	0.44	0.22	0.05	0.03	63.31	0.37	33.49	0.01	-	0.00	98.00	leucoxene
295	0	0.00	0.14	0.03	0.00	0.01	92.55	0.50	8.92	0.00	-	0.17	102.33	leucoxene
296	0.0089	1.00	0.91	0.54	0.12	0.10	66.59	0.34	28.47	0.06	-	0.09	98.22	leucoxene
297	0	0.00	0.06	0.02	0.00	0.00	94.09	0.00	5.77	0.00	-	0.00	99.94	leucoxene
298	0.0097	0.23	1.60	4.27	0.04	0.07	89.12	0.06	2.33	0.02	0.05	0.14	97.94	leucoxene
299	0	1.42	1.35	2.64	0.00	0.15	62.98	0.02	29.98	0.00	-	0.10	98.64	leucoxene
300	0.0001	0.02	0.17	1.43	0.00	0.03	85.57	0.00	0.19	0.00	-	0.77	88.19	leucoxene
301	0.0014	0.06	1.35	1.77	0.05	0.08	92.92	0.02	2.26	0.02	-	0.12	98.65	leucoxene
302	0	0.01	0.12	0.00	0.00	0.02	90.86	0.00	3.61	0.00	-	0.13	94.75	leucoxene
303	-	0.08	0.36	0.37	-	-	0.26	0.05	89.23	-	-	-	90.34	hematite
304	-	0.03	0.41	0.48	-	-	0.14	0.06	90.13	-	-	-	91.24	hematite
305	-	0.02	0.14	0.18	0.04	-	0.23	0.04	91.13	-	-	-	91.79	hematite

Table B.16: EMPA data of grossular 1 and grossular 2

Analytes	MgO	Al_2O_3	SiO_2	P_2O_5	CaO	TiO_2	MnO	FeO	SrO		
LLD	0.02	0.01	0.02	0.03	0.01	0.02	0.02	0.03	0.04		
Grain No.	MgO	Al_2O_3	SiO_2	P_2O_5	CaO	TiO_2	MnO	FeO	SrO	Total	Mineral name
306	0.05	28.70	38.38	0.06	23.54	0.08	0.21	7.69	0.25	98.97	Grossular
307	0.05	27.43	38.51	0.07	23.26	0.08	0.39	9.61	0.18	99.58	Grossular
308	-	24.05	37.93	0.05	23.47	0.14	0.19	13.55	0.42	99.80	Grossular
309	0.05	28.31	38.60	0.05	23.32	0.14	0.24	8.44	0.24	99.40	Grossular
310	0.02	27.01	38.64	0.04	23.67	0.14	0.25	9.53	0.26	99.54	Grossular
311	-	25.98	38.22	0.04	23.78	0.18	0.24	11.10	0.39	99.93	Grossular
312	0.03	25.58	38.42	-	23.76	0.13	0.17	11.34	0.15	99.58	Grossular
313	0.03	26.94	38.43	-	22.54	0.08	0.37	10.85	0.24	99.49	Grossular
314	0.07	26.54	38.62	0.10	23.75	0.20	0.11	9.66	0.36	99.41	Grossular
315	-	24.80	38.28	-	23.34	0.04	0.26	12.41	0.34	99.48	Grossular
316	0.06	27.02	38.21	0.05	23.83	0.11	0.26	9.92	0.26	99.73	Grossular
317	-	27.66	38.42	0.05	23.67	0.02	0.10	9.09	0.80	99.82	Grossular
318	0.03	25.60	38.16	0.05	23.14	0.04	0.44	12.06	0.40	99.92	Grossular
319	0.02	27.00	38.49	0.05	23.81	0.12	0.15	10.13	0.23	99.98	Grossular
320	-	24.13	37.79	-	22.74	0.17	0.33	13.41	0.32	98.89	Grossular
321	0.07	27.55	38.35	-	23.10	0.14	0.23	9.88	0.21	99.54	Grossular
322	0.06	25.54	38.04	0.04	23.25	0.14	0.15	11.61	0.18	99.01	Grossular
323	-	24.86	37.68	-	23.72	0.10	0.10	12.66	0.71	99.83	Grossular
324	-	27.30	39.10	-	22.99	0.41	0.16	9.58	0.18	99.72	Grossular
325	0.08	29.94	39.00	0.07	23.27	0.25	0.34	6.30	0.19	99.45	Grossular
326	0.04	26.62	38.08	-	23.45	0.12	0.34	10.64	0.22	99.49	Grossular
327	0.07	26.85	38.57	0.25	23.63	0.21	0.19	9.58	0.15	99.49	Grossular
328	-	29.79	38.52	-	24.08	0.06	0.14	6.86	0.26	99.70	Grossular
329	0.04	24.82	37.98	0.04	23.29	0.07	0.22	12.61	0.37	99.45	Grossular
330	0.04	27.87	38.72	0.05	23.72	0.20	0.11	8.58	0.18	99.47	Grossular
331	0.02	25.48	38.16	-	23.50	0.16	0.29	11.67	0.35	99.63	Grossular
332	-	28.40	38.95	0.03	23.80	0.07	0.08	8.01	0.20	99.53	Grossular
333	0.07	30.01	38.85	0.04	24.49	0.22	0.11	5.44	0.21	99.44	Grossular
334	0.07	28.91	38.70	0.08	23.87	0.21	0.10	7.56	0.16	99.65	Grossular
335	0.06	29.27	38.81	-	23.85	0.17	0.09	7.07	0.20	99.52	Grossular
336	-	24.78	38.56	-	22.74	0.05	0.21	13.00	0.41	99.75	Grossular
337	0.04	26.41	38.12	0.04	23.76	0.12	0.16	10.69	0.36	99.69	Grossular
338	-	24.69	38.30	0.08	22.87	0.15	0.28	12.78	0.58	99.74	Grossular
339	0.08	30.38	38.65	0.06	23.57	0.15	0.32	6.28	0.20	99.70	Grossular
340	0.04	26.48	38.61	-	23.67	0.12	0.13	10.28	0.23	99.56	Grossular
341	0.03	26.28	38.49	-	23.26	0.13	0.33	10.90	0.20	99.61	Grossular
342	0.02	26.38	38.28	0.05	23.83	0.07	0.27	10.76	0.36	100.01	Grossular
343	-	24.34	38.11	-	22.96	0.15	0.28	13.31	0.57	99.72	Grossular
344	0.04	29.48	38.47	-	23.34	0.08	0.21	7.43	0.79	99.83	Grossular
345	0.04	25.75	38.37	-	22.55	0.10	0.28	11.76	0.52	99.39	Grossular
346	0.03	31.02	39.08	-	24.09	0.08	0.08	5.08	0.21	99.68	Grossular
347	0.03	25.76	38.02	-	23.41	0.07	0.17	11.32	0.27	99.05	Grossular
348	0.03	29.49	38.36	-	24.15	0.06	0.11	6.80	0.41	99.40	Grossular
349	0.06	30.82	38.94	-	23.65	0.18	0.09	6.06	0.19	99.99	Grossular
350	-	24.43	37.86	-	22.87	0.24	0.15	13.47	0.69	99.71	Grossular
351	-	26.30	38.43	-	23.57	0.21	0.12	11.08	0.19	99.91	Grossular
352	-	24.84	37.99	-	23.55	0.16	0.09	12.60	0.43	99.68	Grossular
353	0.16	18.25	38.41	-	32.35	0.22	4.30	7.32	-	101.01	Grossular 2
354	0.20	16.55	38.04	-	33.69	2.22	2.01	7.34	-	100.06	Grossular 2
355	0.09	19.86	39.52	-	35.31	0.35	0.33	5.60	-	101.06	Grossular 2
356	0.04	21.14	38.72	-	33.67	0.79	3.59	2.83	-	100.78	Grossular 2
357	0.09	21.68	38.90	-	35.37	0.57	0.16	3.92	-	100.68	Grossular 2

Table B.17: EMPA data of almandine

Analytes	MgO	Al_2O_3	SiO_2	P_2O_5	CaO	TiO_2	MnO	FeO	SrO	Ce_2O_3	Pr_2O_3	Sm_2O_3	Eu_2O_3	Dy_2O_3	Ho_2O_3		
LLD	0.02	0.01	0.02	0.03	0.01	0.02	0.02	0.03	0.04	0.09	0.09	0.03	0.03	0.05	0.09		
Grain No.	MgO	Al_2O_3	SiO_2	P_2O_5	CaO	TiO_2	MnO	FeO	SrO	Ce_2O_3	Pr_2O_3	Sm_2O_3	Eu_2O_3	Dy_2O_3	Ho_2O_3	Total	Mineral name
358	9.52	21.24	38.81	-	6.82	0.03	0.52	22.44	0.15	-	-	-	-	-	-	99.51	Almandine-pyrope
359	8.05	21.08	37.41	-	6.87	0.03	2.34	22.14	0.17	-	-	-	-	-	-	98.09	Almandine-pyrope
360	8.65	21.57	38.28	-	8.03	0.08	0.34	22.04	0.12	-	-	-	-	-	-	99.11	Almandine-pyrope
361	9.71	21.59	38.96	-	5.54	0.04	0.35	23.42	0.13	-	-	-	-	-	-	99.73	Almandine-pyrope
362	11.03	22.18	39.48	-	2.43	0.20	0.47	24.12	0.14	-	-	-	-	-	-	100.06	Almandine-pyrope
363	2.94	21.30	35.14	0.00	0.87	0.06	20.49	13.25	0.15	-	-	-	0.12	4.71	0.16	99.19	almandine-pyrope-spessartine
364	1.89	20.90	34.26	0.04	1.16	0.05	14.63	24.14	0.14	-	0.10	0.04	0.04	2.48	-	99.86	almandine-pyrope-spessartine
365	2.03	20.62	34.63	0.03	1.12	0.03	14.28	24.00	0.12	0.10	-	-	0.09	3.00	-	100.06	almandine-pyrope-spessartine

APPENDIX C: MASS BALANCE

The tables below show the mass balance sheet of NaOH cracking, water leach and HCl leaching test.

Table C.1: NaOH Cracking test mass balance

NaOH Cracking Mass Balance																				
SOURCE	**La**	**Ce**	**Pr**	**Nd**	**Sm**	**Eu**	**Gd**	**Tb**	**Dy**	**Ho**	**Er**	**Tm**	**Yb**	**Lu**	**Sc**	**Y**	**TREE,**	**TREE excl. Ce & La**	**MREE**	**HREE**
	ppm	**ppm**	**ppm**	**ppm**	**ppm**	**ppm**	**ppm**	**ppm**	**ppm**	**ppm**	**ppm**	**ppm**	**ppm**	**ppm**	**ppm**	**ppm**	**ppm**	**ppm**	**ppm**	**ppm**
Feed Solids	12389	25141	2693	10462	1727	67	1181	171	667	119	345	31	395	68	30	3424	58910	21380	2975	1796
Residue	11490	23647	2531	9575	1577	62	1043	149	643	126	367	44.7	396	71	29.7	3509	55260.4	20123.4	2682	1796.7
PLS	0	0	0	0	0	0	0	0	0	0	0	0	0	0	0	0	0	0	0	0
Wash water	0	0	0	0	0	0	0	0	0	0	0	0	0	0	0	0	0	0	0	0

SOURCE	**La**	**Ce**	**Pr**	**Nd**	**Sm**	**Eu**	**Gd**	**Tb**	**Dy**	**Ho**	**Er**	**Tm**	**Yb**	**Lu**	**Sc**	**Y**	**TREE,**	**TREE excl. Ce & La**	**MREE**	**HREE**
	g	**g**	**g**	**g**	**g**	**g**	**g**	**g**	**g**	**g**	**g**	**g**	**g**	**g**	**g**	**g**	**g**	**g**	**g**	**g**
Feed Solids In (g)	4.96	10.06	1.08	4.18	0.69	0.03	0.47	0.07	0.27	0.05	0.14	0.01	0.16	0.03	0.01	1.37	23.56	8.55	1.19	0.72
Total In (g)	**4.96**	**10.06**	**1.08**	**4.18**	**0.69**	**0.03**	**0.47**	**0.07**	**0.27**	**0.05**	**0.14**	**0.01**	**0.16**	**0.03**	**0.01**	**1.37**	**23.56**	**8.55**	**1.19**	**0.72**
Leach Residue Out (g)	4.30	8.85	0.95	3.58	0.59	0.02	0.39	0.06	0.24	0.05	0.14	0.02	0.15	0.03	0.01	1.31	20.68	7.53	1.00	0.67
PLS Out (g)	0.00	0.00	0.00	0.00	0.00	0.00	0.00	0.00	0.00	0.00	0.00	0.00	0.00	0.00	0.00	0.00	0.00	0.00	0.00	0.00
wash water	0.00	0.00	0.00	0.00	0.00	0.00	0.00	0.00	0.00	0.00	0.00	0.00	0.00	0.00	0.00	0.00	0.00	0.00	0.00	0.00
Total Out, g	**4.30**	**8.85**	**0.95**	**3.58**	**0.59**	**0.02**	**0.39**	**0.06**	**0.24**	**0.05**	**0.14**	**0.02**	**0.15**	**0.03**	**0.01**	**1.31**	**20.68**	**7.53**	**1.00**	**0.67**
Extraction (solid base)	13%	12%	12%	14%	15%	13%	17%	18%	10%	1%	0%	-35%	6%	2%	7%	4%	12%	12%	16%	6%
Extraction (solution base)	0%	0%	0%	0%	0%	0%	0%	0%	0%	0%	0%	0%	0%	0%	0%	0%	0%	0%	0%	0%
Accountability	87%	88%	88%	86%	85%	87%	83%	82%	90%	99%	100%	135%	94%	98%	93%	96%	88%	88%	84%	94%

Table C.2: NaOH Cracking test log sheet

NAOH CRACKING TEST

Test no	MNL-01
Date:	11-08-2016
Feed:	Beach Sand Concentrate

Consumptions:

TOH Consumption, 100%	2000.00	Kg/ton ore

Reaction Conditions:

Temperature	140	°C
Residence time	4.0	hours
Target pH	-	
Solids content	20	% m/v
Grind size	as received	um

Test work Up Data:

Volume of filtrates	3620	mL
Mass of filtrates	4281.7	g
Mass of unwashed cake	641.4	g
Volume of washes	9300	mL
Volume of entrained filtrates	279.0	ml
Mass of washed residues	492	g
Mass of dry solids	311	g
Total Dry mass	374	g
Mass Loss	6.4	%

Moisture content

Wet sub-sample mass	55.00	g
Dry sub-sample mass	34.80	g
Moisture content	36.73	%
Solids content	63.27	%

Feed Data:	**Target**	**Actual**	
Mass of feed solids	400	400	
Required mass of NaOH solution	1600	1600	g
Volume of DI water	800	800	g
Mass of NaOH pellets	800	800	
Reagents conc	**Target**	**Actual**	
NaOH concentration	1000	1000	g/L
NaOH concentration	50	50	% m/m

Sub-samples

Sample name	Container,g	Wet mass, g	Dry mass, g
Primary filter cake	78.40	20.00	12.9
Wash 1	78.90	24.30	15.1
Wash 2	73.4	55.00	34.8

Log Sheet

Time, hours	Solution Temp,°C	Comments/Remarks/Observations
0	145	
0.5	144	
1	150	
1.5	150	
2	140	
2.5	145	
3	140	
3.5	140	
4	140	
Average	**144**	

Table C.3: Water leaching test mass balance

Water Leach Mass Balance																				
SOURCE	**La**	**Ce**	**Pr**	**Nd**	**Sm**	**Eu**	**Gd**	**Tb**	**Dy**	**Ho**	**Er**	**Tm**	**Yb**	**Lu**	**Sc**	**Y**	**TREE,**	**TREE excl. Ce & La**	**MREE**	**HREE**
	ppm	**ppm**	**ppm**	**ppm**	**ppm**	**ppm**	**ppm**	**ppm**	**ppm**	**ppm**	**ppm**	**ppm**	**ppm**	**ppm**	**ppm**	**ppm**	**ppm**	**ppm**	**ppm**	**ppm**
Feed Solids	11490	23647	2531	9575	1577	62	1043	149	643	126	367	44.7	396	71	29.7	3509	55260	20123	2682	1797
Residue	10573	21453	2296	8917	1488	61	1065	152	594	113	308	41	361	63	24	3076	50585	18559	2614	1632
PLS	0	0	0	0	0	0	0	0	0	0	0	0	0	0	0	0	0	0	0	0
SOURCE	**La**	**Ce**	**Pr**	**Nd**	**Sm**	**Eu**	**Gd**	**Tb**	**Dy**	**Ho**	**Er**	**Tm**	**Yb**	**Lu**	**Sc**	**Y**	**TREE,**	**TREE excl. Ce & La**	**MREE**	**HREE**
	g	**g**	**g**	**g**	**g**	**g**	**g**	**g**	**g**	**g**	**g**	**g**	**g**	**g**	**g**	**g**	**g**	**g**	**g**	**g**
Feed Solids In (g)	3.88	7.99	0.86	3.24	0.53	0.02	0.35	0.05	0.22	0.04	0.12	0.02	0.13	0.02	0.01	1.19	18.68	6.80	0.91	0.61
Total In (g)	**3.88**	**7.99**	**0.86**	**3.24**	**0.53**	**0.02**	**0.35**	**0.05**	**0.22**	**0.04**	**0.12**	**0.02**	**0.13**	**0.02**	**0.01**	**1.19**	**18.68**	**6.80**	**0.91**	**0.61**
Leach Residue Out (g)	3.43	6.96	0.74	2.89	0.48	0.02	0.35	0.05	0.19	0.04	0.10	0.01	0.12	0.02	0.01	1.00	16.40	6.02	0.85	0.53
PLS Out (g)	0.00	0.00	0.00	0.00	0.00	0.00	0.00	0.00	0.00	0.00	0.00	0.00	0.00	0.00	0.00	0.00	0.00	0.00	0.00	0.00
Total Out, g	**3.43**	**6.96**	**0.74**	**2.89**	**0.48**	**0.02**	**0.35**	**0.05**	**0.19**	**0.04**	**0.10**	**0.01**	**0.12**	**0.02**	**0.01**	**1.00**	**16.40**	**6.02**	**0.85**	**0.53**
Extraction (solid base)	12%	13%	13%	11%	9%	6%	2%	2%	11%	14%	20%	12%	13%	15%	22%	16%	12%	12%	7%	13%
Extraction (solution base)	0%	0%	0%	0%	0%	0%	0%	0%	0%	0%	0%	0%	0%	0%	0%	0%	0%	0%	0%	0%
Accountability	88%	87%	87%	89%	91%	94%	98%	98%	89%	86%	80%	88%	87%	85%	78%	84%	88%	88%	93%	87%

Table C.4: Water leaching test log sheet

WATER LEACH TEST

Test no	MNL-01
Date:	Aug-16
Feed:	Caustic cracked solids

Reaction Conditions:

Parameter	**Target**	
Temperature	60	°C
Residence time	4.0	hours
Target pH	Varies	
Initial pulp density	20.0	% (m/m)
Feed Data:	**Target**	
Mass of feed wet solids	488.32	g
Mass of dry feed solids	338.00	g
Mass of DI water	1201.68	g

Test work Up Data:

Volume of filtrates	999	mL
Density of filtrate	0.99	g/ml
Mass of filtrates	988	g
Volume of washes	2160	mL
Volume of entrained filtrates	139.7	mL
Mass of unwashed cake	449.6	g
Mass of washed residues	440.7	g
Mass of dry washed residues	311.3	g
Total dry residue mass	324.2	g
Mass loss	4%	

Sub-samples

Sample name	**Wet mass, g**	**Dry mass, g**
Primary filter cake	20	12.9

Log Sheet

Time, hours	Solution Temp,°C	pH of solution	Eh of solution, mV(vs Ag/AgCl)	Comments/ Remarks
0	60.00	8.25	194.50	Readings taken before solids addition
0.5	62.50	11.05	18.00	
1	59.00	11.14	46.50	
1.5	58.90	11.14	56.00	
2	59.90	11.11	54.45	
2.5	62.00	11.06	43.00	
3	58.90	11.13	46.50	
3.5	59.70	11.11	32.75	
4	60.20	11.10	45.80	
Total	**60.12**	**10.79**	**59.72**	

Table C.5: The HCl leaching test mass balance

HCl Leach Mass Balance																				
SOURCE	**La ppm**	**Ce ppm**	**Pr ppm**	**Nd ppm**	**Sm ppm**	**Eu ppm**	**Gd ppm**	**Tb ppm**	**Dy ppm**	**Ho ppm**	**Er ppm**	**Tm ppm**	**Yb ppm**	**Lu ppm**	**Sc ppm**	**Y ppm**	**TREE, ppm**	**TREE excl. Ce & La ppm**	**MREE ppm**	**HREE ppm**
Feed Solids	10573	21453	2296	8917	1488	61	1065	152	594	113	308	41	361	63	24	3076	50585	18559	2614	1632
Leach Residue	4365	11294	1162	4462	915	41	648	108	468	95	267	37.5	325	58	10.8	2302	26558	10899	1604	1359
Final PLS	1678	2842	323	1270	170	6.04	117	11.4	44.3	7.13	9.97	0.86	14.4	2.36	2.08	232	6731	2211	293	90
Wash water	51.3	82	10.2	35.4	4.81	0.183	3.21	0.32	1.65	0.721	1.14	0	0.41	0.031	0.071	7.3	199	65	8	4
SOURCE	**La g**	**Ce g**	**Pr g**	**Nd g**	**Sm g**	**Eu g**	**Gd g**	**Tb g**	**Dy g**	**Ho g**	**Er g**	**Tm g**	**Yb g**	**Lu g**	**Sc g**	**Y g**	**TREE, g**	**TREE excl. Ce & La g**	**MREE g**	**HREE g**
Feed Solids In (g)	3.17	6.44	0.69	2.68	0.45	0.02	0.32	0.05	0.18	0.03	0.09	0.01	0.11	0.02	0.01	0.92	15.18	5.57	0.78	0.49
Total In (g)	**3.17**	**6.44**	**0.69**	**2.68**	**0.45**	**0.02**	**0.32**	**0.05**	**0.18**	**0.03**	**0.09**	**0.01**	**0.11**	**0.02**	**0.01**	**0.92**	**15.18**	**5.57**	**0.78**	**0.49**
Leach Residue Out, g	1.12	2.90	0.30	1.14	0.23	0.01	0.17	0.03	0.12	0.02	0.07	0.01	0.08	0.01	0.00	0.59	6.81	2.79	0.41	0.35
Final PLS Out, g	1.83	3.09	0.35	1.38	0.19	0.01	0.13	0.01	0.05	0.01	0.01	0.00	0.02	0.00	0.00	0.25	7.33	2.41	0.32	0.10
Wash water, g	0.27	0.43	0.05	0.19	0.03	0.00	0.02	0.00	0.01	0.00	0.01	0.00	0.00	0.00	0.00	0.04	1.05	0.35	0.04	0.02
Total Out, g	**3.22**	**6.42**	**0.70**	**2.71**	**0.45**	**0.02**	**0.31**	**0.04**	**0.18**	**0.04**	**0.09**	**0.01**	**0.10**	**0.02**	**0.01**	**0.88**	15.19	5.55	0.77	0.47
Extraction (solid base)	65%	55%	57%	57%	47%	43%	48%	39%	33%	28%	26%	22%	23%	21%	62%	36%	55%	50%	48%	29%
Extraction (solution base)	66%	55%	59%	59%	47%	41%	45%	31%	32%	34%	18%	8%	16%	14%	37%	32%	55%	49%	46%	25%
Accountability	101%	100%	102%	101%	100%	99%	97%	92%	99%	106%	92%	86%	93%	93%	75%	96%	100%	100%	99%	96%

Table C.6: The HCl leaching test log sheet

REE HCL LEACH

Test no	MNL-01
Date:	2016/08/17
Feed:	Water leach residue

HCl consumption:

Total Acid Added	212.8	kg HCl/kg solids
Total Acid Consumption	212.8	kg HCl/kg solids

Reaction Conditions:

Parameter	**Target**	**Actual**	
Temperature	ambient	21	°C
Residence time	4.0	4.0	hours
Target pH	3.00	3.29	
Target Eh	ambient		mV
Feed Data:	**Target**	**Actual**	
Required mass of dry feed solids	300	300	g
Solids content	20	20	%
Mass of DI water	1200	1200	g

Test work Up Data:

Volume of filtrates	1089	mL
Density of filtrate	1.01	g/ml
Mass of filtrates	1101	g
Volume of washes	5290	mL
Volume of entrained filtrates	96.1	mL
Mass of unwashed cake	353.6	g
Mass of washed residues	286.9	g
Mass of dry washed residues	209.3	g
Total mass of dry solids	256.4	g
Final pulp density		% (m/m)
Mass Loss	14.5	%

Wash Data:

Wash ratio	**5X the mass of unwashed cake**
Wash 1	1800 mL
Wash 2	1730 mL
Wash 3	1760 mL

Sub-samples

Sample name	**Wet mass, g**	**Dry mass, g**
Primary filter cake	25.6	18.9
Wash 1	23.5	17.1
Wash 2	15.4	11.1

Log Sheet

Time, hours	Solution Temp,°C	pH of solution	Eh of solution, mV(vs Ag/AgCl)	Volume of HCl added, mL	Comments/ Remarks
0	19.4	10.9	-39.5		
0.5	21.6	4.1	423.88	35	
1	21.9	3.6	528.13	9	
1.5	21.9	3.52	551.5	6	
2	21.9	2.84		2	
2.5	21.6	3.048	524.13	1	
3	21.5	3.084	508	2	
3.5	21.4	3.054	518.25	1	
4	21.4	3.054	519.88	0.5	
Total	**21.4**	**3.3**	**441.8**	**56.5**	

APPENDIX D: MASS BALANCE CALCULATIONS

The following formula was used to calculate the HREE and MREE leach efficiency, TREE extraction efficiency and TREE accountability.

- TREE = Final PLS of (all analysed REE's) 6731ppm
- MREE = (Sm + Eu + Gd)of Final PLS 293pp
- HREE = (Tb + Dy + Ho + Er + Tm + Yb + Lu)of Final PLS….90ppm

Calculations and conversions from ppm to grams

The calculations below show how the feed solid in (g), leach residue out (g), wash water (g) and final PLS out (g) of an individual REE element measured.

$$\text{Feed Solids in (g)} = \frac{\text{REE (of Feed Solids in ppm)}}{1000000} \times \text{Required mass of dry solids}$$

$$\text{Feed Solids in (g)} = \frac{\text{REE (of Feed Solids in ppm)}}{1000000} \times 300\text{g}$$

$$\text{Leach Residue out(g)} = \frac{\text{REE (of leach residue in ppm)}}{1000000} \times \text{Total mass of dry solids}$$

$$\text{Leach Residue out (g)} = \frac{\text{REE (of leach residue in ppm)}}{1000000} \times 256.4\text{g}$$

$$\text{Wash water (g)} = \frac{\text{REE(wash water)}}{1000} \times \frac{\text{Volume of wash water}}{1000}$$

$$\text{Wash water (g)} = \frac{\text{REE(wash water)}}{1000} \times \frac{529\text{ ml}}{1000}$$

$$\text{Final PLS out (g)} = \frac{\text{REE(Final PLS out)}}{1000} \times \frac{\text{Volume of Filtrates}}{1000}$$

$$\text{Final PLS out (g)} = \frac{\text{REE(Final PLS out)}}{1000} \times \frac{1089\text{ ml}}{1000}$$

Calculations of TREE leach Efficiency (Extraction Efficiency)

TREE Feed solids = 15.18g

TREE Leach Residue out= 6.81g

TREE Final PLS out = 7.33g

TREE Wash water = 1.05g

$$\text{TREE leach efficiency} = \frac{\text{TREE \{Feed Solids in(g)} - \text{Leach Residue out in (g)\}}}{\text{TREE (Feed solids in (g))}}$$

$$\text{TREE leach efficiency} = \frac{15.18 - 6.81}{15.81} \times 100\%$$

TREE leach efficiency = 55%

Calculations of MREE leach Efficiency

MREE Feed solids = 0.78g

MREE Leach Residue out= 0.41g

MREE Final PLS out = 0.32g

MREE Wash water = 0.04g

$$\text{MREE leach efficiency} = \frac{\text{MREE \{Final PLS out(g)} + \text{wash water (g)\}}}{\text{MREE (Feed solids in (g))}}$$

$$\text{MREE leach efficiency} = \frac{0.32 + 0.04}{0.78} \times 100\%$$

MREE leach efficiency = 46%

Calculations of HREE leach Efficiency

HREE Feed solids = 0.49g

HREE Leach Residue out= 0.35g

HREE Final PLS out = 0.10g

HREE Wash water = 0.02g

$$\text{HREE leach efficiency} = \frac{\text{HREE \{Final PLS out(g) + wash water (g)\}}}{\text{HREE (Feed solids in (g))}}$$

$$\text{HREE leach efficiency} = \frac{0.10 + 0.02}{0.49} \times 100\%$$

HREE leach efficiency = 25%

TREE accountability calculations

Total in (TREE) = Feed solids in

= 15.18g

Total out (TREE) = Leach Residue out +Final PLS out +Wash water out

=6.81g +7.33g +1.05g

=15.19g

$$\text{Accountability of TREE} = \frac{\text{Total Out (g)}}{\text{Total In (g)}}$$

$$\text{Accountability of TREE} = \frac{15.19}{15.18} \text{X}100\%$$

Accountability of TREE = 100%

APPENDIX E: CALCULATED ZR/SI RATIO

The table and figure below show the calculated zircon Zr: Si ratio of the analysed leached residues.

Table E.1: Calculated Zr/Si ratio of unreacted zircon

Sample number	Sample	Si	Zr	Zr/Si	Comments
1	NaOH crack	10	40	0.25	Unreacted zircon
2	NaOH crack	10	38	0.26	Unreacted zircon
3	NaOH Repulp Wash 1	13	50	0.26	Unreacted zircon
4	NaOH Repulp Wash 1	12	46	0.26	Unreacted zircon
5	NaOH Repulp Wash 2	11	43	0.26	Unreacted zircon
6	NaOH Plug Wash 3	10	41	0.24	Unreacted zircon
7	HCl leach unwashed	9	36	0.25	Unreacted zircon
8	HCl leach wash 1	9	36	0.25	Unreacted zircon
9	HCl leach wash 1	8	33	0.24	Unreacted zircon
10	HCl leach wash 2	10	39	0.26	Unreacted zircon
11	HCl leach wash 3	10	39	0.26	Unreacted Zircon
12	HCl leach wash 3	11	39	0.28	Unreacted zircon
13	Water Leach	11	42	0.26	Unreacted zircon
14	Water Leach repulp Wash 1	9	36	0.25	Unreacted zircon
15	Water Leach repulp Wash 1	10	38	0.26	Unreacted zircon

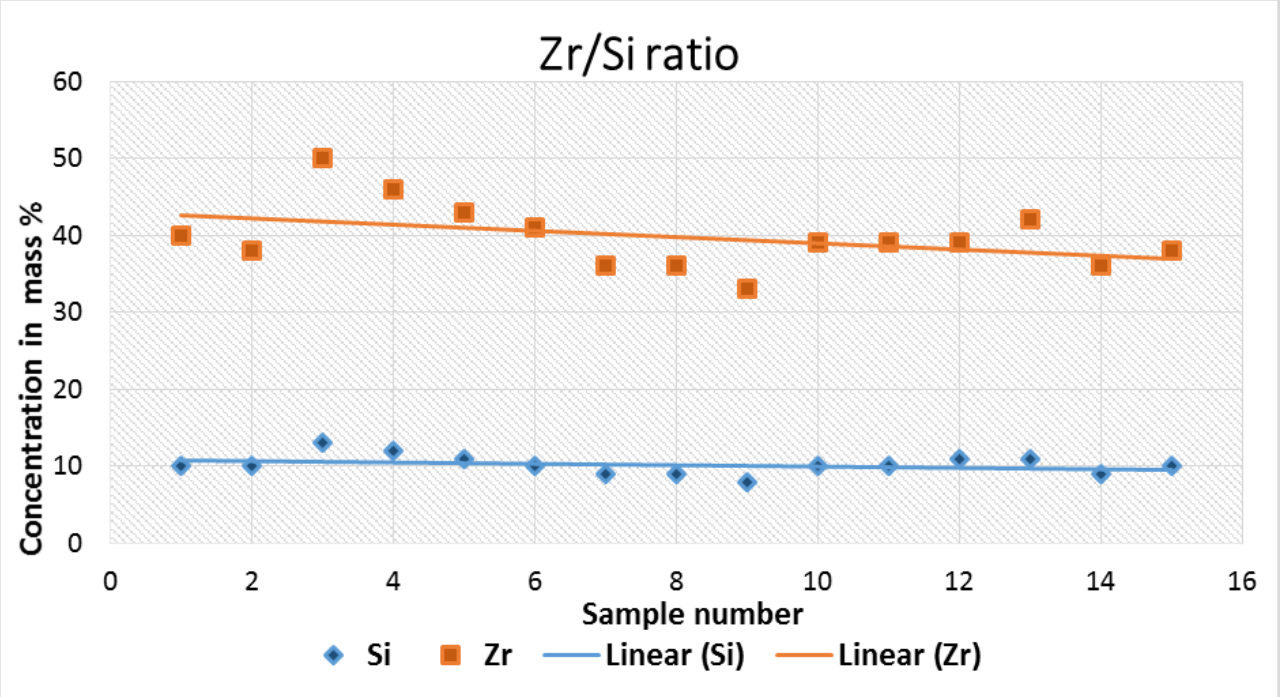


Figure E.1: Calculated Zr/Si ratio of unreacted zircon

APPENDIX F: BULK MODAL MINERALOGY

Table F.1 XRD results of the bulk sample.

Mineral name	Chemical formula	+212 µm	-212+150 µm	-150+106 µm	-106 µm
Amphibole	$Ca_2(Mg, Fe)_5Si_8O_{22}(OH)_2$	xx	xx	xx	nd
Almandine	$(Fe,Mg,Mn)_3Al_2Si_3O_{12}$	xx	xx	xx	nd
Epidote	$Ca_2(Fe,Al)Al_2(SiO_4)(Si_2O_7)O(OH).$	xxxxx	xxxxx	xxx	nd
Grossular	$Ca_3Al_2 (SiO_4)_3$	xx	xx	xx	nd
Ilmenite	$(Fe,Mg) (Ti,Fe)O_3$	nd	nd	nd	xx
Monazite	$(Ce,La,Y,Nd,Th)PO_4$	x	x	xx	xxx
Quartz	SiO_2	xx	x	xx	nd
Rutile	TiO_2	nd	nd	nd	xx
Zircon	$Zr(SiO_4)$	x	xx	xxxx	xxxxx

*nd –not detected, trace (**x**)< 5mass%, minor (**xx**) 5-15mass%, intermediate (**xxx**) 15-25mass%, major (**xxxx**)25-50mass%, predominant (**xxxxx**)>50mass%*

Table F.2: Repeatability tests for modal mineral abundance

Mineral	Mineral	Chemical Formulae	Head	+212 µm	–212µm	–150µm	–106 µm
Mass Distribution of repeat test %			**100**	**12.2**	**40.0**	**37.2**	**10.5**
Mass Distribution of original test %			**100**	**8.5**	**40.4**	**34**	**17.1**
REE-containing species	Monazite	$(Ce,La,Nd,Th)PO_4$	5.7	0.4	1.8	7.4	24.3
	Xenotime	YPO_4	0.1	0.1	0.1	<0.1	0.1
	Zircon	$ZrSiO_4.$	30.8	4.0	12.7	53.0	60.8
	Almandine	$Fe_3Al_2Si_3O_{12}$	1.5	3.0	1.4	1.3	0.2
	Grossular	$Ca_3Al_2(SiO_4)_3$	1.3	2.4	1.8	0.8	<0.1
	Titanite	$CaTiSiO_5$	0.9	0.6	1.5	0.5	<0.1
	Thorite	$(Th,U)SiO_4$	0.1	0.1	0.2	0.1	<0.1
	Leucoxene		1.3	0.3	1.9	1.3	0.2
	Leucoxene_Nb		<0.1	<0.1	<0.1	<0.1	<0.1
Oxides	Rutile	TiO_2	12.1	2.6	11.4	17.9	6.5
	Ilmenite	$FeTiO_3$	4.6	0.6	2.7	7.7	6.1
	FeO/OH	$FeO(OH)$	1.6	2.0	2.1	1.1	0.4
	Chromite	$FeCr_2O_4$	0.2	0.1	0.1	0.4	0.2
	Magnetite_Ti	Fe_2O_4	0.6	0.2	0.6	1.0	0.2
	Spinel	$MgAl_2O_4$	0.3	0.3	0.2	0.4	<0.1
Phosphates	Apatite	$Ca_5(PO_4)_3(OH,F,Cl)$	<0.1	<0.1	<0.1	0.1	<0.1
Silicates	Augite	$(Ca,Na)(Mg,Fe,Al,Ti)(Si,Al)_2O_6$	11.7	20.6	20.1	2.2	0.1
	Actinolite	$Ca_2(Mg,Fe)_5Si_8O_{22}(OH)_2$	2.6	9.6	2.7	0.4	0.1
	Enstatite	$Mg_2Si_2O_6$	1.7	2.4	3.0	0.4	<0.1
	Diopside	$Ca_3Al_2(SiO_4)_3$	<0.1	<0.1	<0.1	<0.1	<0.1
	Epidote	$Ca_2(Fe,Al)_3(SiO_4)_3(OH)$	20.4	44.8	32.5	3.3	0.2
	Albite	$NaAlSi_3O_8$	0.1	0.2	0.2	0.1	<0.1
	Olivine	$(Mg, Fe)_2SiO_4$	<0.1	<0.1	<0.1	<0.1	<0.1
	Microcline	$KAlSi_3O_8$	0.2	0.3	0.2	0.1	0.1
	Quartz	SiO_2	0.5	0.8	0.5	0.4	0.1
	Kaolinite	$Al_2Si_2O_5(OH)_4$	0.1	0.2	0.2	0.1	<0.1
	Andalusite	Al_2SiO_5	1.5	4.3	2.1	0.1	<0.1
	Others		<0.1	<0.1	<0.1	<0.1	<0.1
	Total		**100**	**100**	**100**	**100**	**100**

Table F.3 shows the experimental errors obtained through reproducing the MLA data that was used as a guide for process selection. A 2 kg aliquot of the remaining sample (**Figure 8**) was sub-sampled and screened into the four size fractions, and the same number of polished sections was prepared from subsamples, as for the first set of samples. These sections were subjected to MLA analysis using the same mineral standards reference file for processing. The repeated data is underestimated as a result of sampling and varying screened mass proportion between the original test and the repeat test, as shown above in (**Table F.2**). The equation used to calculate the relative standard deviation (RSD) is shown below:-

$$Relative\ standard\ Deviation(RSD) = \frac{Original\ Test\ - Repeat\ Test}{Original\ Test} \times 100$$

Table F.3: Comparison of original test and repeated test head compositions %

Mineral groups	Mineral	Original test	Repeat test	Average	Variance	RSD
REE-containing species	Monazite	5.3	5.7	5.5	-0.4	-7.5
	Xenotime	<0.1	0.1	0.1	<0.1	<0.1
	Zircon	31.3	30.8	31	0.5	1.6
	Almandine	1.6	1.5	1.5	0.1	6.3
	Grossular	1.2	1.3	1.3	-0.1	-8.3
	Titanite	0.9	0.9	0.9	0	0
	Thorite	0.1	0.1	0.1	0	0
	Leucoxene	1.5	1.3	1.4	0.2	13.3
	Leucoxene_Nb	<01	<0.1	<0.1	<0.1	<0.1
Oxides	Rutile	11.9	12.1	12	-0.2	-1.7
	Ilmenite	4	4.6	4.3	-0.6	-15
	FeO/OH	1.4	1.6	1.5	-0.2	-
	Chromite	0.3	0.2	0.3	0.1	33.3
	Magnetite_Ti	0.6	0.6	0.6	0	0
	Spinel	0.3	0.3	0.3	0	0
Phosphates	Apatite	<0.1	<0.1	<0.1	<0.1	<0.1
Silicates	Augite	12.8	11.7	12.2	1.1	8.6
	Actinolite	2.5	2.6	2.5	-0.1	-4
	Enstatite	1.7	1.7	1.7	0	0
	Diopside	<0.1	<0.1	<0.1	<0.1	<0.1
	Epidote	20.4	20.4	20.4	0	0
	Albite	0.1	0.1	0.1	0	0
	Olivine	<0.1	<0.1	<0.1	<0.1	<0.1
	Microcline	0.1	0.2	0.1	-0.1	-100
	Quartz	0.4	0.5	0.4	-0.1	-25
	Kaolinite	<0.1	0.1	0.1	<0.1	<0.1
	Andalusite	1.4	1.5	1.5	-0.1	-7.1
	Others	<0.1	<0.1	<0.1	<0.1	<0.1
Total		**100**	**100**	**100**		